Distribution
Category UC-94E

SAND86-0694

Physical and Numerical Simulations of Fluid-Filled Cavities In A Creeping Material

by

D. S. Preece

and

H. J. Sutherland

Sandia National Laboratories
Albuquerque, NM 87185

ABSTRACT

Centrifuge creep experiments have been performed on six models of fluid-filled cylindrical cavities in a cylindrical block of the modeling material plasticine. Three of the experiments treated a single cavity on the axis of the plasticine cylinder. The other three experiments each treated an array of four cavities with three cavities symmetrically arranged around one central cavity. The three multi-cavity models differed in the spacing between the central and satellite cavities. The experiments were designed to physically model petroleum-filled caverns leached in rock salt. The experiments were performed for several reasons. First, plasticine is a creeping material which has a mathematical formulation similar to rock salt. Finite element computer programs that include material models for creep have been exercised by performing finite element analyses of the experiments using the plasticine creep model and comparing numerical and experimental results. Both two- and three-dimensional finite element analyses were performed. Second, the multi-cavity experiments were designed to gain an understanding of the behavior of arrays of cavities, specifically, how spacing between cavities influences their creep response. Three-dimensional finite element simulations of the multi-cavity experiments acted as a validation exercise for the code and provided information such as stress distribution that could not be measured experimentally. Third, information obtained about the interaction of cavities in plasticine can also be applied to cavities in rock salt.

CONTENTS

CONTENTS CONTINUED

LIST OF TABLES

FIGURES

FIGURES CONTINUED

FIGURES CONTINUED

FIGURES CONTINUED

Page

APPENDICES

INTRODUCTION

The U. S. Strategic Petroleum Reserve (SPR) was created as a result of the Energy Conservation Act of 1975. The SPR plan calls for storage of a supply of crude oil to be used during supply interruptions. It was designed to store a total of 750 million barrels of crude oil in five different Gulf Coast Salt domes. At each dome the crude oil was to be placed in existing solution mined caverns, in newly leached caverns and in an existing room and pillar salt mine. The reserve currently contains approximately 500 million barrels with new cavern leaching taking place at most of the sites.

Safe cavern spacing has been a concern since the reserve was created. The newly leached caverns at each site were spaced to have a pillar to diameter ratio (P/D) of 1.8. This pillar size is based on the successful experience of the French and Germans in leaching and operating salt caverns [1]. This spacing has also been verified by extensive finite element structural creep analyses [2]. There are some cases where this spacing criterion for the newly leached caverns is not met. Particular examples are the caverns which were purchased at the time the SPR was created and used for immediate crude oil storage. These caverns were typically leached to provide brine for commercial chemical extraction. Leaching was sometimes not very well controlled and caverns with odd shapes and small spacing were sometimes produced. An example of this is shown in Figure 1 which is a cross-section of the West Hackberry salt dome. Caverns 6 and 9 are relatively close together and have a P/D value of approximately 0.4. The wells for these two caverns were drilled in 1947 and 1949 and the two have had their present size and shape for at least twenty years with no apparent structural stability problems. Sometimes preferential directional leaching happens during creation of the new caverns which results in a P/D ratio smaller than 1.8. Preferential leaching occurs when the salt is more soluble in one direction than another. It usually makes the cavern elliptical rather than circular and results in a smaller P/D to the next cavern in the preferred leaching direction. Another aspect of cavern spacing (other than structural stability) is the variability of creep closure and volume loss as a function of spacing. Neither field data nor two-dimensional finite element studies have ever adequately answered the

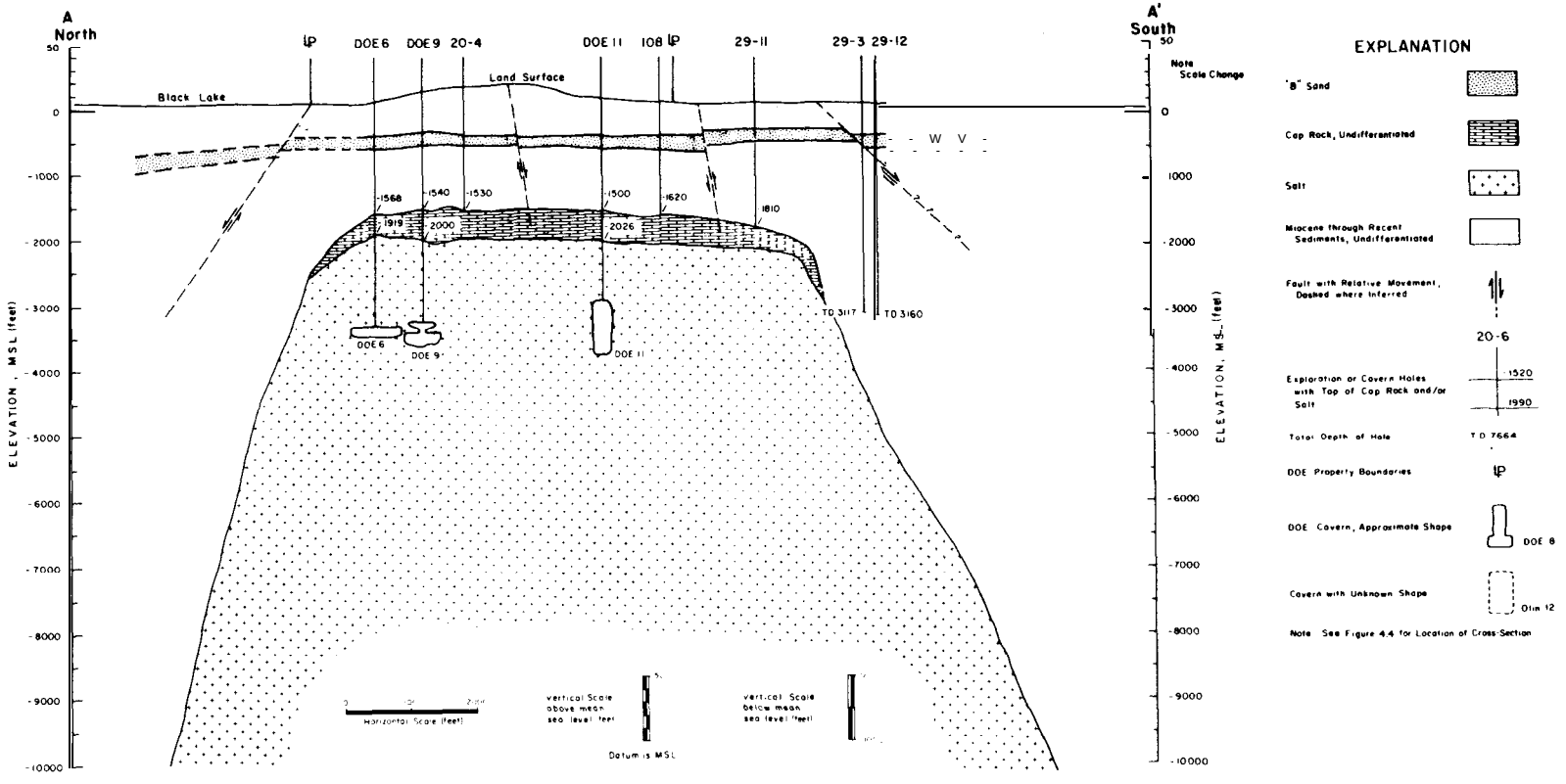

Figure 1: Cross-Section of West Hackberry SPR Site.

question of whether a cavern in an array of caverns experiences more or less creep than a single cavern or one on the edge of the cavern array.

The close spacing of some old caverns, preferential leaching of new caverns and the unknown influence of cavern spacing on creep closure has motivated the present study of cavern spacing. The study included a suite of centrifuge experiments as well as two- and three-dimensional finite element analyses. The first objective of the study was to gain a better understanding of the influence of spacing on the structural response of fluid-filled cavities in a creeping material. The prototypes of these are petroleum-filled caverns in rock salt. In the laboratory these are alcohol-filled cavities in plasticine. Results and conclusions from the laboratory where conditions are better known and controlled should be applicable to understanding the behavior of caverns in rock salt. The second objective of the study was to exercise both two- and three-dimensional finite element computer programs on the single cavity experiments, which have an axisymmetric geometry, and compare computations from the two programs with each other and with the centrifuge test results. This is the first real test of the three-dimensional finite element creep capability and serves as a validation technique for the code but not necessarily for creeping materials other than plasticine. The third objective is to exercise the three-dimensional finite element program on the multiple cavity centrifuge experiments which do not have an axisymmetric geometry. This further validates the computer program and aids in understanding the centrifuge test results.

MATERIAL PROPERTIES OF PLASTICINE

Plasticine has been used by several investigators to simulate the behavior of creeping materials like salt; e.g., see Ramberg's discussion of modeling materials for centrifuge simulations [3]. A detailed description of plasticine's mechanical behavior is given by McClay [4] and Crandall, et. al. [5]. As discussed by McClay, the creep behavior of plasticine can be described by a constitutive model using a power law in stress. The constitutive constants for this formulation change with manufacturer, grade and color. Through careful material control and characterization, plasticine becomes a very good physical model material for creep simulations.

Material Description

As the original plasticine material tested by McClay was no longer available, a material had to be characterized. The material was obtained in several premixed colors: ivory, green, gray and black. Also the color was modified by mixing tempera pigment with the ivory plasticine. The colors tested here were red and blue.

Material Tests

The density of the plasticine was measured using the standard water displacement technique. The density for the ivory, green, gray and black plasticine was found to be 1.71 gm/cm^3 with a standard deviation of 0.004 gm/cm^3. With the red or blue pigment added to the ivory, the density increased to 1.75 gm/cm^3 with a standard deviation of 0.009 gm/cm^3.

The plasticine was tested in uniaxial compression at several constant strain rates. The test specimens were 1 in (25.4 mm) in diameter and 2 in (50.8 mm) in length. The tests were conducted at strain rates varying from 1x10-3/s to 3x10-6/s. The temperature of the sample was controlled to

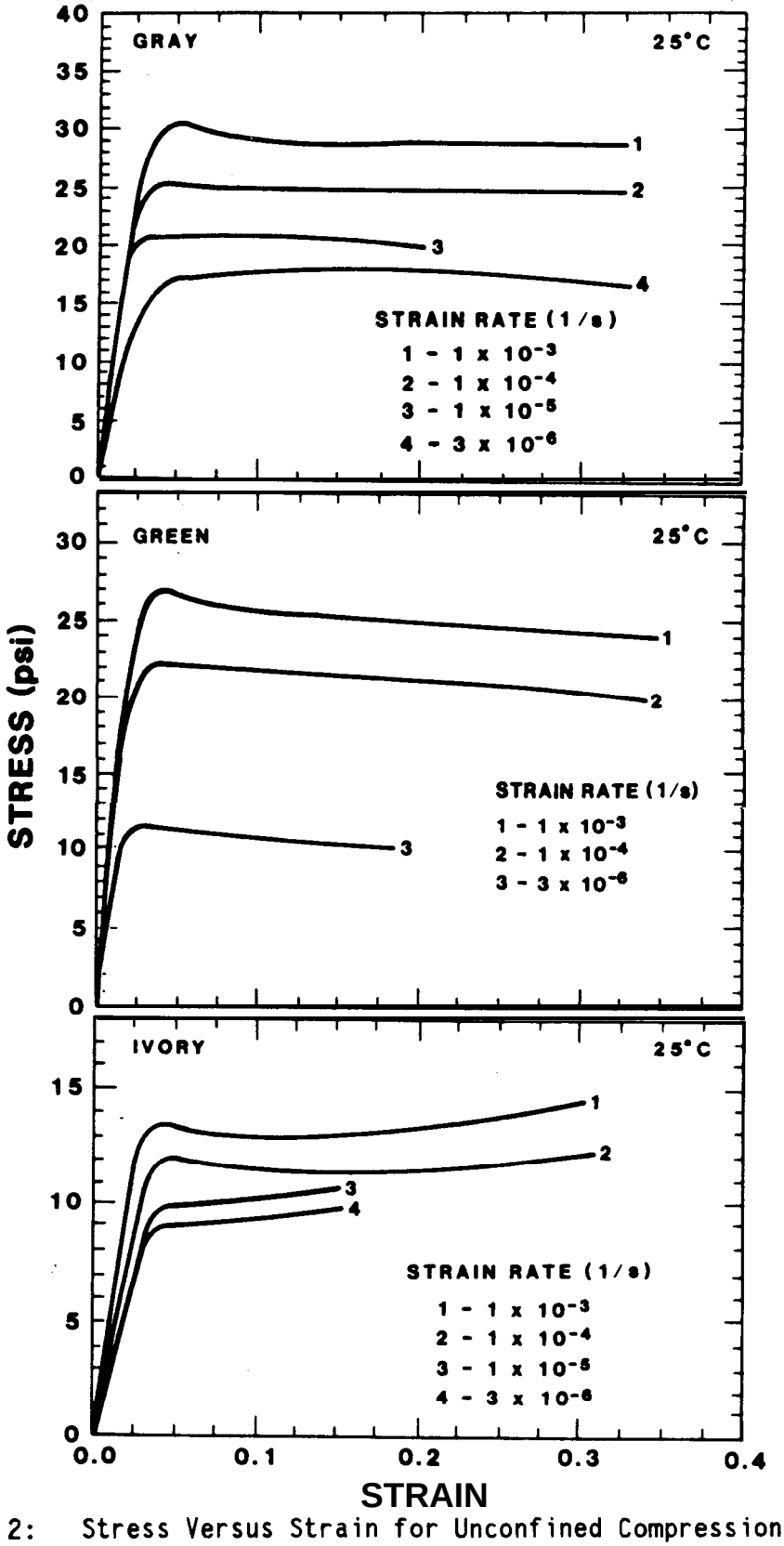

Figure 2: Stress Versus Strain for Unconfined Compression Tests of Plasticine Cylinders at Different Strain Rates.

25^{o} C $\pm$ 0.5^{o} c. A typical set of stress-strain plots, from the tests of ivory, green and gray plasticine is shown in Figure 2.

The constitutive data obtained for the various plasticines are summarized in Table I and in Figure 3. These data were fitted using a linear regression analysis [6] to a power law constitutive equation of the form:

$$\dot{e} = K(\sigma)^{n} \qquad (1)$$

where $\dot{e}$ is the effective creep strain rate, K is the leading coefficient, a is the effective stress and n is the power law exponent. This formulation implies steady state secondary creep.

The unconfined compression tests summarized in Table I gave a creep model and a longitudinal (Youngs') modulus. They did not, however, provide any measurement of Poisson's ratio which is necessary for finite element calculations. McClay [4] gives a partial list of the ingredients used to produce plasticine, all of which are quite incompressible. Even with this information it was deemed necessary to perform some experiments on the plasticine used here to accurately determine Poisson's ratio. This problem has been considered previously for modeling clay which is similar in many respects to plasticine. Crandall [5] measured longitudinal and shear wave speeds obtained from resonance experiments to determine Poisson's ratio for modeling clay. In this study, longitudinal and shear wave speed experiments were conducted on specimens of green and gray plasticine in the Ultrasonics Laboratory at Sandia. The longitudinal wave speed was measured at 0.0670 to 0.0685 in/μsec (1.70E2 to 1.74E2 m/sec) but the shear wave speed was impossible to measure since the material would not carry shear waves but seemed to convert a shear wave input into an attenuated longitudinal wave. Another way to calculate Poisson's ratio without using the shear wave speed is to use the density and small strain modulus in the equation for longitudinal wave speed [6]. The only unknown is Poisson's ratio which is calculated as 0.4998 for a small strain modulus of 1000 psi (6895 kPa), a density of 1.6167x10-4 lb-sec/in^{4} (1.71 gm/cm^{3}) and a longitudinal wave speed of 0.06775 in/μsec (1.72E-2 m/sec). The sensitivity of Poisson's ratio to

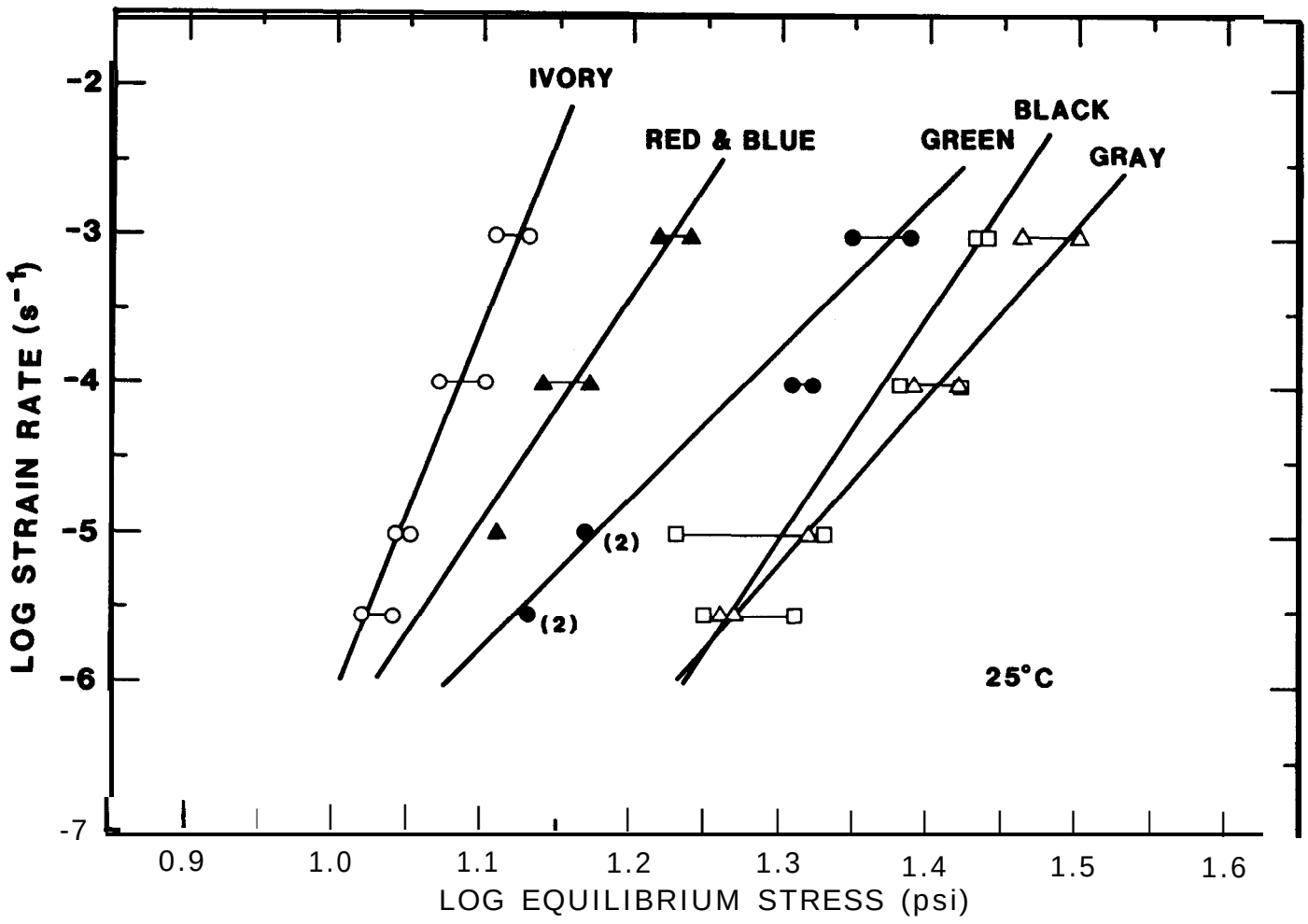

Figure 3: **Log equilibrium Stress Versus Log Strain Rate for Various Types of Plasticine.**

small strain modulus was determined by calculating the small strain modulus corresponding to various values of Poisson's ratio. For a Poisson's ratio of .4999 the corresponding small strain modulus is calculated as 445 psi (3068 kPa) and for a Poisson's ratio of ,499 it is 4440 psi (30613 kPa). It will be shown later that changing Poisson's ratio from 0.4998 to 0.499 does not significantly impact the finite element results. The bounds on small strain modulus are ± 50 psi (345 kPa) which implies that this method of determining Poisson's ratio yields good results.

Table I

Plasticine Material Properties at 25° C

		Creep Model Curve Fit (Eq. 1)		
Material Description	Longitudinal Modulus psi (kPa)	Leading Coefficient	Exponent	Determination Coefficient
Ivory	330 (2290)	1.45E-31 (2.82E-52)	24.7	0.95 [4]
Green	990 (6830)	1.19E-17 (3.88E-26)	10.1	0.99 [5]
Gray	940 (6490)	1.82E-20 (7.25E-30)	11.2	0.99
Black	710 (4880)	2.74E-24 (4.04E-36)	14.1	0.90
Red & Blue [6]	510 (3500)	1.64E-22 (2.43E-35)	15.3	0.94

Notes:
1. Strain rate in l/s.
2. Stress in psi (kPa).
3. Longitudinal Modulus at l.OE-4/s strain rate.
4. Exclude one 1.0E-4 strain rate data point.
5. Exclude 1.0E-4 strain rate data.
6. Standard ivory plasticine colored with tempera pigment.

EXPERIMENTAL TECHNIQUES

Specimen Fabrication

The experiments required large, uniform cylindrical blocks of plasticine. The procedures developed for the casting, machining and assembly are described in detail by Sutherland and Preece [6]. In general, a casting process was used to form the plasticine models. First, the appropriate quantities of plasticine were melted and poured into the fixture used for the centrifuge experiment. Then, the blocks were parted, appropriate cavities and surfaces were cut and the model was reassembled. The lateral boundaries between the plasticine and the fixture were lined with Teflon to insure a very low coefficient of friction on these boundaries.

During the preparation of the plasticine test specimens, appropriate cylindrical cavities were machined into the block of plasticine. To insure that creep closure in the period between model preparation and testing did not affect our results, the cavities were filled with rubber coated salt plugs. The cavities were connected to the "surface" through plastic pipes or risers. These risers permitted the removal of the salt plugs by a "lost wax" processing technique and allowed the filling of the cavities with alcohol.

The salt plugs were removed immediately before testing using a spray of water, through the riser, to dissolve the plug. This process also provided the cavities with leak proof plastic liners. After salt plug removal a right angle bend with a short tube parallel to the top, flat surface was attached to the riser tube. This design permitted the specimen to be turned on its side, for mounting onto the fixed platform of the centrifuge, without draining the cavity.

Centrifuge

The Sandia CA-2 centrifuge was used to conduct these simulations. This machine has a test radius that varies from 5 ft (1.52 m) to 7 ft (2.13 m). Its maximum rated capabilities are 500 lb (227 kg) static payload, 150 g acceleration, and 30,000 g-lb (13,600 g-kg) dynamic load. Fifty slip rings are available on this machine for data acquisition.

Single Cavity Experiments

The single cavity experiments are shown schematically in Figure 4. These simulations were conducted in experimental fixtures that were 11.25 in (0.285 m) inside diameter by 11.5 in (0.292 m) high. All of the models were constructed using the green plasticine because it is the "best" material for simulating the salt in that it has the closest stress exponent to that for salt. Each plasticine cylinder was 10 in (0.254 m) high with a flat top. A single cavity was machined about the centerline of each of three specimens as shown in Figure 4. The cavity was 2 in (50.8 mm) in diameter and 4 in (101.6 mm) high. Thus, the overburden and the underburden were 3 in (76.2 mm). The riser, in all cases, reached to a height of 4.59 in (117 mm) above the top of the cavity. To increase the overburden stress on the specimen, the upper surface of the specimen was covered with a single lead sheet that was 0.25 in (6.35 mm) thick. A layer of teflon was placed between the plasticine and the lead to yield a low coefficient of friction between them.

The tests were conducted for a nominal two hours each. Three models were tested, one each at loads of 100 g, 125 g, and 150 g. A graph of g-load versus time for these experiments is given in Figure 5. These experiments are designated as SE100, SE125 and SE150, respectively. Figure 6 contains cross-sectional views of the single cavity experiments after the tests were completed.

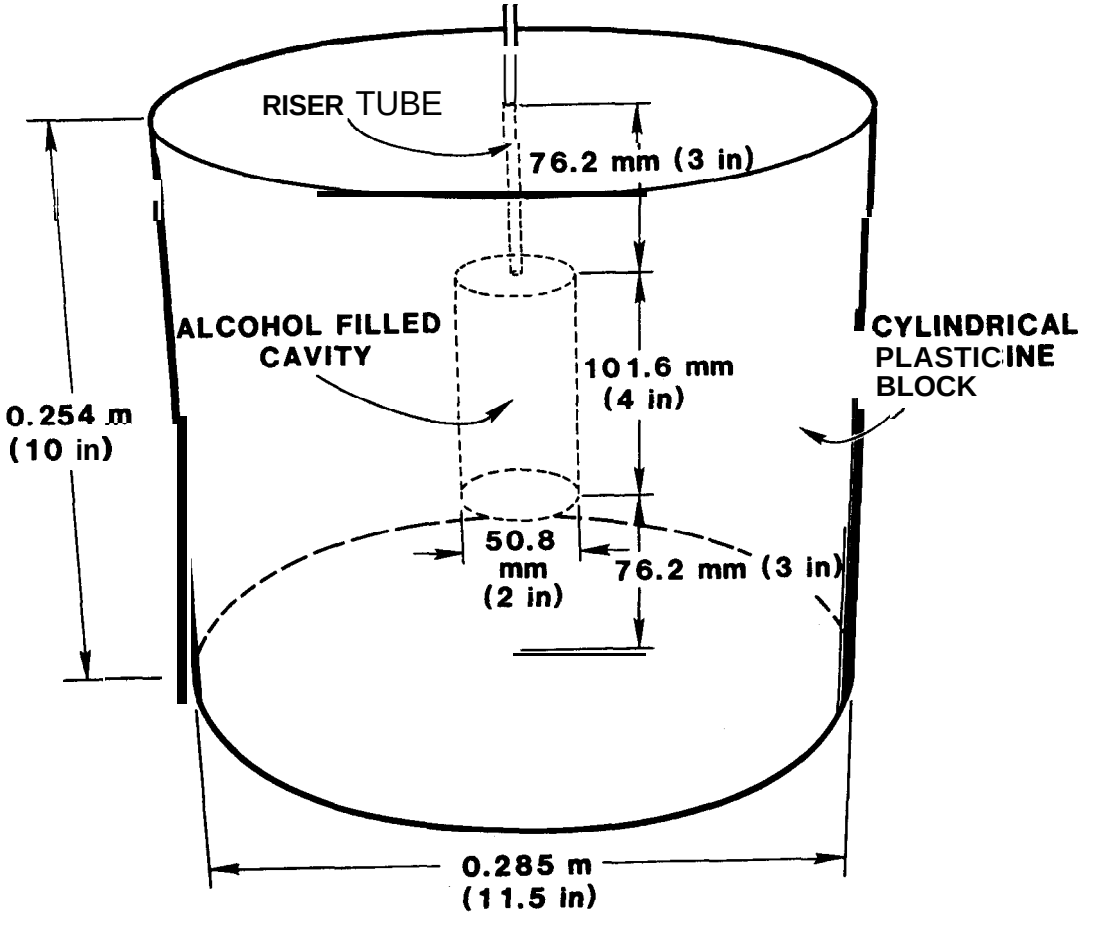

Figure 4: Schematic of Single Cavity Centrifuge Experiments

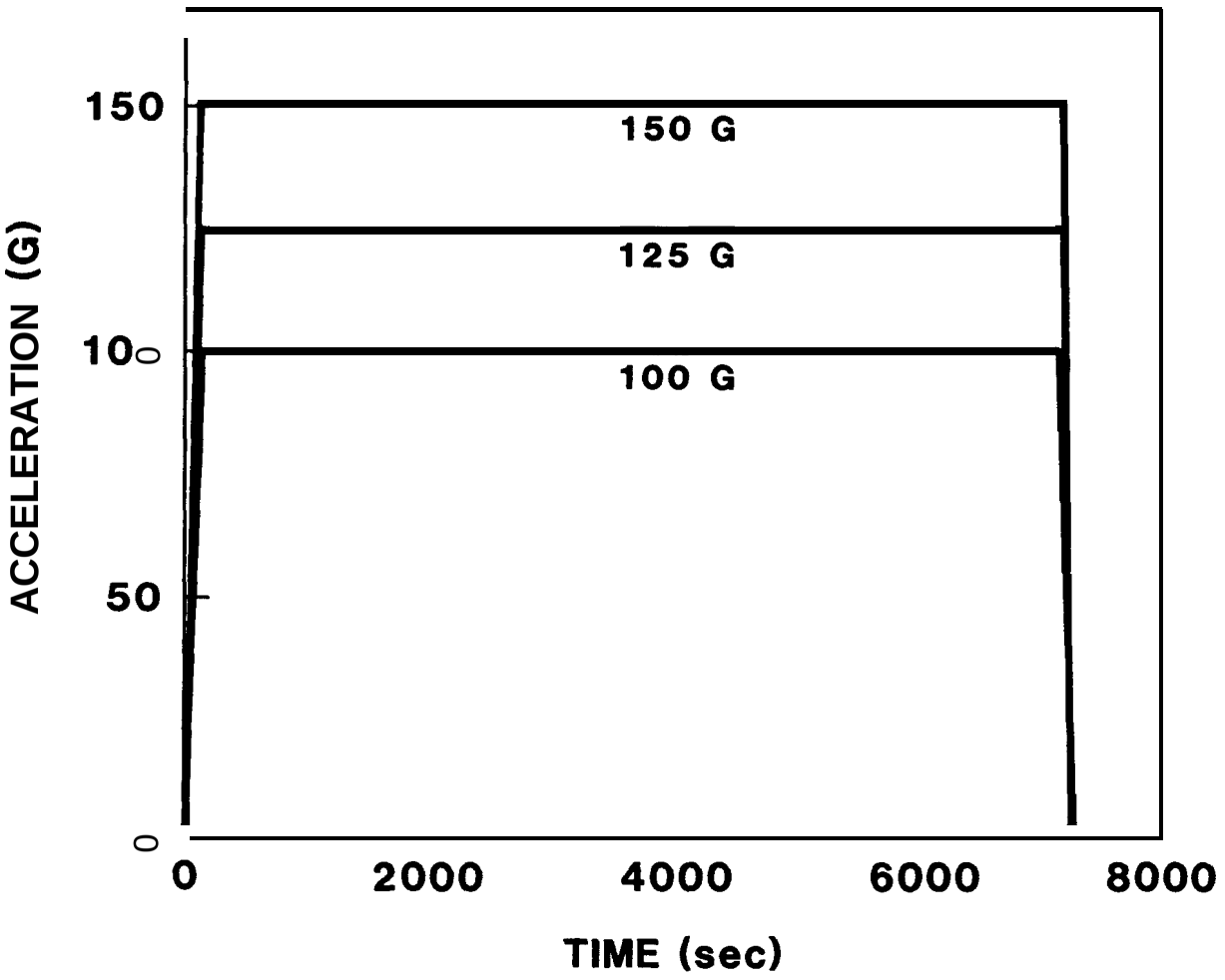

Figure 5: G Load Versus Time for Single Cavity Centrifuge Experiments.

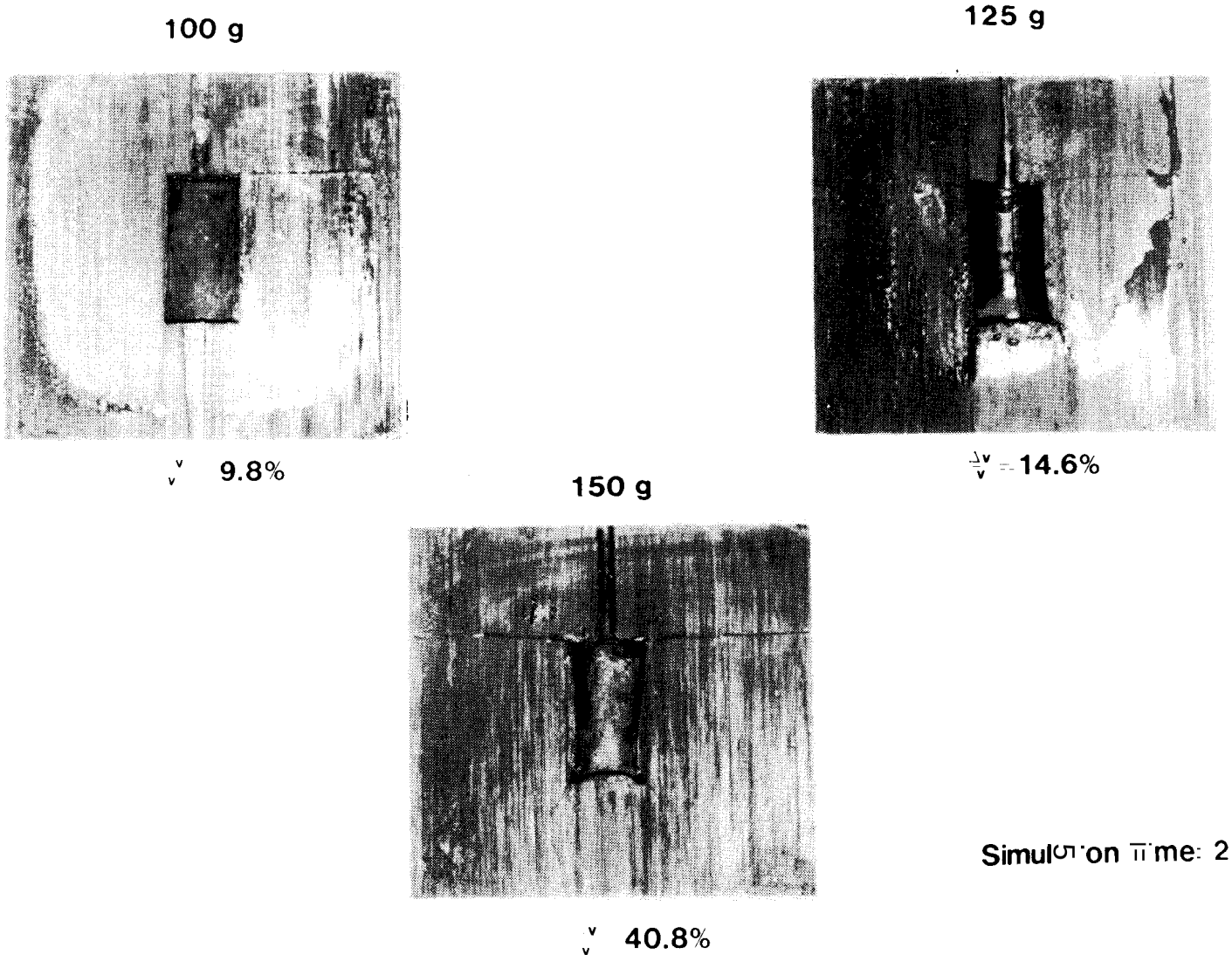

Figure 6: Cross-Sectional Views of the Single Cavity Experiments

Multi-Cavity Experiments

The multi-cavity experiments are shown schematically in Figure 7. The simulations were conducted in experimental fixtures that were 17.25 in (0.438 m) inside diameter by 11.5 in (0.292 m) high. Each model was 10 in (0.254 m) high with a flat top. A single cavity was machined about the centerline of each specimen (cavity A). The other three cavities (B, C, and D) in each specimen were machined symmetrically as shown in Figure 7 (i.e., at 120 degrees relative to one another). Each cavity was 2 in (50.8 mm) in diameter and 4 in (101.6 mm) high. The three models were constructed with spacings of 1 in (25.4 mm), 2 in (50.8 mm) and 3 in (76.2 mm) between the central and satellite cavities (dimension CC in Figure 7 is 3 in, 4 in and 5 in respectively). This gives pillar to diameter ratios (P/D) for the three models of 0.5, 1.0 and 1.5. The first and last models were constructed from green plasticine and the other from the gray plasticine. The green plasticine offered the "best" simulation of the salt and the gray plasticine was used to check for systematic scaling errors [6]. The plasticine overburden and underburden were 3 in (76.2 mm). The riser, in all cases, reached a height of 4.75 in (121 mm) above the top of the cavity. To increase the overburden stress on the specimen, the upper surface of the specimen was covered with eight lead sheets that had a combined thickness of 0.25 in (6.35 mm). A layer of teflon was placed between the lead and the plasticine. Thus, the single-cavity and the multi-cavity simulations were equivalent with the exception of the number and placement of the cavities and a slight difference in the fluid head.

The multi-cavity tests were conducted for a nominal three hours and fifteen minutes at 100 g. A graph of g-load versus time is given in Figure 8 for the multi-cavity tests. Based on the pillar sizes of 1 in (25.4 mm), 2 in (50.8 mm) and 3 in (76.2 mm), these tests are designated as ME1, ME2 and ME3, respectively. Figure 9 contains cross-sectional views of the multi-cavity experiments after the tests were completed.

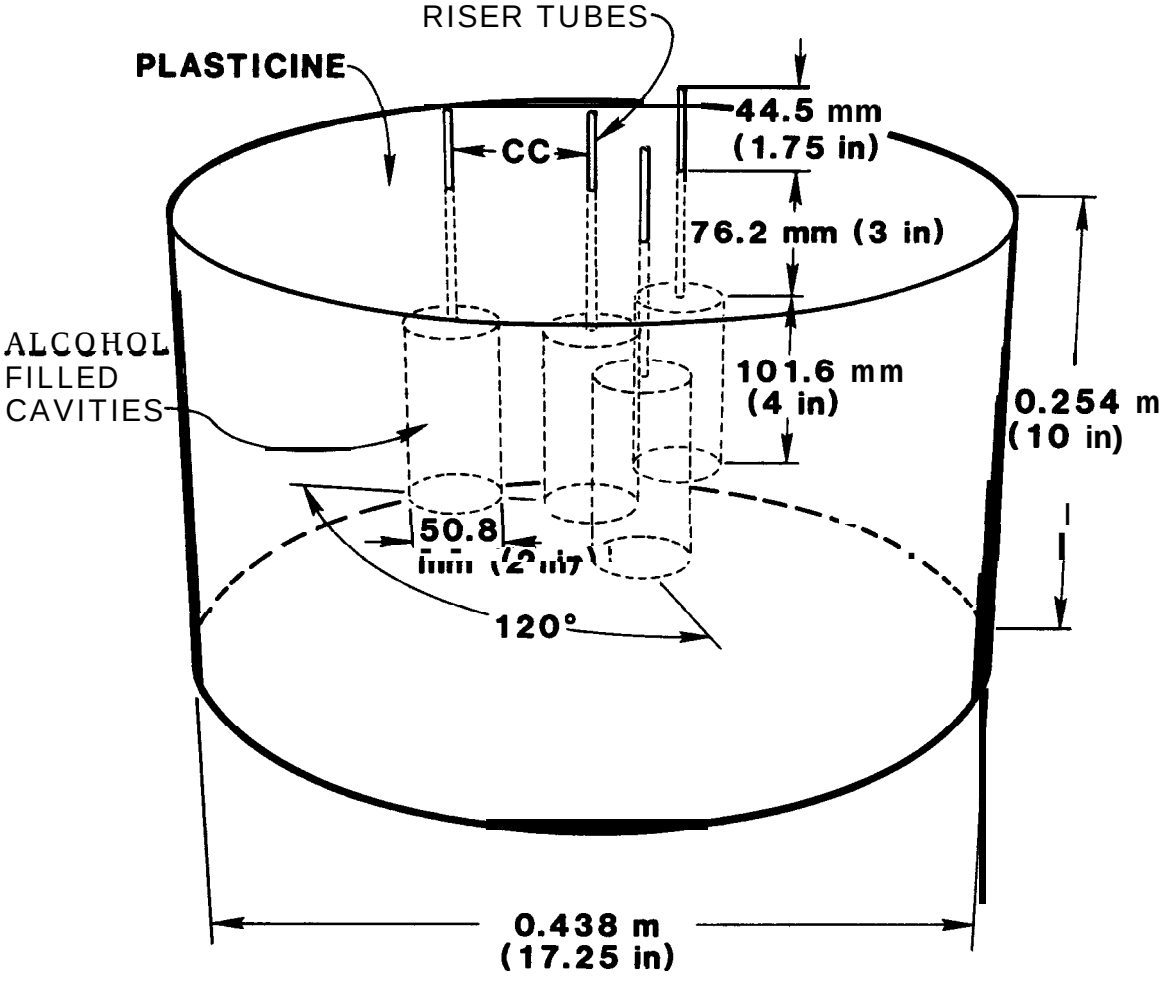

Figure 7: Schematic of Multiple Cavity Centrifuge Experiments.

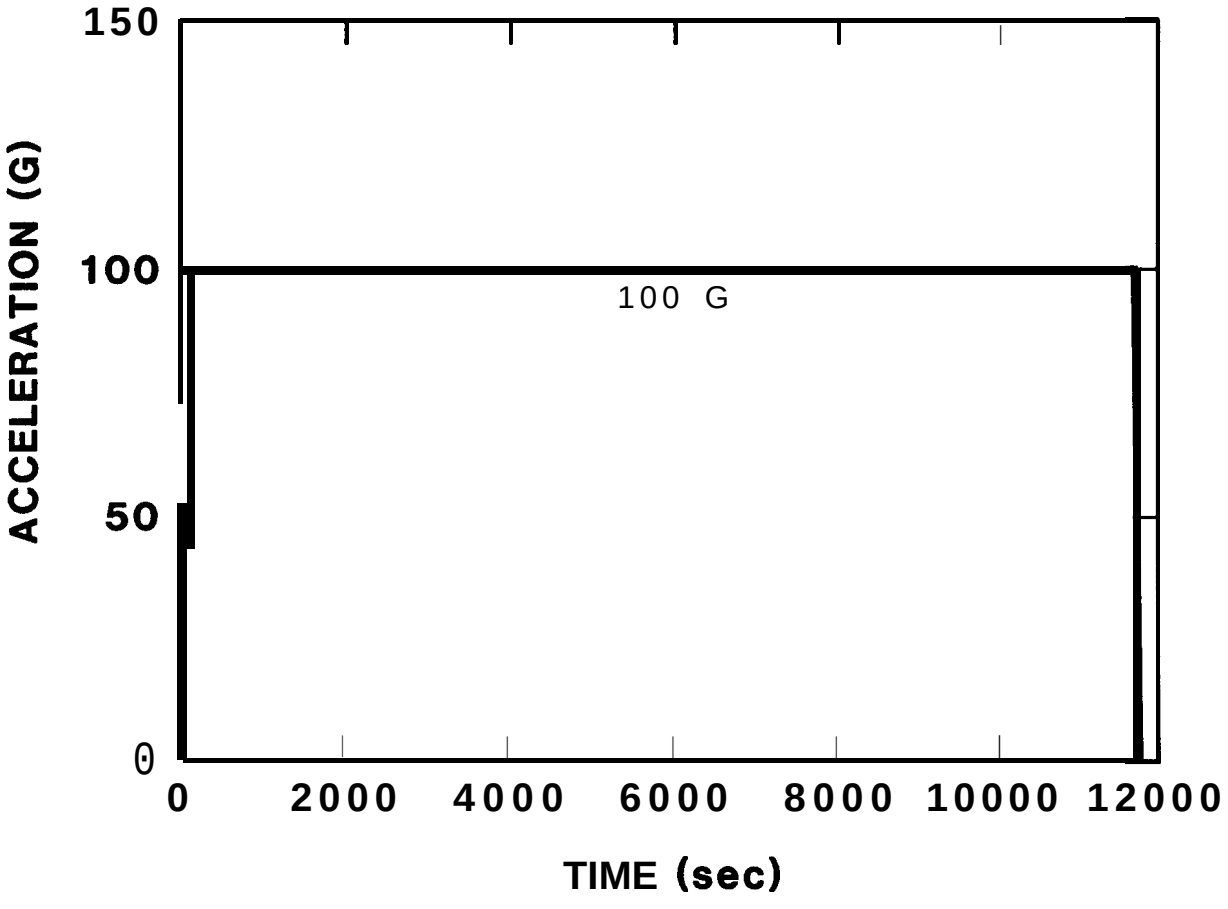

Figure 8: **G Load Versus Time for Multiple Cavity Centrifuge Experiments.**

P:D = 0.5

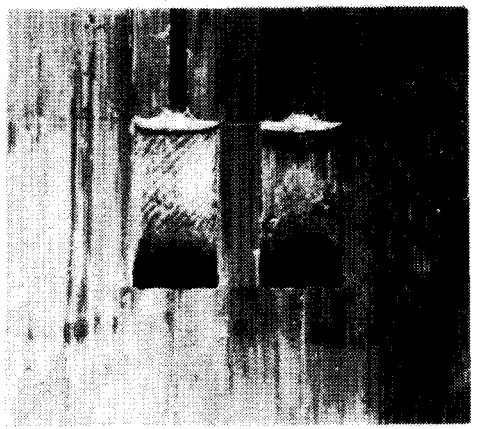

Cavity A Cavity B

P:D = 1.0

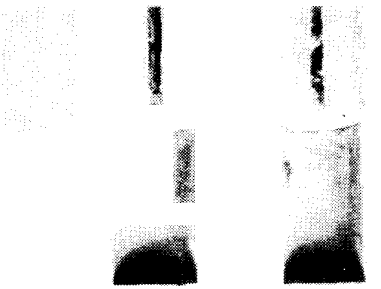

Cavity A Cavity B

P:D = 1.5

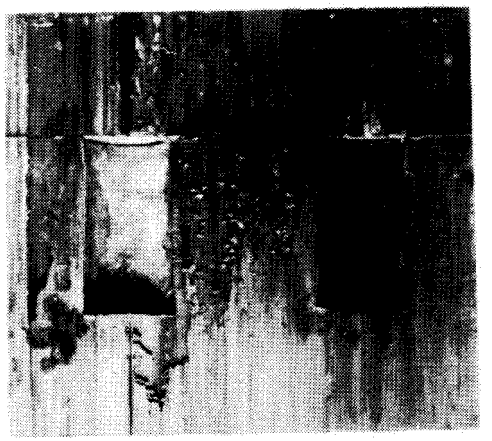

Cavity A Cavity D

Simulation :
3hr 15 min
100 g

Figure 9 Cross-Sectional Views of the Multi-Cavity Experiments

Post Test Analysis

After a simulation was completed, the specimen was stabilized by freezing. Then, the test fixture was removed and the specimen was sectioned in an appropriate manner. For the single-cavity experiments, the specimen was sliced in half along a diameter to form two semi-cylindrical pieces. For the multi-cavity specimens, the specimen was sectioned first along a diameter through two cavities and then along two radii. Each cut was chosen to divide an "outlying" cavity in half.

After sectioning, all of the cut surfaces were photographed for digitizing for computer calculation of final volume. The digitizing process and subsequent calculational techniques are described in detail by Sutherland and Preece [6]. The results of the analysis are summarized in Table II for the single cavity simulations and in Table III for the multi-cavity simulations. In the multi-cavity experiments the central cavity was labeled cavity A and the satellite cavities were labeled B, C and D.

Table II

Final Cavity Volumes for Single Cavity Tests. Test time 2 hours.

g's	Orig. Vol. in^3 (cm^3)	Final Vol. in^3 (cm^3)	Stand. Dev.	%loss
100	12.79 (209.5)	11.54 (189.0)	0.329	9.77
125	13.44 (220.2)	11.48 (188.1)	0.396	14.6
150	13.82 (226.5)	8.19 (134.2)	0.327	40.7

Table III

Final Cavity Volumes for Multi-Cavity Tests
Test time 3 hours, 15 min at 100 g's

P/D	Cavity	Orig. Vol. in^3 (cm^3)	Final Vol. in^3 (cm^3)	Stand. Dev.	% loss
	(cm^3)				
0.5	A	12.61 (206.7)	11.18 (183.1)	0.242	11.3
"	B	12.51 (205.0)	11.08 (181.6)	0.177	11.4
"	C	12.64 (207.1)	11.44 (187.5)	0.190	9.5
"	D	12.64 (207.1)	11.42 (187.1)	0.492	9.6
1.0	A	12.43 (203.7)	11.80 (192.3)	0.064	5.1
"	B	12.37 (202.6)	11.53 (189.0)	0.268	6.8
"	C	12.51 (205.1)	11.69 (191.6)	0.233	6.5
"	D	12.49 (204.6)	11.85 (194.2)	0.064	5.1
1.5	A	12.67 (207.7)	10.12 (165.8)	0.260	20.1
"	B	12.79 (209.7)	8.21 (134.6)	0.623	35.8
"	C	12.88 (210.9)	11.06 (181.3)	0.375	14.1
"	D	12.87 (210.9)	11.06 (181.3)	0.400	14.1

Note: The 0.5 and 1.5 P/D models were made from green plasticine and the 1.0 P/D model was made from gray plasticine.

FINITE ELEMENT COMPUTER PROGRAMS

Two finite element computer programs were used to analyze the centrifuge experiments. The finite element simulations served two purposes. First, the computer simulations aided in understanding the experimental results by providing calculated stress, strain and displacement fields that could not be directly measured. Second, comparison of calculated and measured final cavity volumes serves as a validation technique for the finite element programs. The two finite element programs used in this study were JAC [8] and JAC3D. JAC is a two-dimensional finite element program developed for quasi-static analysis of non-linear solids. It employs the conjugate gradient iterative technique to obtain a solution. Spatial integration is performed using a single gauss point in each four node quadrilateral element. An hourglass viscosity technique is used to control the zero energy modes that occur with single point integration. The single point integration combined with the explicit nature of the program and extensive vectorization makes JAC execute very quickly on a CRAY-1 computer. JAC3D was derived from JAC to treat three-dimensional finite element models and has many of the same characteristics including single point integration, hourglass viscosity and vectorization. These characteristics have made three-dimensional creep analyses more reasonable to do by significantly reducing the computation time.

Creep Model Integration Accuracy

The stress exponent in the secondary creep model (Equation 1) for plasticine was found to vary from 10.1 to 24.7 (see Table I). Many calculations have been made using the secondary creep model with the stress exponent for rock salt of approximately 5 [9]. A factor in the choice of green and gray plasticine for these experiments was the lower stress exponents. They are probably more accurate in the numerical calculations and make these two materials behave more like salt. A single element calculation was made to check the accuracy of integration of the green plasticine creep model. The green plasticine creep model was input in a plane strain single element calculation with all the parameters the same as

for a normal calculation except that Poisson's ratio was set to zero. This value of Poisson's ratio causes the calculated strain rate to match the strain rate in Equation (1) if there is no numerical error. The boundary condition for stress was set at 10 psi (68.95 kPa) which, as discussed later, corresponds to the approximate average effective stress the model experiences in the secondary creep stress state. Under the above conditions the single finite element calculation gave a strain rate of 1.485E-7/sec and Equation (1) gives 1.498E-7/sec which is a difference of 0.87 percent. This indicates that the numerical integration error of the creep model with the 10.1 stress exponent is acceptable.

VOLUME CALCULATION ALGORITHMS

Storage cavities in a creeping material such as rock salt experience gradual volume losses due to creep closure. In a typical petroleum storage cavern an easily measured quantity is pressure rise at the wellhead which is directly related to volume change due to creep closure. (It is also related to fluid thermal expansion and solutioning whose contribution to pressure build-up can generally be separated from that of creep closure). In the centrifuge experiments, volume change was chosen as the basic measured quantity since it could be determined after the test was completed and could be compared with actual petroleum storage caverns in the field through scaling laws. In order to compare finite element calculations with centrifuge experiments, methods were developed to convert nodal displacements on the cavity boundary at each time step to a cavity volume. The cavity volume typically decreases between time steps due to creep closure.

Nodal Loop Method for Calculating Cavity Volumes

Two-dimensional axisymmetric finite element creep calculations lend themselves well to nodal loop methods for volume calculation using the theorems of Pappus-Guldinus [10]. The nodal loop method is briefly documented in Reference [11] and has been used previously for finite element cavity volume change calculations [2, 12, 13]. A discussion of the nodal loop method is included here for completeness. A deformed two-dimensional axisymmetric finite element model is shown in Figure 10. The deformed volume of the cylindrical cavity can be calculated using the area and centroid of the region enclosed by the loop of nodes on the cavity boundary.

$$V = 2\pi \bar{X} A \qquad (2)$$

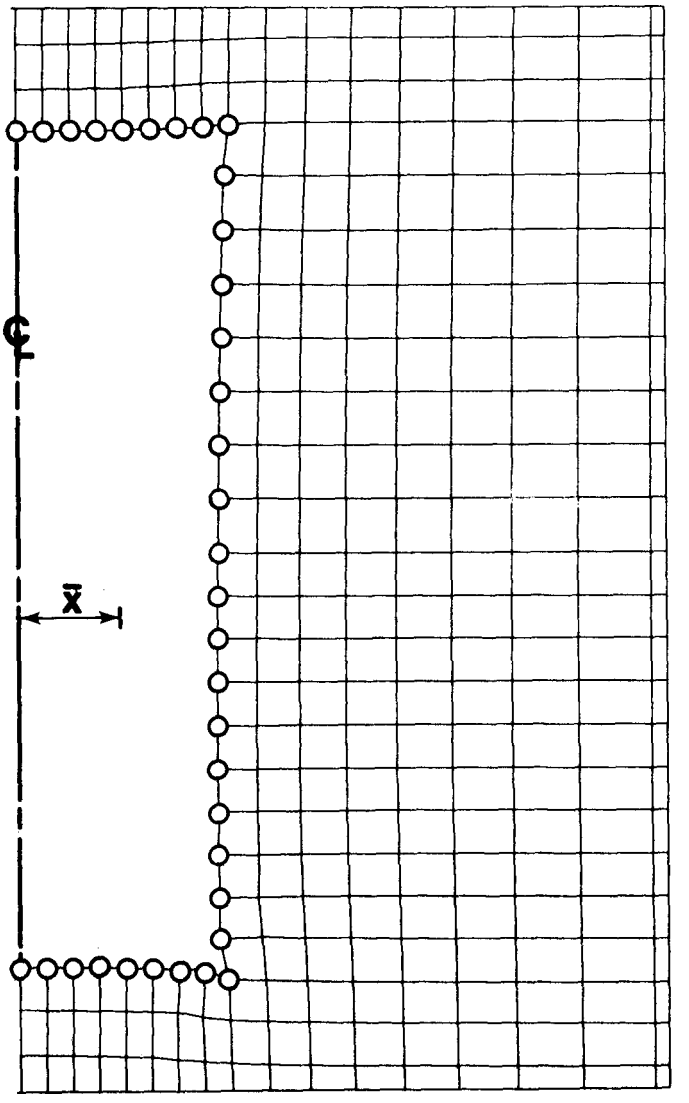

Figure 10: Nodal Loop Method for Calculating Cavity Volume Change.

The area and centroid of the region enclosed by the nodal points are calculated from the following equations

$$A = \sum_{i=0}^{n} (Z_{i+1} - Z_i)(R_{i+1} + R_i)/2 \qquad (3)$$

$$\bar{X} = -\frac{1}{\bar{A}} \sum_{i=0}^{n} \left[\frac{1}{8}(Z_{i+1} - Z_i)\right]\left[(R_{i+1} + R_i)^2 + \frac{1}{3}(R_{i+1} - R_i)^2\right] \qquad (4)$$

Where R and Z are calculated by adding the nodal displacements to the undeformed coordinates. Appendix A contains a listing of the FORTRAN source code for VOLCAV.FOR. This program reads a list of user supplied node numbers (nodal loop) to define the boundary of the cavity. It also reads the post finite element plotting database from JAC and uses the displacements at each time step to calculate the cavity volume. It performs a linear regression in two variables, time and volume, to obtain what is called cavity flowrate or the rate of volume change with time.

Hexahedral Method for Calculating Three-Dimensional Cavity Volumes

Three-dimensional models present new problems for calculating cavity volume. The loop method works well for three-dimensional models when all the deformation is axisymmetric. However, the very nature and reason for three-dimensional analysis suggests that most models analyzed will have asymmetric deformation.

Figure 11 shows a three-dimensional finite element which has one face and four nodes on the cavity surface. These four nodes and their corresponding displacement vectors are used to create a hexahedron. The volume of the hexahedron can be calculated as 1/64 times the Jacobian of the hexahedron [14]. A hexahedral volume is calculated for each face in the

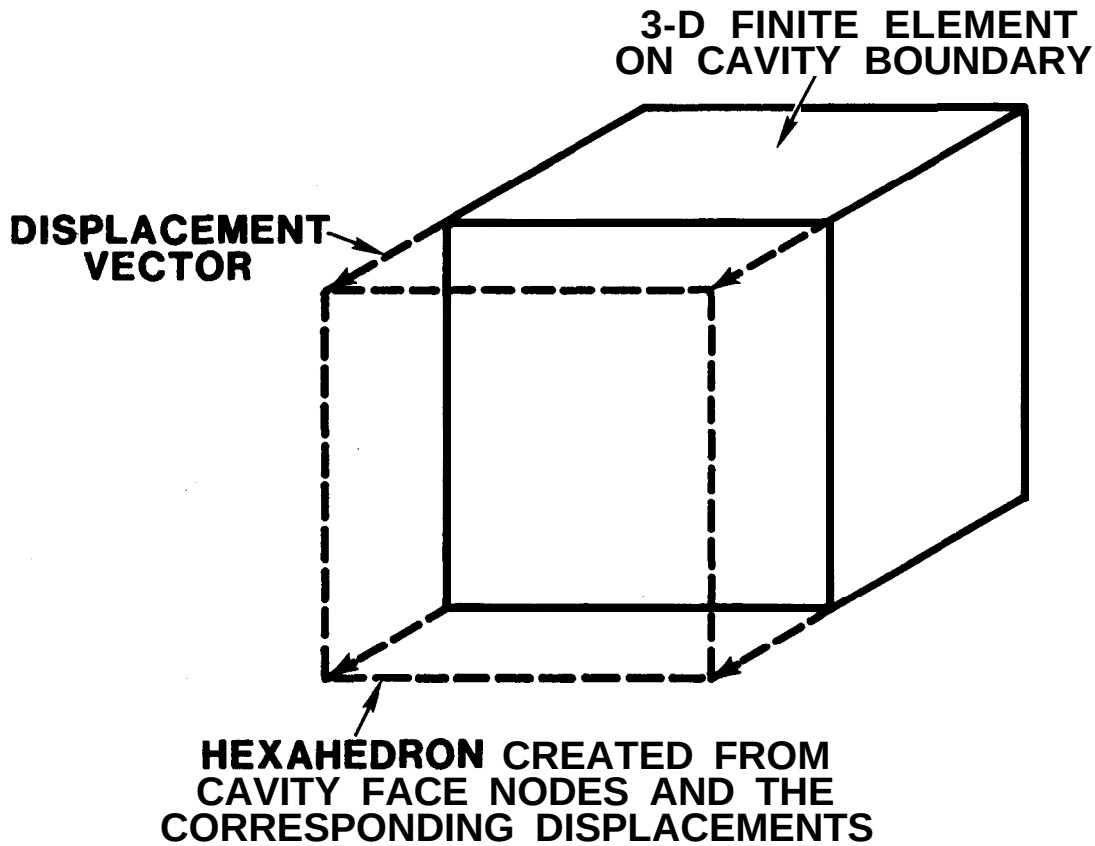

Figure 11: Hexahedron Method for Calculating Cavity Volume Change of 3-D Models.

cavity and summed to obtain the cavity volume loss at each time step. The FORTRAN program VOL3D.FOR was written to implement the algorithm and is given in Appendix B. The program reads the input file for the finite element program and extracts from the cavity pressure data the numbers of the nodes that form the faces of the cavity. It then reads the post finite element plotting database, creates hexahedrons from the surface faces and displacements, calculates the hexahedral volume and sums over the cavity surface to obtain the volume loss at each time step. The cavity volume at each time step is calculated by subtracting the volume loss from the undeformed cylindrical volume.

The hexahedral and nodal loop methods for volume calculation were both utilized on the three-dimensional single cavity finite element model. The analysis of this model will be discussed in the next section but a comparison of volume calculations for the two methods will be presented here. The model, though three-dimensional, has axisymmetric geometry and experiences axisymmetric closure. For the same set of displacements the nodal loop method calculates a volume of 11.2389 in^3 (184.17 cm^3) and the hexahedral method gives a volume of 11.2466 in^3 (184.30 cm^3) which is a difference of 0.068%. The major part of this difference exists because the nodal loop volume is calculated assuming a smooth cylindrical cavity surface while the hexahedral volume depends on a series of flat faces along that smooth cylindrical surface.

SINGLE CAVITY FINITE ELEMENT CALCULATIONS

Finite element calculations of the single cavity centrifuge experiments were performed for several reasons. First, the influence of sources of error in these finite element calculations was studied using the two-dimensional axisymmetric program JAC [8]. The calculations were significantly less expensive using the two-dimensional program. The important error sources are mesh refinement, time step size, convergence tolerance, hourglass viscosity and Poisson's ratio. A balance between error minimization and computational expedience was obtained and the centrifuge experiment was calculated using both JAC and JAC3D and the results of the two were compared. Finally, the finite element results were compared with the centrifuge experimental results.

Baseline Calculation

The influence of sources of error on computational results was determined by comparing all calculations to a baseline calculation. This calculation was performed last in a manner which balanced error minimization and computational efficiency. The baseline calculation was performed using the two-dimensional finite element model of the single cavity centrifuge experiments shown in Figure 12. The boundary conditions of this model consist of displacement constraints represented by rollers on Figure 12 where displacement is allowed parallel to the roller but not perpendicular to it. A surcharge pressure is applied to the top and alcohol fluid pressure is applied inside the cavity with 4.6 inches (116.84 mm) of head above the top of the cavity. Acceleration induced body force loadings are applied and vary with time as shown in Figure 5. The floor and wall of the model are treated as slidelines to prevent them from numerically passing through each other if large deformations occur. This calculation was done with the material properties and parameters shown in Table IV.

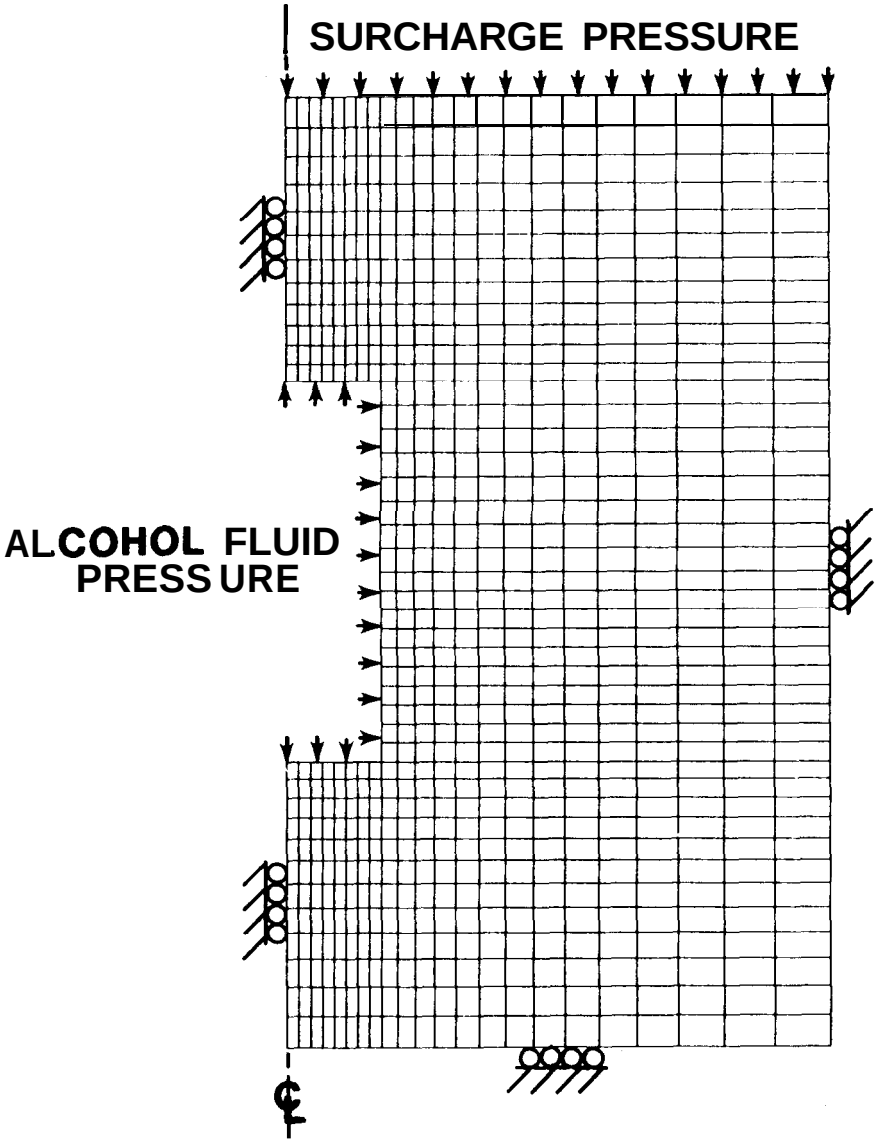

Figure 12: 2-D Axisymmetric Finite Element Model of Single Cavity Experiment For Use With JAC.

Table IV

Material Properties and Computational Parameters

for Baseline Calculation

Elastic Material Properties:

Youngs' Modulus = 800 psi (5516 kPa)

Poisson's Ratio = 0.4998

Creep Material Properties (Equation 1):

A = 1.19 E-17 (units in psi and seconds)

= 3.88 E-26 (units in KPa and seconds)

N = 10.1

Computational Parameters:

Hourglass viscosity = 1.0

Convergence tolerance = 0.01

Time step size = 400 sec.

The influence of the various numerical parameters on the solution was studied by varying one value at a time from the baseline calculation and observing the percent difference from the calculated volume change. When the difference was not significant for a reasonable variation of the parameter no more calculations were made.

Mesh Refinement

The influence of mesh refinement was studied by cutting the size of the elements around the cavity in half as shown in Figure 13. The result was a 0.49% increase in the volume change. This is considered insignificant and the coarser model shown in Figure 12 was used in all subsequent calculations.

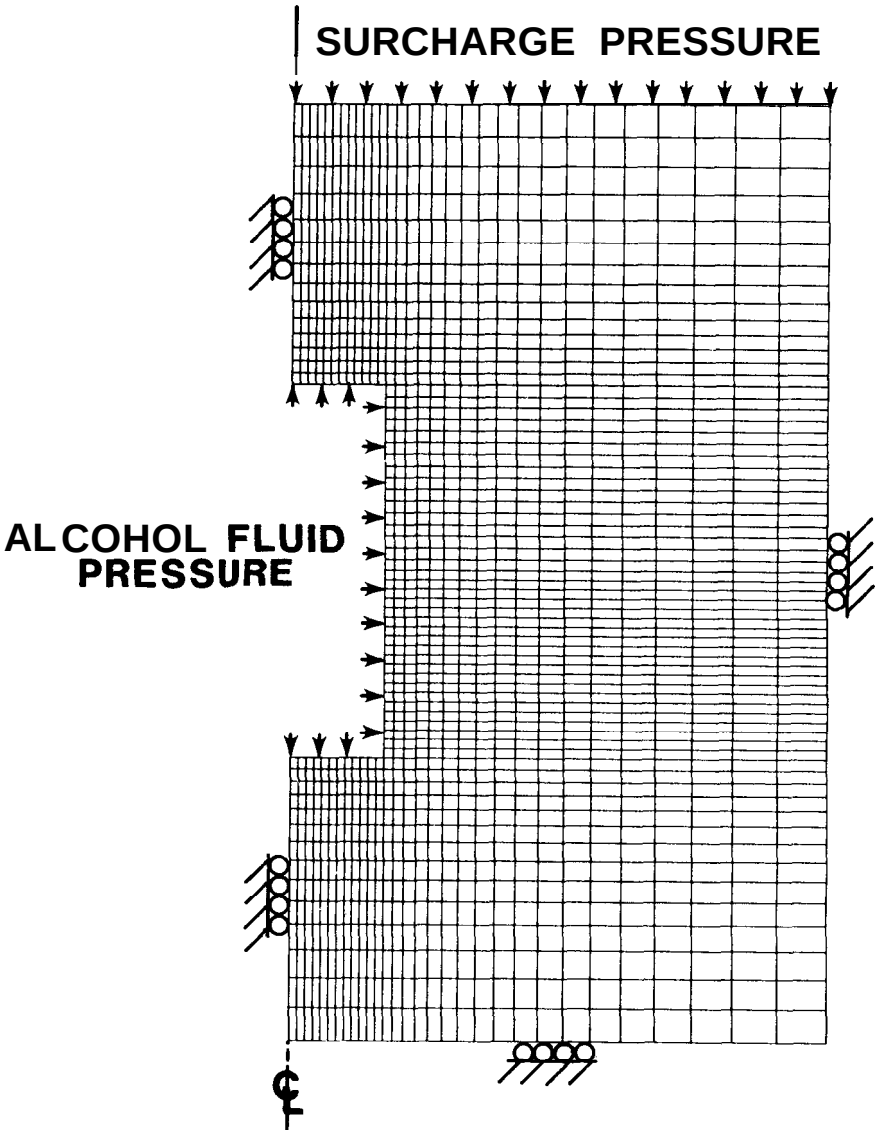

Figure 13: Refined 2-D Axisymmetric Finite Element Model of Single Cavity Experiment Used to Check Mesh Convergence.

Time Step Size

The time step was varied throughout each calculation by making it shorter at the beginning of the analysis when the volumetric closure rate is highest and lengthening it as stress relaxation takes place and the closure rate approaches steady state. The influence of the size of the time step was determined by dividing it in half throughout the entire analysis. The time step at the beginning of the analysis was thus changed from 400 seconds in the baseline calculation to 200 seconds. This change produced a 2.08% difference in the volume change which is considered a tolerable error. The baseline time step sequence was used in subsequent calculations.

Convergence Tolerance

JAC and JAC3D employ an iterative solution scheme and thus require the user to input a convergence tolerance. The convergence tolerance used is usually a compromise between computational accuracy and economy. There are two tolerances required by JAC. One is a displacement norm tolerance which compares the two-norm of the displacement vector at two succeeding iterations. The other, which exercises the most control over the solution, is the residual force norm convergence tolerance which compares the two-norm of the residual force vector at two succeeding iterations [8]. The residual force norm convergence tolerance is usually encountered first. The method used to determine an adequate convergence tolerance consisted of performing the calculation at one tolerance then dividing that tolerance in half and performing the calculation again. If the two results are close to each other then the first is an adequate tolerance. Dividing the baseline residual force norm convergence tolerance by two produced a 0.26% difference in volume change which is considered insignificant. The baseline residual force norm convergence of 0.01 was used with confidence in all other calculations.

Hourglass Viscosity

The hourglass viscosity controls the zero energy modes that are possible with single point integration [8]. The program user can exercise control of the hourglass viscosity with an input parameter. The baseline hourglass viscosity parameter was 1.0. Higher values of the hourglass viscosity parameter will sometimes give less deformation since the elements will be stiffer in resisting hourglass type deformations. A calculation was made with the hourglass viscosity parameter doubled to 2.0. This resulted in a volume change difference from the baseline calculation of 0.13% which is considered insignificant. The baseline hourglass viscosity of 1.0 was used in all other calculations.

Poisson's Ratio

The value of Poisson's ratio used in the calculations was found to have a significant impact on the results. The loads applied to the centrifuge model shown in Figure 12 are the surcharge pressure on top, the body forces due to acceleration loading and the fluid pressure in the cavity. The surcharge pressure and body forces act in a direction parallel to the cavity axis and provide the driving force which causes cavity creep closure. Poisson's ratio controls the portion of these forces that contribute to stresses in the radial direction. Larger radial stresses result in larger deviatoric stresses which directly influence cavity creep closure. Thus, values of Poisson's ratio that are closest to 0.5 result in the most transfer of the axial surcharge and body force loadings to the radial direction producing larger deviatoric stresses and more cavity closure. Another aspect of Poisson's ratio is its' direct influence on bulk and shear modulus whose equations are given below [15].

$$G = \frac{E}{2(1+\nu)} \qquad (5)$$

$$K = \frac{E}{3(1-2v)} \qquad (6)$$

Where

E = Youngs' modulus

G = Shear modulus

K = Bulk modulus

v = Poisson's ratio

As Poisson's ratio approaches 0.5 the shear modulus approaches one-third of Youngs' modulus and the bulk modulus approaches infinity. In the range close to 0.5, small changes in Poisson's ratio can cause order of magnitude changes in bulk modulus. Higher values of bulk and shear modulus result in less elastic cavity closure. It has also been demonstrated that bulk and shear modulus have some influence on cavity creep closure though the reasons for this are not fully understood at this time [16]. In summary it seems that the various influences of Poisson's ratio (radial stress and elastic moduli) interact in a very complex manner that is handled naturally in the finite element formulation. The single point numerical integration with hourglass stiffness will treat incompressible materials without locking. The results of the parametric study of the influence of Poisson's ratio on closure is given in Table V.

Table V

Influence of Poisson's Ratio on Cavity Closure

Poisson's Ratio	ΔV (in^3)	% difference from baseline calculated volume change	
0.4998	.7997	0. 0	(baseline)
0.4997	.7988	-0.113	
0.499	.7828	-2.11	
0.49	7154	10.54	

As can be seen in Table V, the calculated volume change decreases significantly when Poisson's ratio is changed from 0.4997 to 0.49. There is not much change between 0.4998 and 0.4997. As mentioned previously the value obtained from material property tests was 0.4998 which was the value used in all subsequent finite element calculations.

Three-Dimensional Single Cavity Finite Element Model

The three-dimensional finite element model of the single cavity centrifuge experiment is shown in Figure 14. The dimensions of this model exactly match those of the actual experimental model. PATRAN-G [17] is the three-dimensional mesh generator used to create this model which has 6256 nodal points and 5072 three-dimensional elements. The model was created by defining the geometry of the top surface and translating that surface (or portions of it) to generate the remainder of the model geometry. This geometric model was then filled with three-dimensional finite elements. High stress gradients were expected immediately adjacent to the cavity so the mesh was graded from smaller elements around the cavity to larger elements at the outer boundaries. A similarity in the size and distribution of finite elements exists between the two-dimensional finite element model (Figure 12) and the three-dimensional finite element model. The

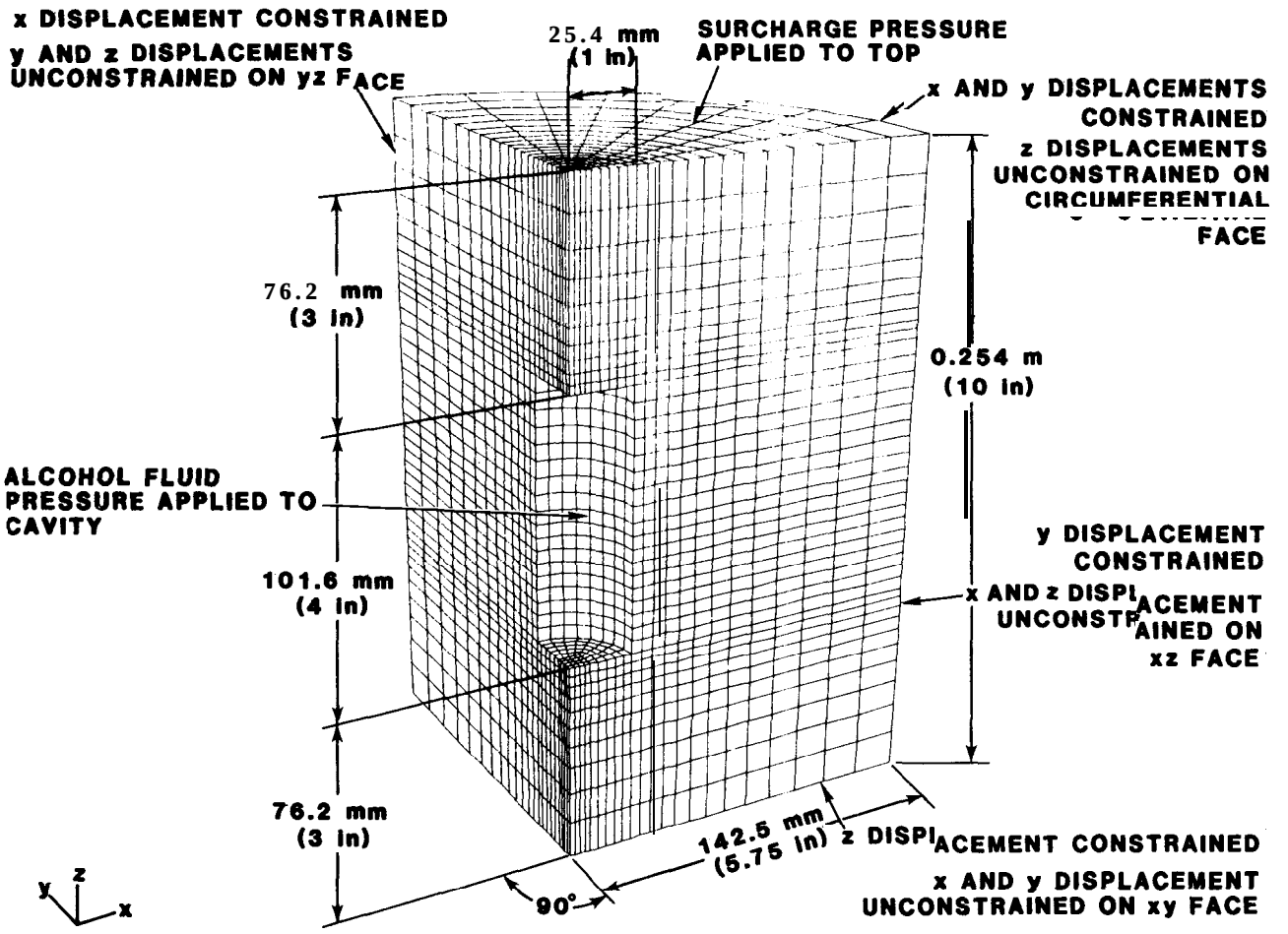

Figure 14: 3-D Finite Element Model of Single Cavity Experiment for Use With JAC3D.

displacement constraints have been set (as shown in Figure 14) to provide symmetry boundary conditions on the XZ and YZ faces of the model. These boundary conditions make the model axisymmetric. The loading is the same as that applied to the two-dimensional finite element model (Figure 12) with a surcharge pressure applied to the top of the model, alcohol fluid pressure with 4.6 in (116.84 mm) of head above the top of the cavity, and acceleration induced body force loadings parallel to the cavity axis that vary with time as shown in Figure 5. The material properties and computational parameters assumed for the three-dimensional calculations were the same as those for the baseline two-dimensional calculations and are given in Table IV.

Comparison of JAC and JAC3D Computational Results

An important part of this study is the benchmarking of JAC3D with JAC on a structural creep problem. JAC was a participant in an extensive benchmark exercise between nine two-dimensional structural creep programs in 1981 [9]. A benchmark between JAC and JAC3D also implies benchmarking with the other nine two-dimensional programs.

Deformed finite element models calculated by JAC and JAC3D at the end of the experiment but before the 100 g gravity load is removed are shown in Figures 15 and 16 respectively. The deformed shapes are almost identical with the two-dimensional model giving a deformed volume of 10.7806 in^3 (176.66 cm^3) compared to 10.7712 in^3 (176.51 cm^3) for the three-dimensional model.

Contour plots of various stress components as calculated by JAC and JAC3D are given in Figures 17 through 22. The contour plots from the JAC calculations were made with the finite element post-processing program DETOUR [18] and the three-dimensional JAC3D contour plots were made with MOVIE.BYU [19] and included hidden line removal. Contour plots of axial stress immediately after the 100 g gravity load is reached and immediately before it is removed are shown in Figures 17 and 18 respectively. Similar contour plots are given for radial stress in Figures 19 and 20 and for Von

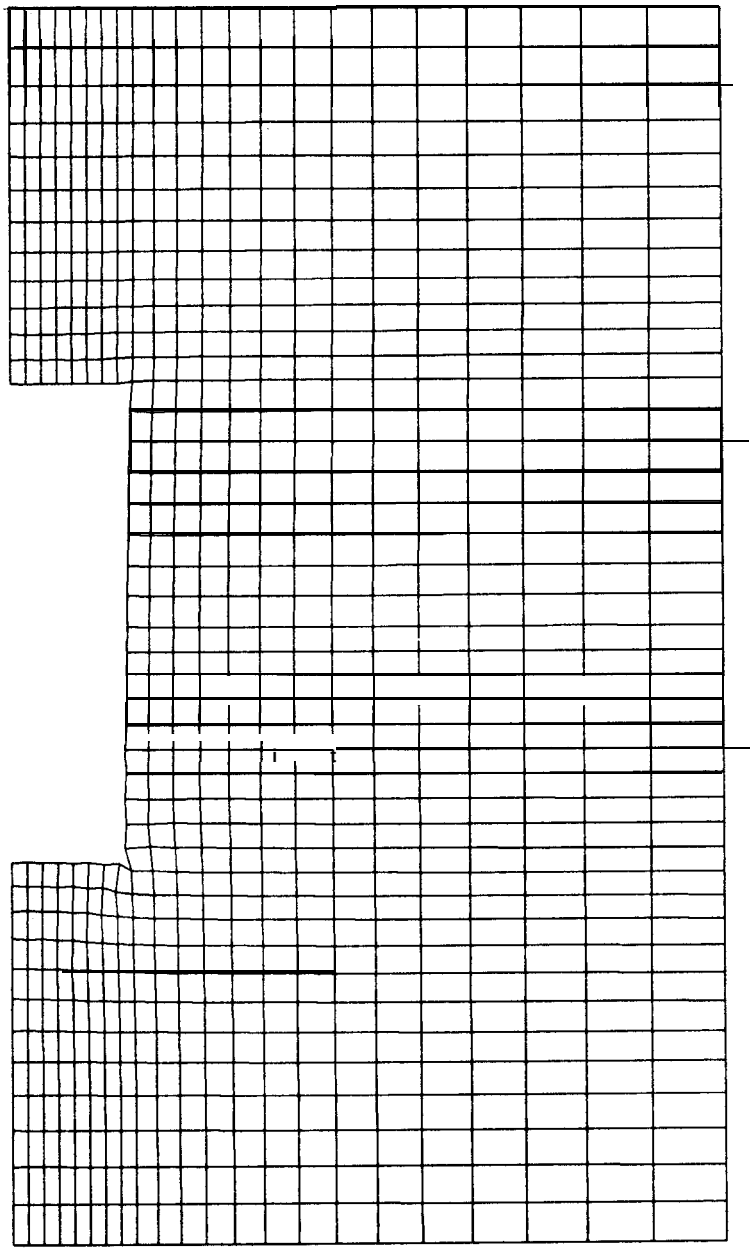

Figure 15: Deformed Finite Element Model of Single Cavity Experiment Immediately Before 100 g Gravity Load is Removed. Calculated by JAC.

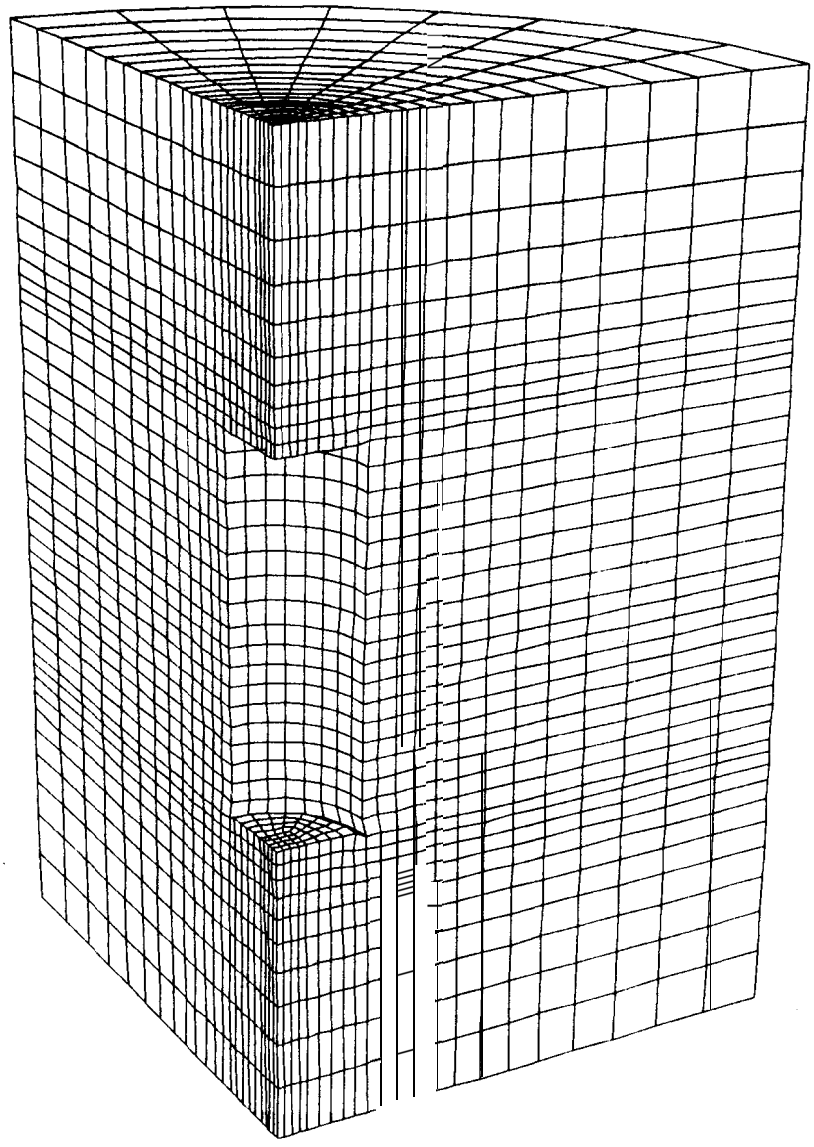

Figure 16: Deformed Finite Element Model of Single Cavity Experiment Immediately Before 100 g Gravity Load is Removed. Calculated by JAC3D.

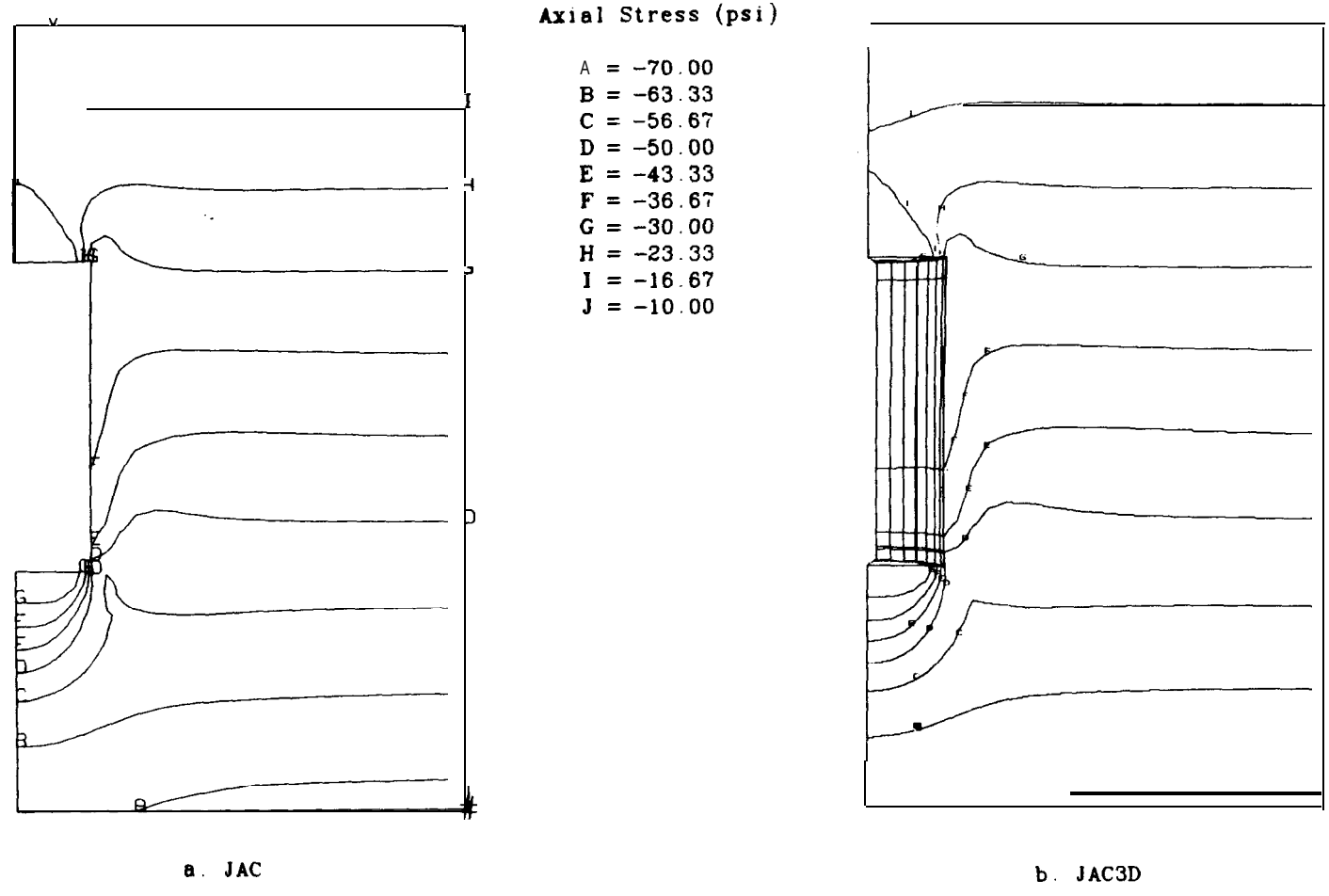

Figure 17: Calculated Axial Stress Immediately After Application of 100 g Gravity Load.

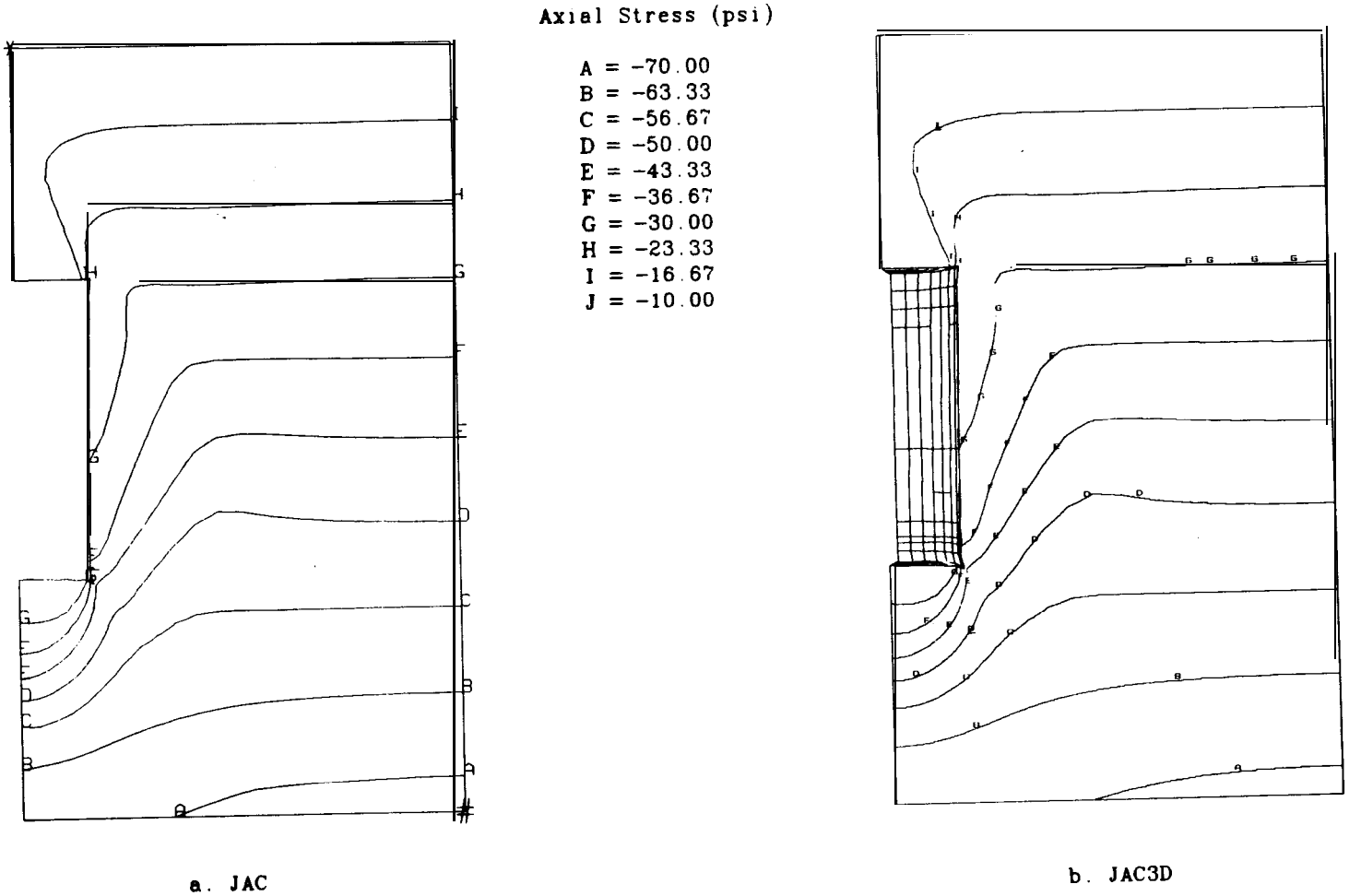

Figure 18: Calculated Axial Stress Immediately Before 100 g Gravity Load is Removed.

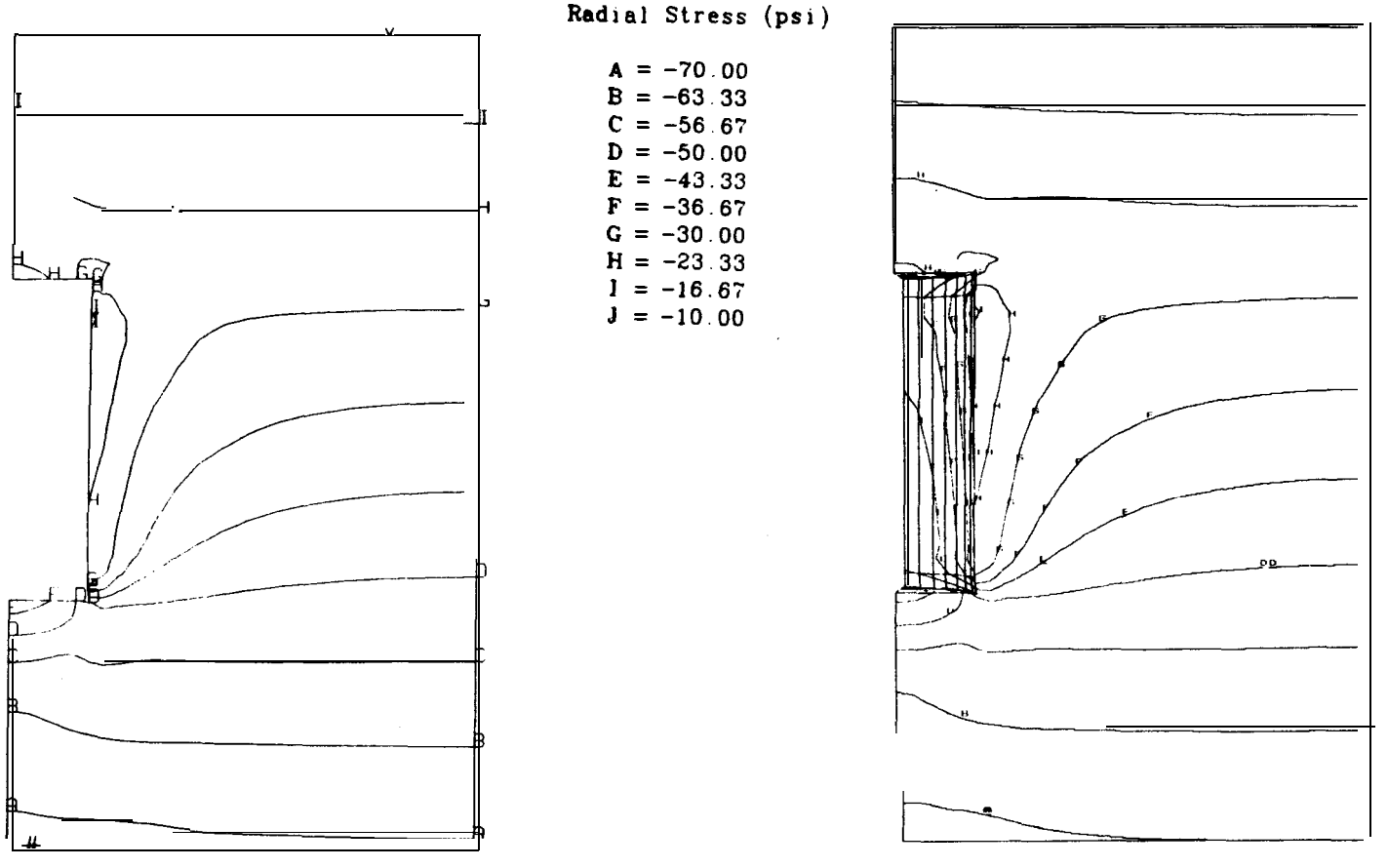

a. JAC

b. JAC3D

Figure 19: Calculated Radial Stress Immediately After Application of 100 g Gravity Load.

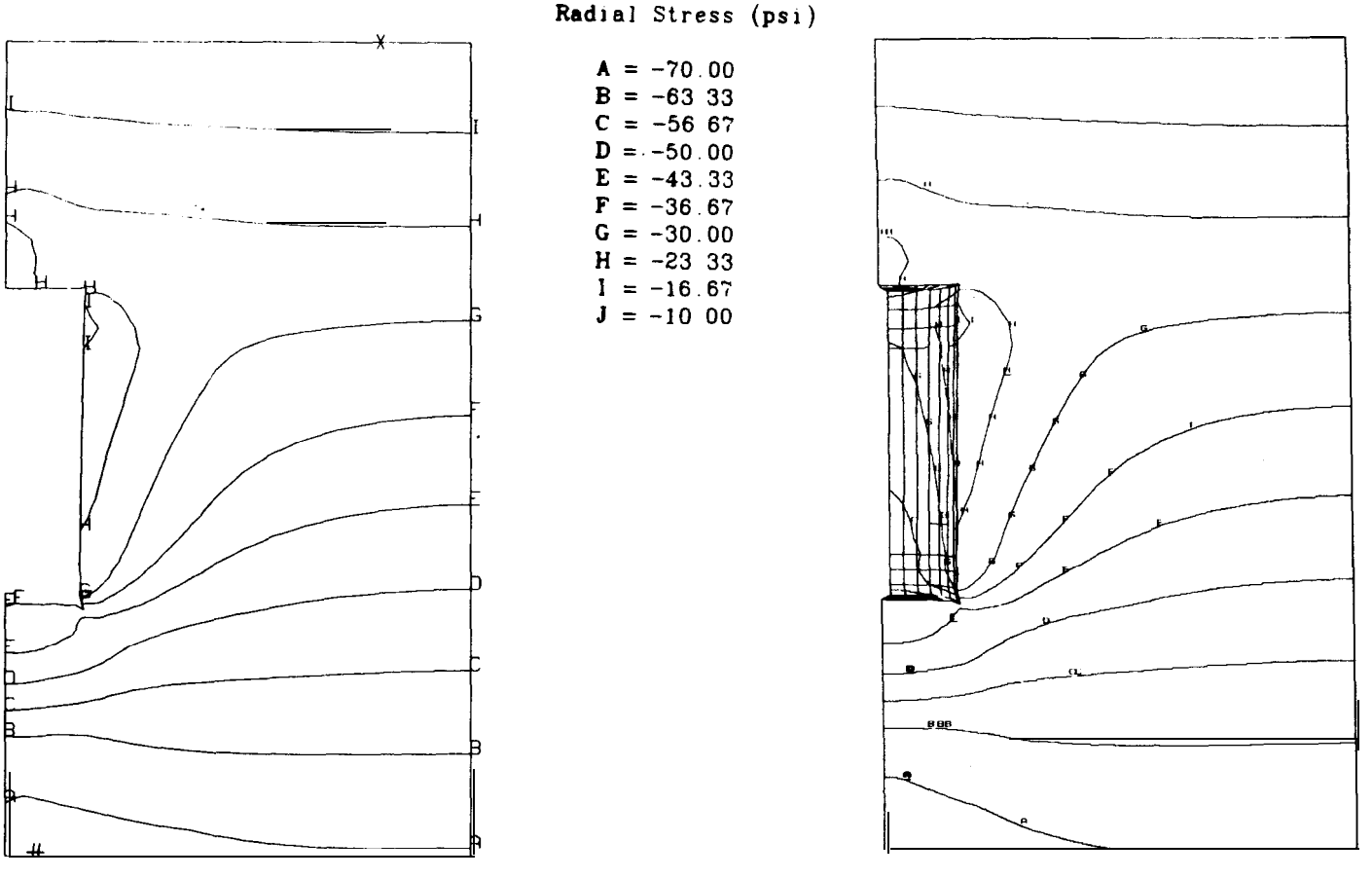

a. JAC

b. JAC3D

Figure 20: Calculated Radial Stress Immediately Before 100 g Gravity Load is Removed.

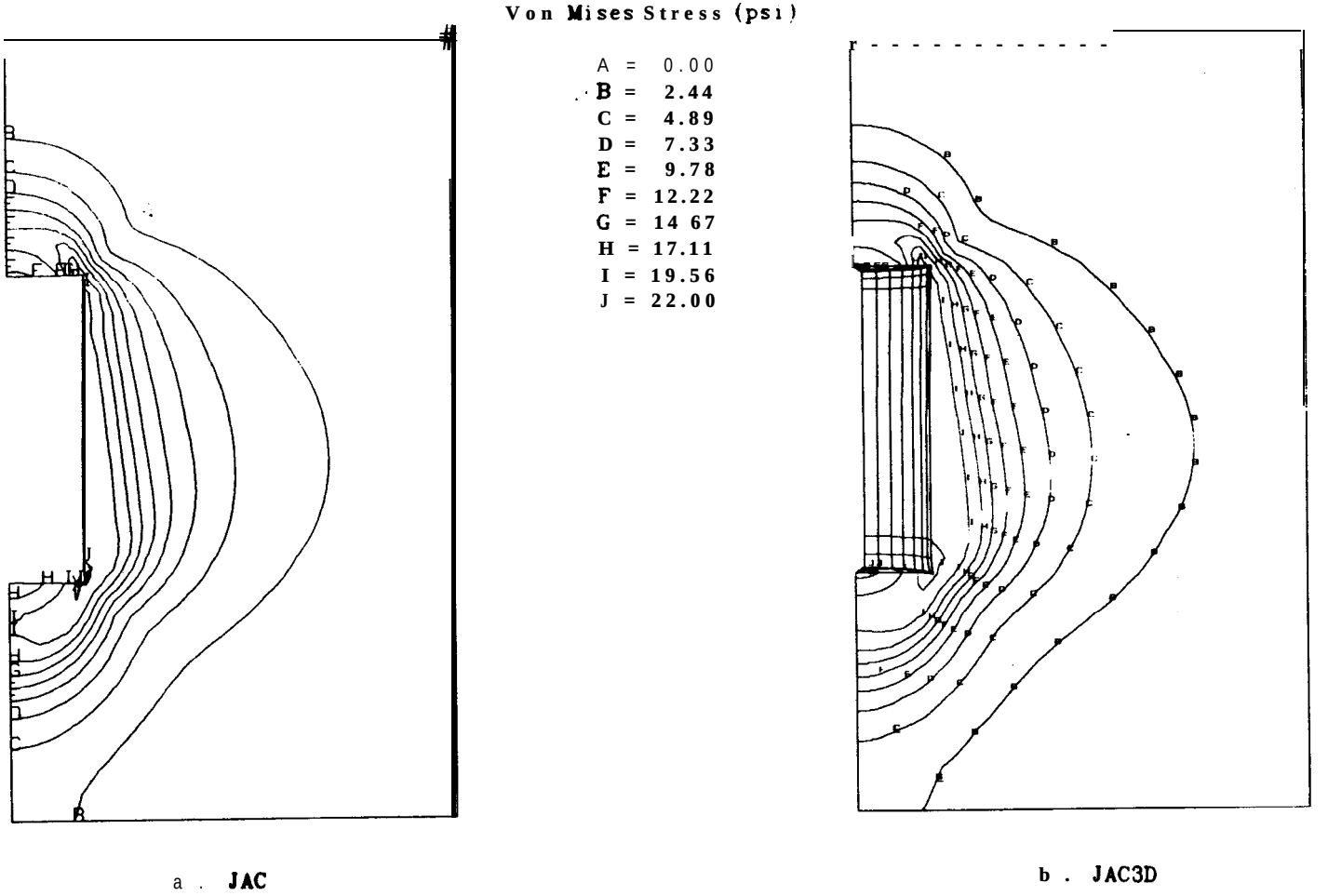

Figure 21: Calculated Von Mises Stress Immediately After Application of 100 g Gravity Load.

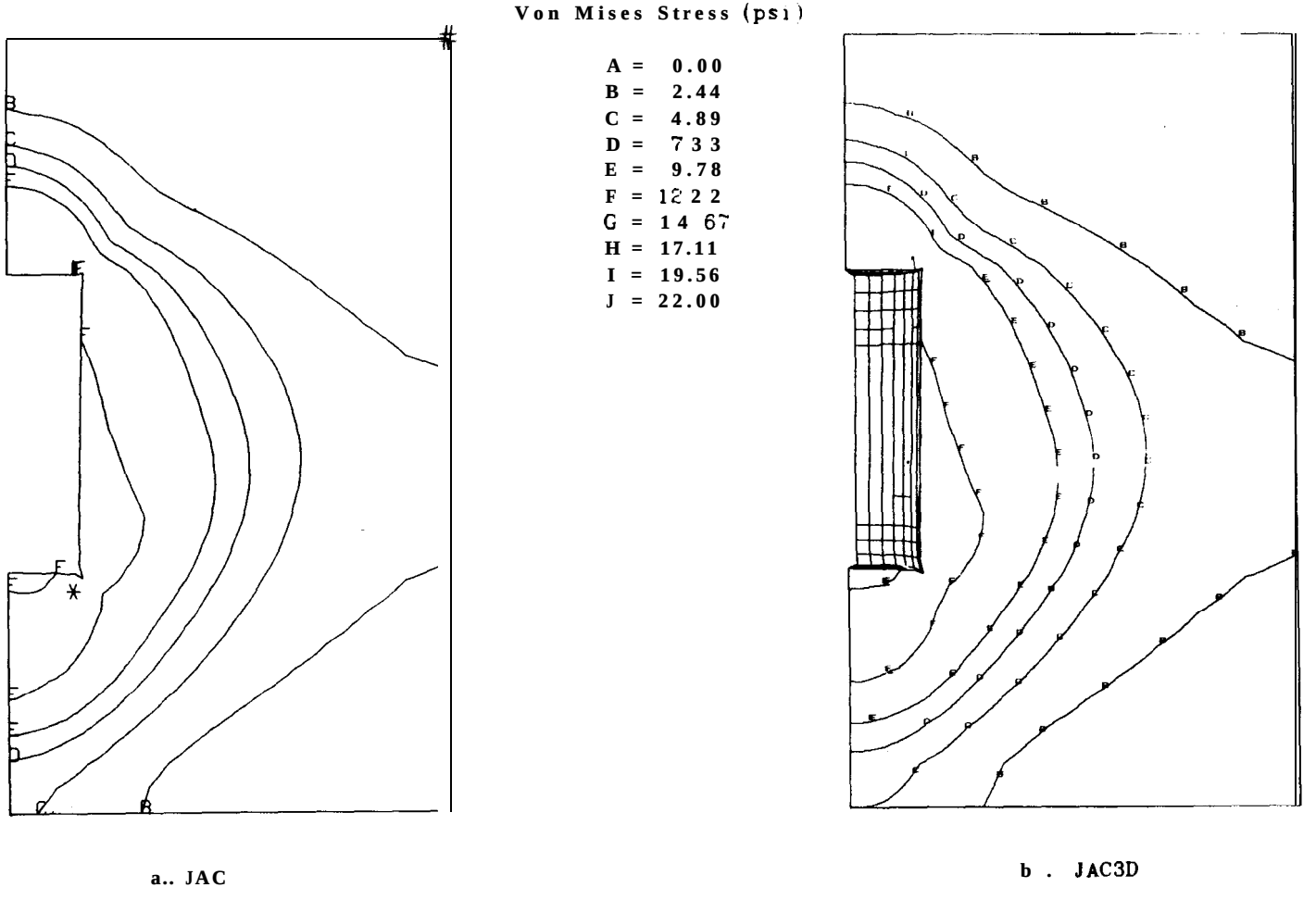

Figure 22: Calculated Von Mises Stress Immediately Before 100 g Gravity Load is Removed.

Mises stress in Figures 21 and 22. Von Mises stress gives the proximity to the yield surface in principal stress space for a Von Mises yield criteria and is also directly proportional to the second invariant of the deviatoric stress tensor [20]. These figures show that the stress distributions calculated by JAC and JAC3D are almost exactly the same. The figures also show that stress relief occurs around the cavity as creep closure takes place since differences can be seen in the stress distributions between initial loading and immediately before unloading. This is most obvious in the contour plots of Von Mises stress which shows the stresses immediately adjacent to the cavity dropping from 19.56 psi (134.86 kPa) to 12.22 psi (84.25 kPa).

Figure 23 shows calculated volume versus time for both JAC and JAC3D. It is interesting to note that the volume curves for JAC and JAC3D deviate very little from each other throughout the calculation. At the start of the experiment when the acceleration loading is being increased from 1 g to 100 g (Figure 5) the cavity experiences a significant volumetric elastic closure due to the relatively low elastic moduli (Table V). Along with this elastic response a small amount of creep closure is also taking place. The initial response is followed by what appears to be primary creep as the volume curves bend around quickly. This portion of the response has been characterized by others [21] as structural primary creep which corresponds to redistribution and relief of stresses. Material primary creep is not a possible result from these calculations since it is not included in the formulation of the creep model given in Equation (1). After approximately 2000 sec the volume curves appear to become linear but they actually continue to gradually change. The volumetric closure rate at the end of the experiment has been calculated as 5.0457E-3 in^3/sec (8.2684E-2 mm^3/sec) from the two-dimensional model and 5.0154E-3 in^3/sec (8.2188E-2 mm^3/sec) from the three-dimensional model. The end of the experiment is marked by an elastic rebound as the acceleration loading is reduced from 100 g to 1 g.

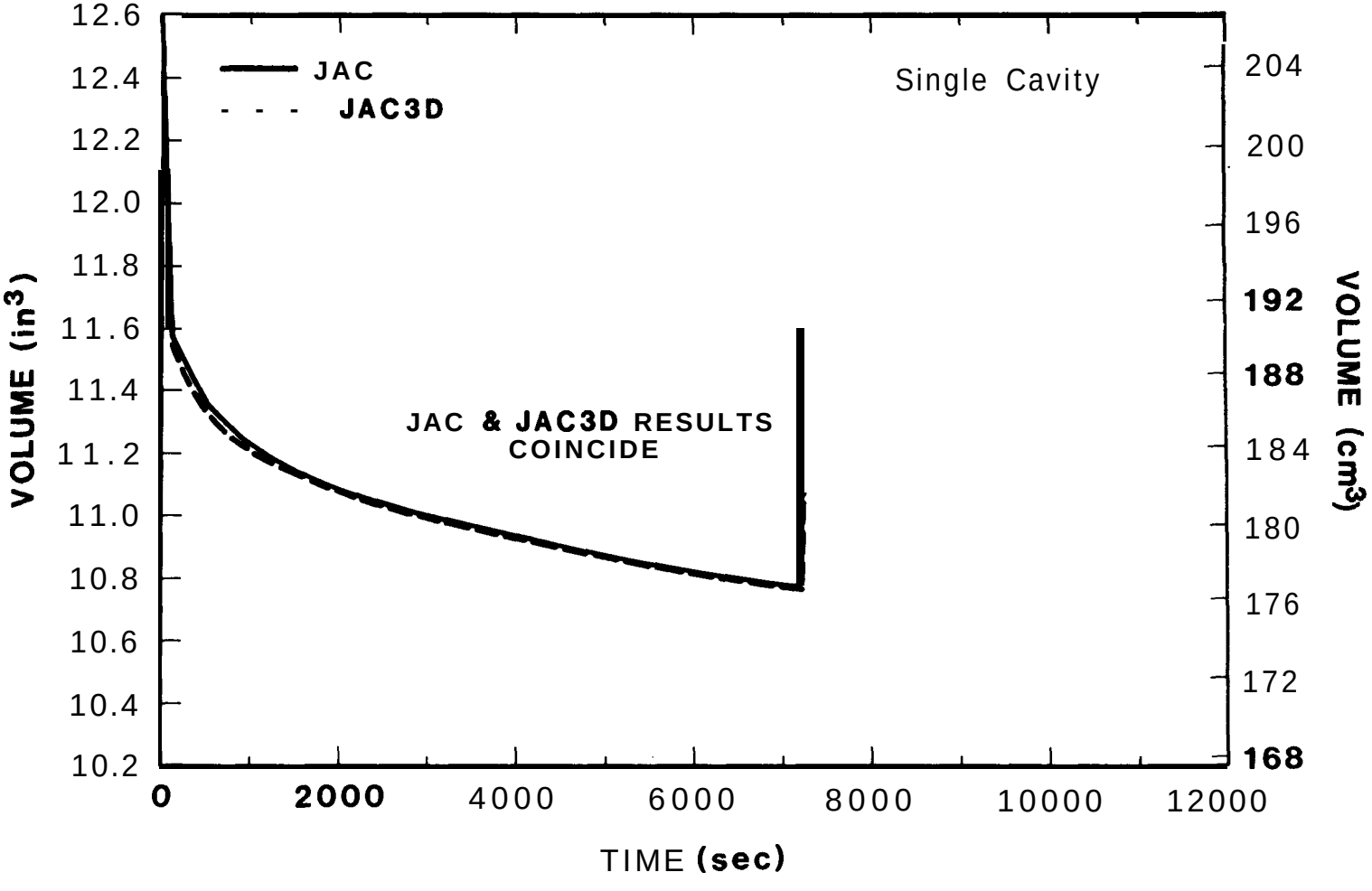

Figure 23: Calculated Volume Versus Time for Single Cavity Experiments.

Comparison of Finite Element Calculations and Centrifuge Experiments

The centrifuge test results in terms of percent volume loss are given in Table II and are plotted against acceleration in Figure 24. Finite element calculated percent volume loss versus acceleration are also plotted against acceleration in Figure 24. There is a good correlation between the finite element calculations and the centrifuge experiments for the 100 g and 125 g experiments but a significant discrepancy at 150 g. As has been mentioned previously it is likely that a leak developed in the riser tube during the 150 g experiment which reduced the fluid head inside the cavity and resulted in a larger volume loss. A finite element calculation was performed assuming the fluid level was at the top of the cavity. This calculation is labeled as "reduced fluid head" in Figure 24 and shows that fluid head loss has a significant impact on the amount of creep closure. The dashed line between the last two points was used to indicate that the final volume was extrapolated from midway through the 150 g reduced head calculation. This was necessary because mesh grading on the cavity wall resulted in a mismatch of master and slave slide lines in the lower corner of the model when large deformations cause slideline contact for a significant distance from the corner.

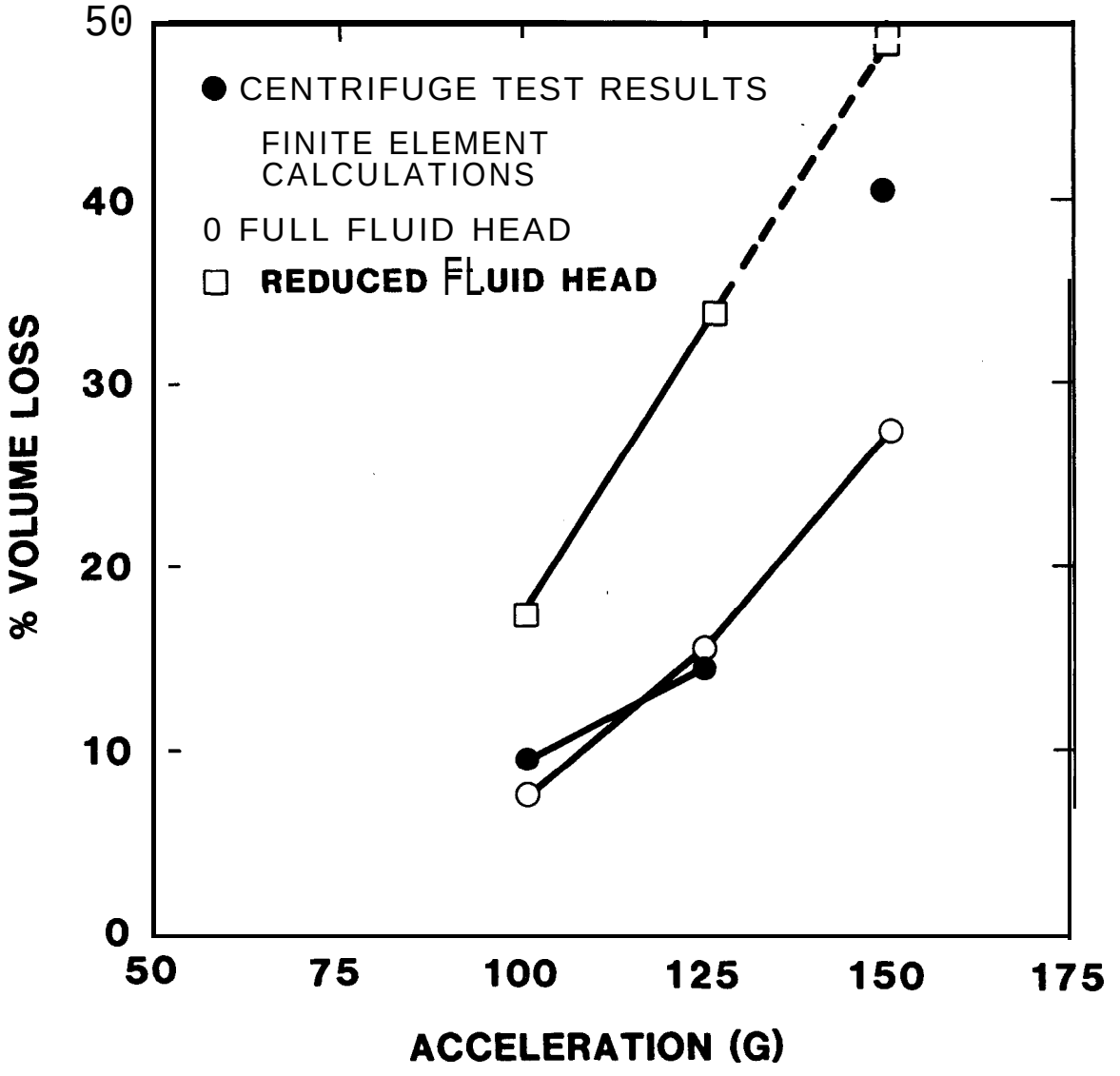

Figure 24: Comparison of Calculated Volume Losses With Centrifuge Test Results.

MULTI-CAVITY FINITE ELEMENT ANALYSES

The multi-cavity centrifuge experiments which have been described previously were performed to gain some understanding of the behavior of arrays of creeping fluid-filled cavities. The geometry of these experiments is shown in Figure 7. Three-dimensional finite element analyses of the experiments were performed to help clarify the centrifuge test results and to calculate quantities that could not be measured during the experiment such as volume versus time and stress distribution.

Three-Dimensional Finite Element Model Generation

A three-dimensional finite element model was generated for each of the three multi-cavity experiments. These experiments treated pillar to diameter ratios (P/D) of 0.5, 1.0, and 1.5 by varying the spacing between the central cavity and the three satellite cavities. The three-dimensional models were generated using PATRAN-G [17]. One of the models, for P/D of 0.5, is shown in Figure 25. The models were generated by defining the basic geometry of the top surface and then translating it (or portions of it) to generate the remainder of the geometrical model. The geometrical model was then filled with three-dimensional finite elements. The mesh was graded from the cavities outward to give smaller elements immediately adjacent to the cavities because of the high stress gradients expected in this area. Each model has symmetry boundary conditions on the vertical surfaces as shown in Figure 25 where displacements are allowed parallel to the face but not perpendicular to it. The symmetry boundary condition for the face that is 60 degrees from the XZ face was made using a sliding surface with a coefficient of friction of zero. The top of the model has a surcharge pressure applied to the top and alcohol fluid pressure inside the cavity with 4.75 inch (120.65 mm) head above the top of the cavity.

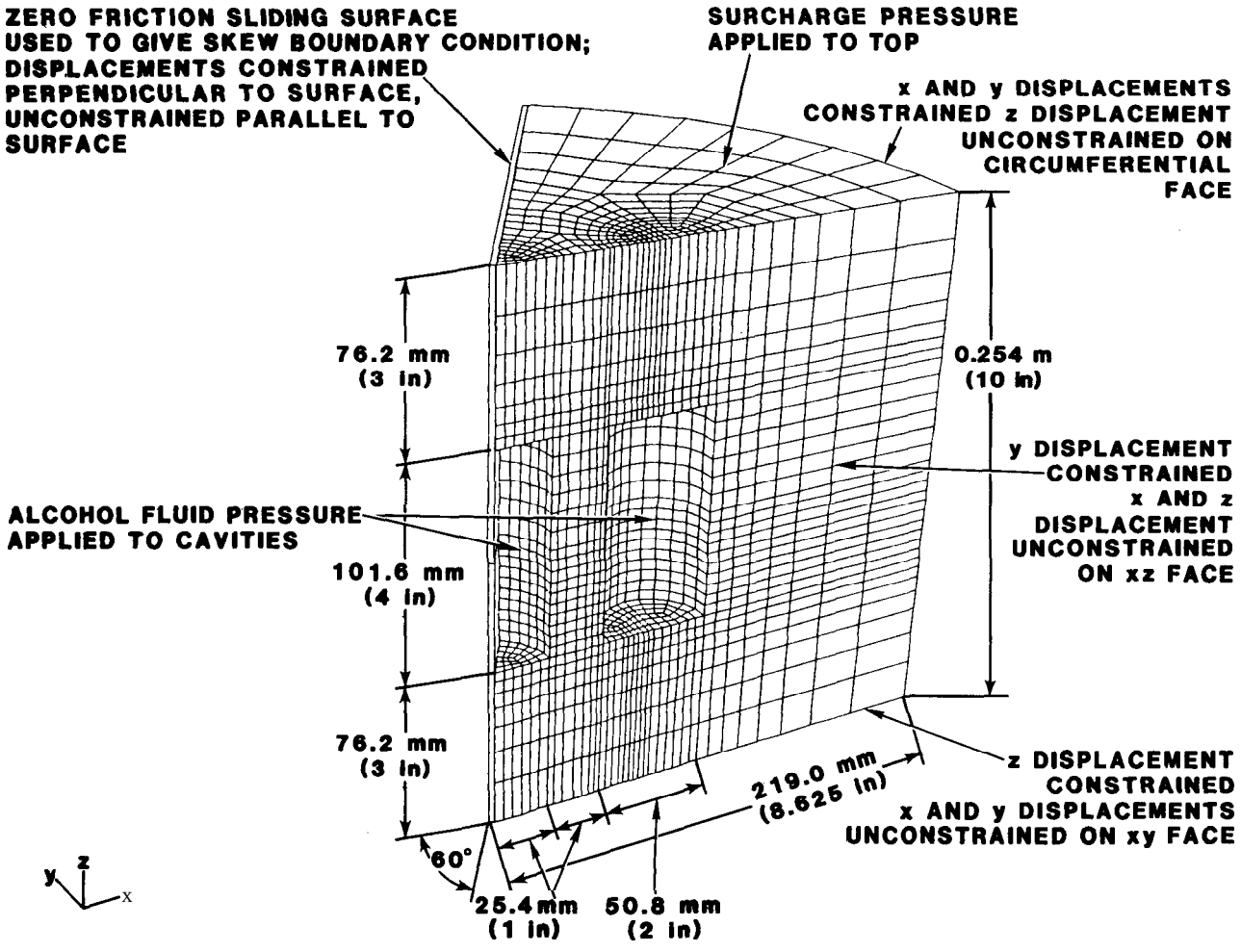

Figure 25: 3-D Finite Element Model of Multiple Cavity Centrifuge Experiment With P/D = 0.5.

Finite Element Analysis of Centrifuge Experiment With P/D = 0.5

Dimensions and boundary conditions for the 0.5 P/D three-dimensional finite element model are shown in Figure 25. The finite element model was made to match the experimental model. Figure 26 shows this same model as it has been mathematically clipped at midheight by the computer program SECTION [22] and displayed by MOVIE.BYU [19]. Clipping the model allows observation of the finite element grid immediately adjacent to the cavities. This model was made with 6662 nodal points and 5347 three-dimensional finite elements. The analysis was performed using JAC3D.

Figure 27 shows the calculated displacements at the end of the centrifuge experiment but before the 100 g gravity load has been removed. The pillar (this is not a pillar in the classical mining sense but is referred to as such) between the cavities deforms more at the bottom since this is where the largest difference exists between the geostatic stress and the alcohol fluid pressure. Close observation also shows that the deformation of both cavities is not symmetric but that there is more deformation on the side of the cavity immediately adjacent to another cavity. Asymmetric deformation was the reason the deformed volumes of these cavities were calculated using the hexahedron method rather than the loop method both of which were described earlier in this report.

Calculated volume versus time is shown in Figure 28. Similar behavior to that of the single cavity experiments is observed where the closure rate is greater during the early portion of the experiment and decreases as the test progresses. Figure 28 also shows that the central cavity closes more than the outer cavity, both elastically and through creep. Larger central cavity closure can be explained by examining the stress distribution around the cavities, which is done in detail below. Final percent volume loss for the 0.5 P/D experiment is given in Table VI and again shows the central cavity closing more than the outer cavity. Contour plots of axial stress immediately after loading and immediately before unloading are given in Figures 29 and 30 respectively. These figures show some relief and redistribution of axial stress as evidenced by the downward movement of the "C", "D" and "E" contours. It is also interesting to note that the axial

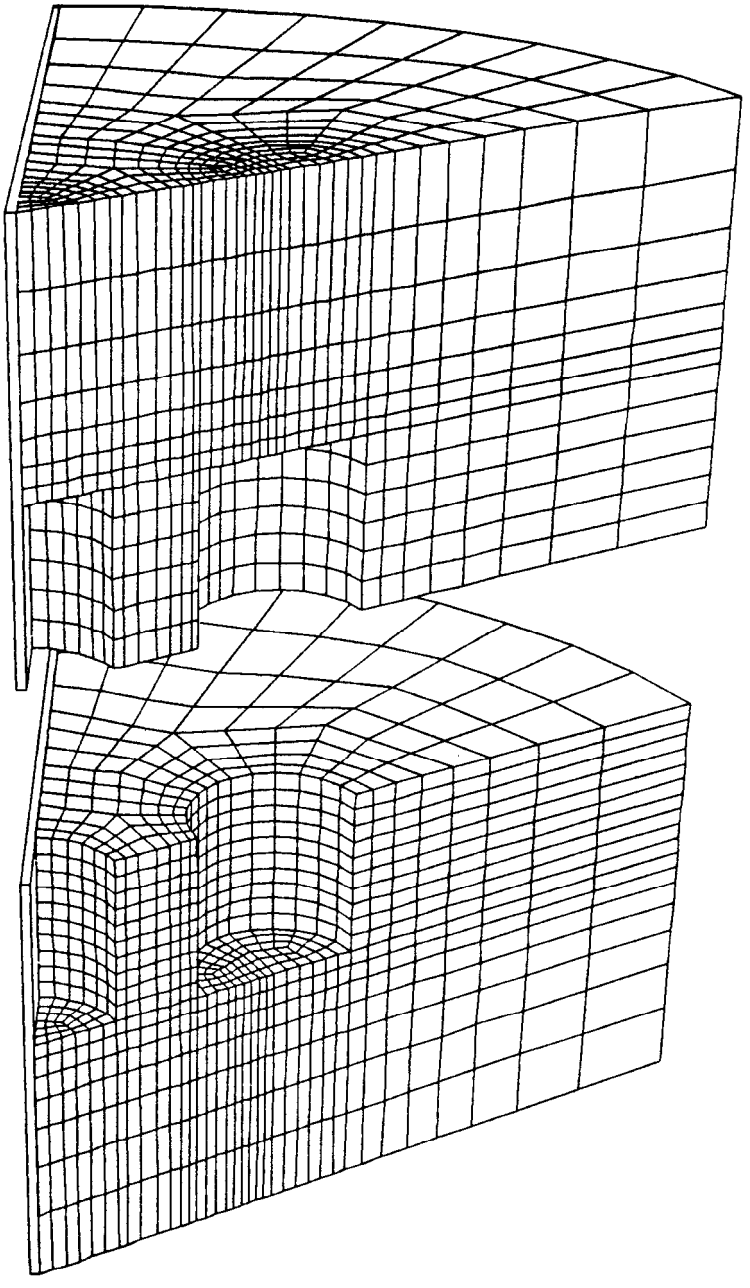

Figure 26: Sectioned 3-D Finite Element Model of Multiple Cavity Centrifuge Experiment With P/D = 0.5.

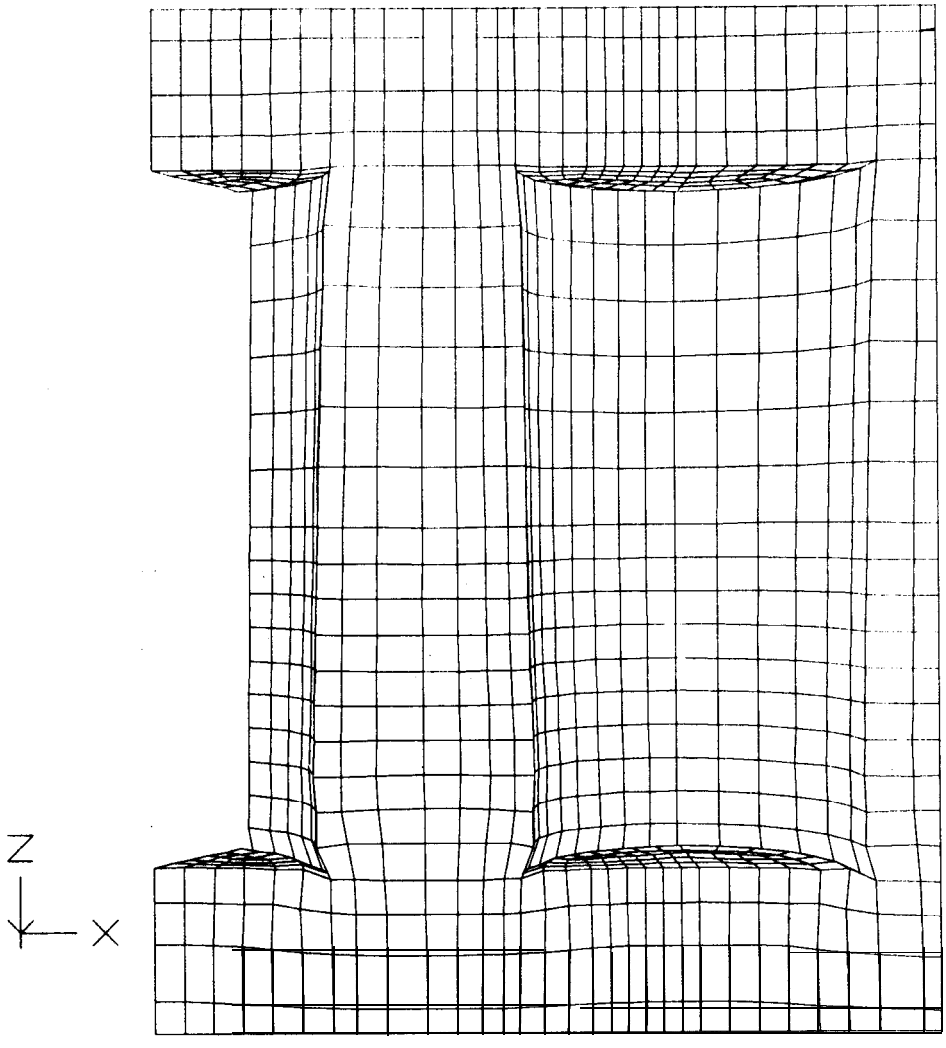

Figure 27: Deformed 3-D Finite Element Model of Multiple Cavity Centrifuge Experiment Immediately Before 100 g Gravity Load is Removed P/D = 0.5.

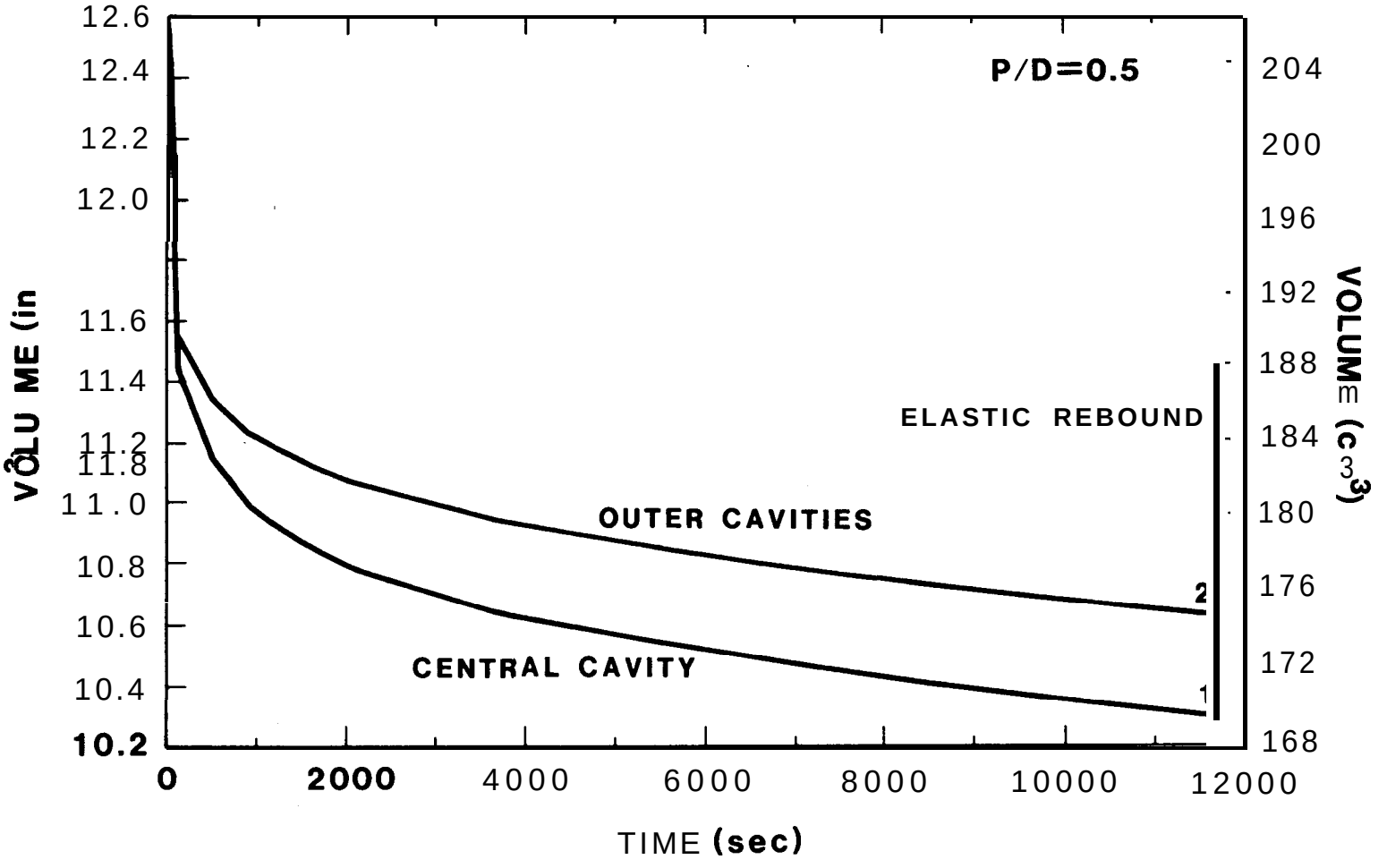

Figure 28: **Calculated Volume Versus Time for** Inner **and Outer Cavities. P/D = 0.5.**

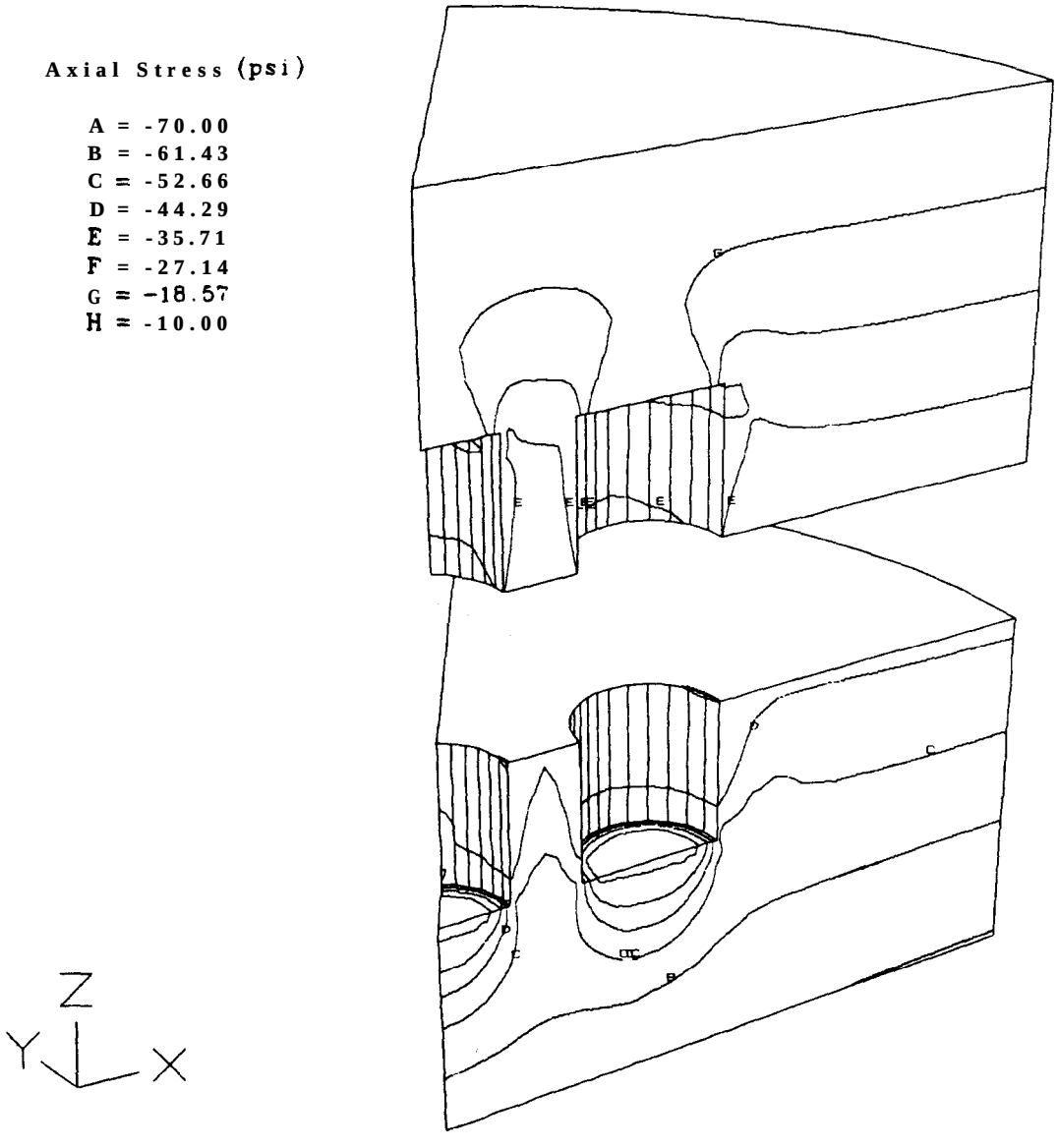

Figure 29: **Calculated Axial Stress Immediately After 100 g Gravity Load is Reached. P/D = 0.5, Sectioned Model.**

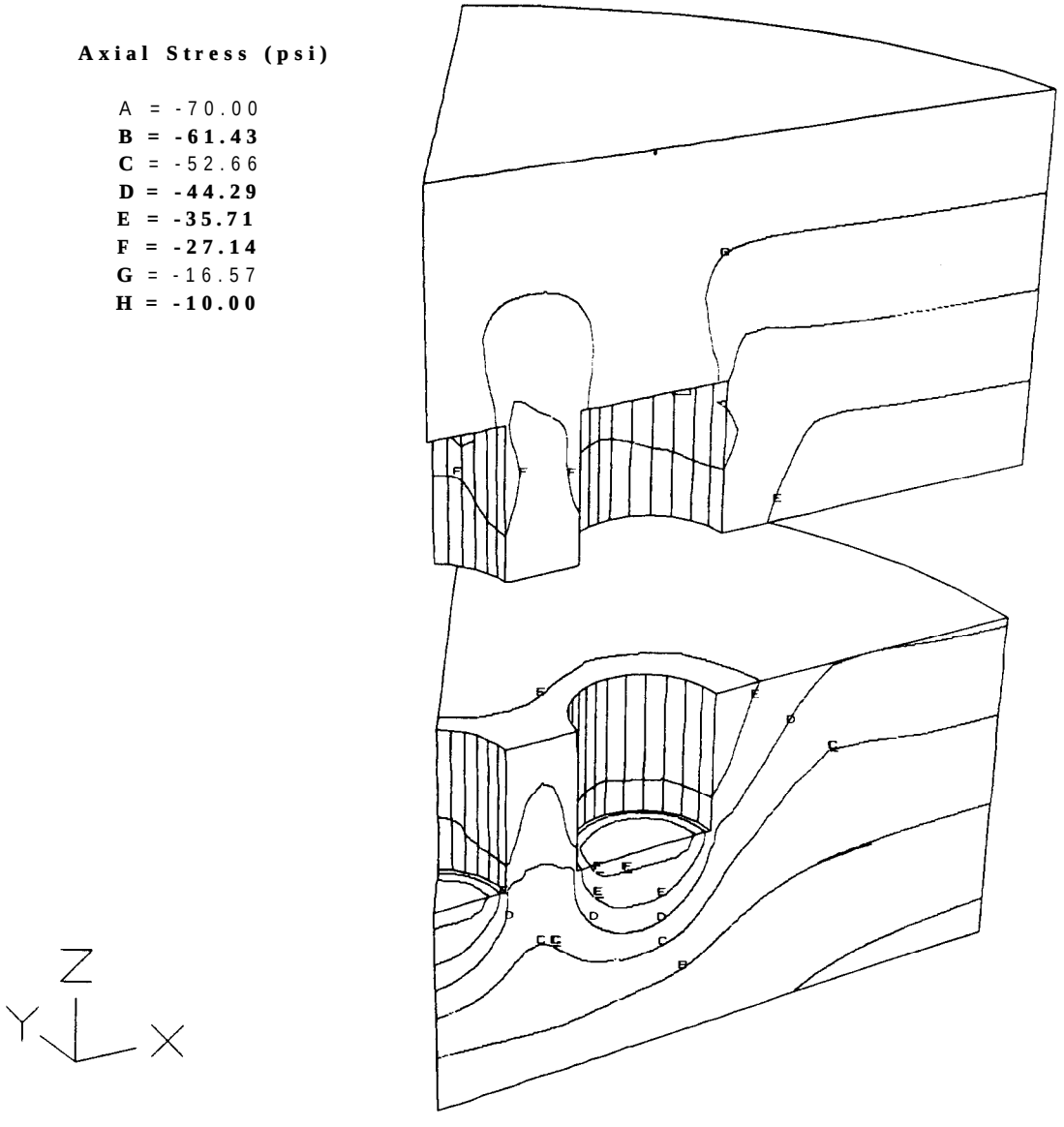

Figure 30: Calculated Axial Stress Immediately Before the 100 g Gravity Load is Removed. P/D = 0.5, Sectioned Model.

stress in the pillar has decreased from lithostatic in Figure 29 to something less in Figure 30 due to creep. Initially the axial stress in the pillar is bounded by the "D" and "E" contours (Figure 29) but after relief it is bounded by the "E" and "F" contours (Figure 30). Contour plots of Von Mises Stress are given in Figures 31 and 32 for the start and end of the experiment respectively. A significant amount of Von Mises stress relief is observed between Figure 31 and 32, however, it should be noted that the highest Von Mises stresses on the model are immediately adjacent to the cavity and in the pillar between the cavities. The highest Von Mises stress covers a larger volume of material in the pillar than on the other side of the cavity which explains why a cavity deforms more on the pillar side. The majority of the stress relief occurs between 0 and 2000 seconds (Figure 28) when the volumetric closure rate is rapidly decreasing.

Table VI

Calculated Percent Volume Loss for Multi-Cavity Configuration Based on Final Volume

P/D	Central Cavity % Vol. Loss	Outer Cavity % Vol. Loss
0.5	10.89	8.91
1.0	10.69	8.77
1.5	10.21	8.96
Single Cavity	8.67	---

Notes:

(1) The single cavity model had the same dimensions and fluid head as the multi-cavity experiments but did not include the outer cavity.

Finite Element Analysis of Centrifuge Experiment With P/D = 1.0

The finite element model of the 1.0 P/D centrifuge experiment is shown in Figure 33. This model is identical to the 0.5 P/D model in loading and boundary conditions except that there is a 2 inch (50.8 mm) spacing between

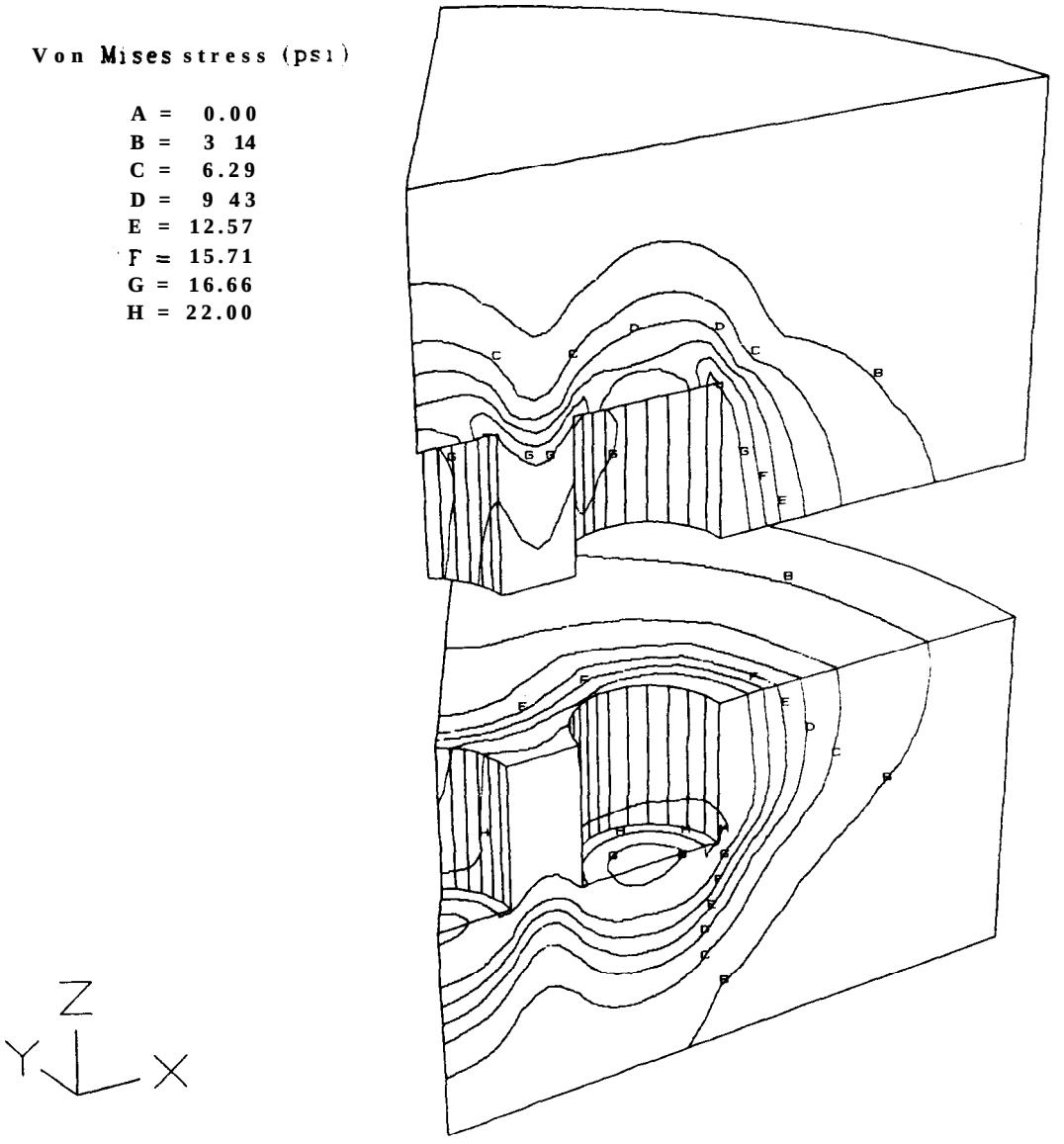

Figure 31: Calculated Von Mises Stress Immediately After 100 g Gravity Load is Reached. P/D = 0.5, Sectioned Model.

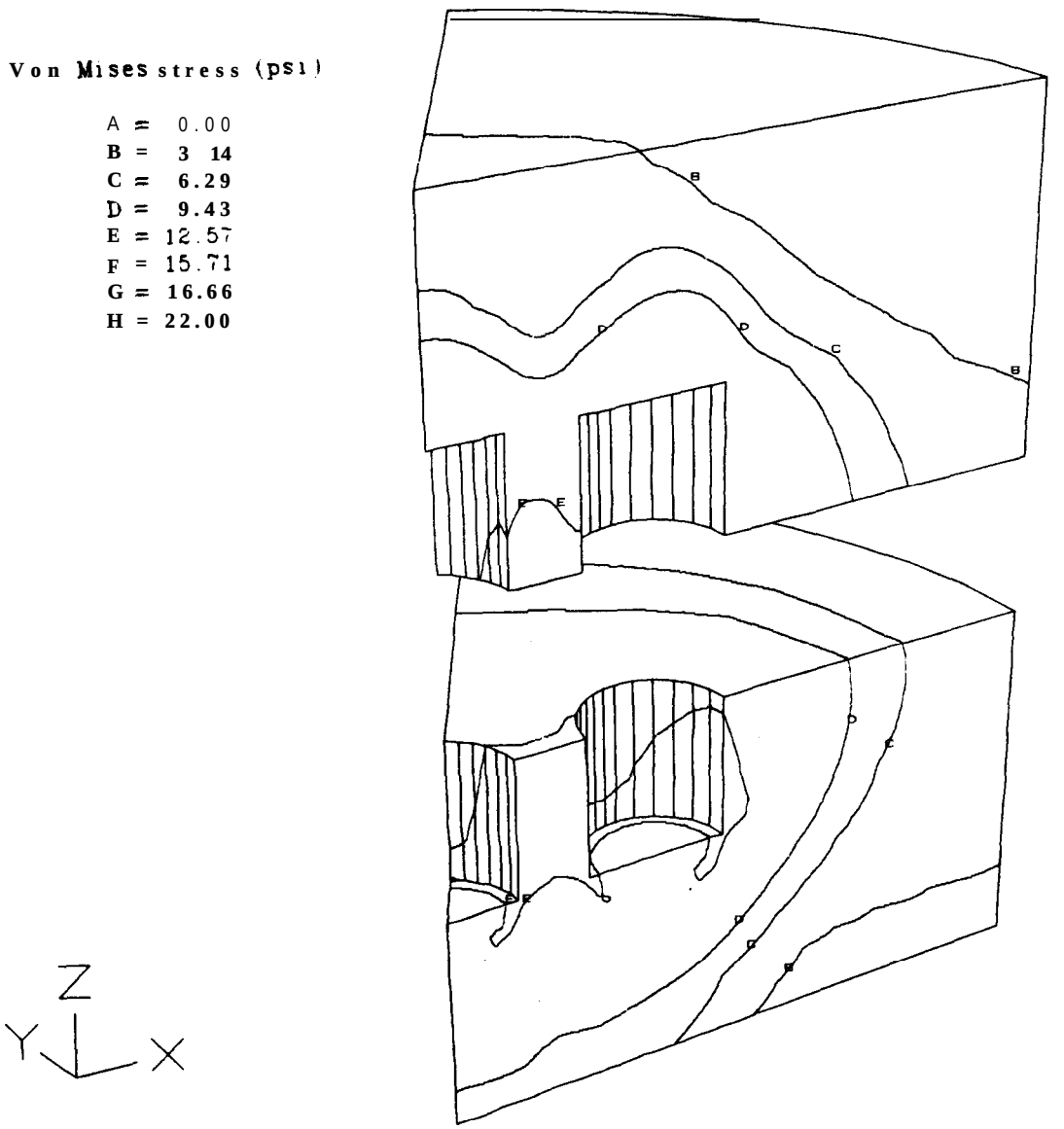

Figure 32: Calculated Von Mises Stress Immediately Before 100 g Gravity Load is Removed. P/D = 0.5, Sectioned Model.

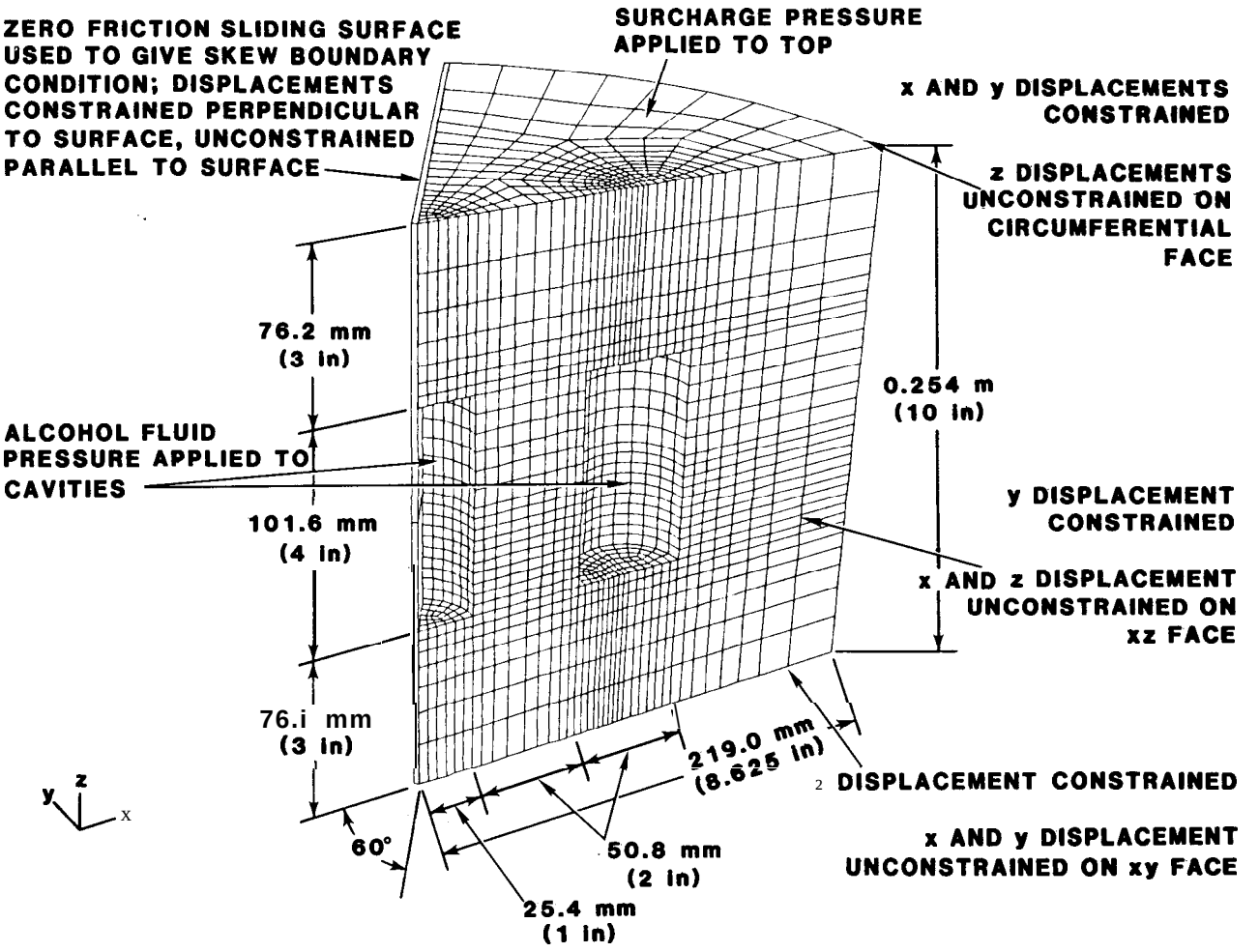

Figure 33: 3-D Finite Element Model of Multiple Cavity Centrifuge Experiment With P/D = 1.0.

the cavities. Figure 34 shows this model mathematically clipped at its midheight to display the mesh immediately adjacent to the cavities. The greater cavity spacing required more three-dimensional elements between the cavities than the 0.5 P/D model. This model had 7065 nodal points and 5707 three-dimensional elements.

Figure 35 shows the calculated displacements at the end of the centrifuge experiment but before the 100 g gravity load has been removed. The pillar between the cavities still shows asymmetric deformation though an analysis of the displacements shows that the asymmetry is less than for the 0.5 P/D model. As with the 0.5 P/D model more deformation is seen on the side that is adjacent to another cavity.

The calculated volume versus time for the inner and outer cavities is shown in Figure 36. This curve is similar to that of Figure 28 for the 0.5 P/D model in that the inner cavity experiences more closure both elastically and through creep. The 1.0 P/D curves are slightly closer together but the inner cavity experiences slightly less elastic rebound than the 0.5 P/D model and the final volumes of the 0.5 P/D model and the 1.0 P/D model are not significantly different. It is interesting to note that for both the central and outer cavities the percent volume loss decreases as P/D is increased from 0.5 to 1.0 as shown in Table VI.

Figures 37 and 38 show contours of axial stress immediately after loading and immediately before unloading. Similar behavior to the 0.5 P/D model is observed where the axial stress in the pillar and immediately adjacent to the cavities is relieved through creep. The axial stress in the middle of the pillar is relieved to slightly less than lithostatic (Figure 38) based on the position of the "D" and "E" contours. The pillar maximum axial stress is closer to lithostatic than it is in the 0.5 P/D model (Figure 30). Figures 39 and 40 show contours of Von Mises stress at the beginning and end of the experiment. As with the 0.5 P/D model the highest stresses are adjacent to the cavity and on the pillar. It is evident from the "H" contour (Figure 39) that more material is at a higher Von Mises stress in the pillar than on the other side of the cavity. Comparing Figures 31 and 39 it is also evident that there is less pillar

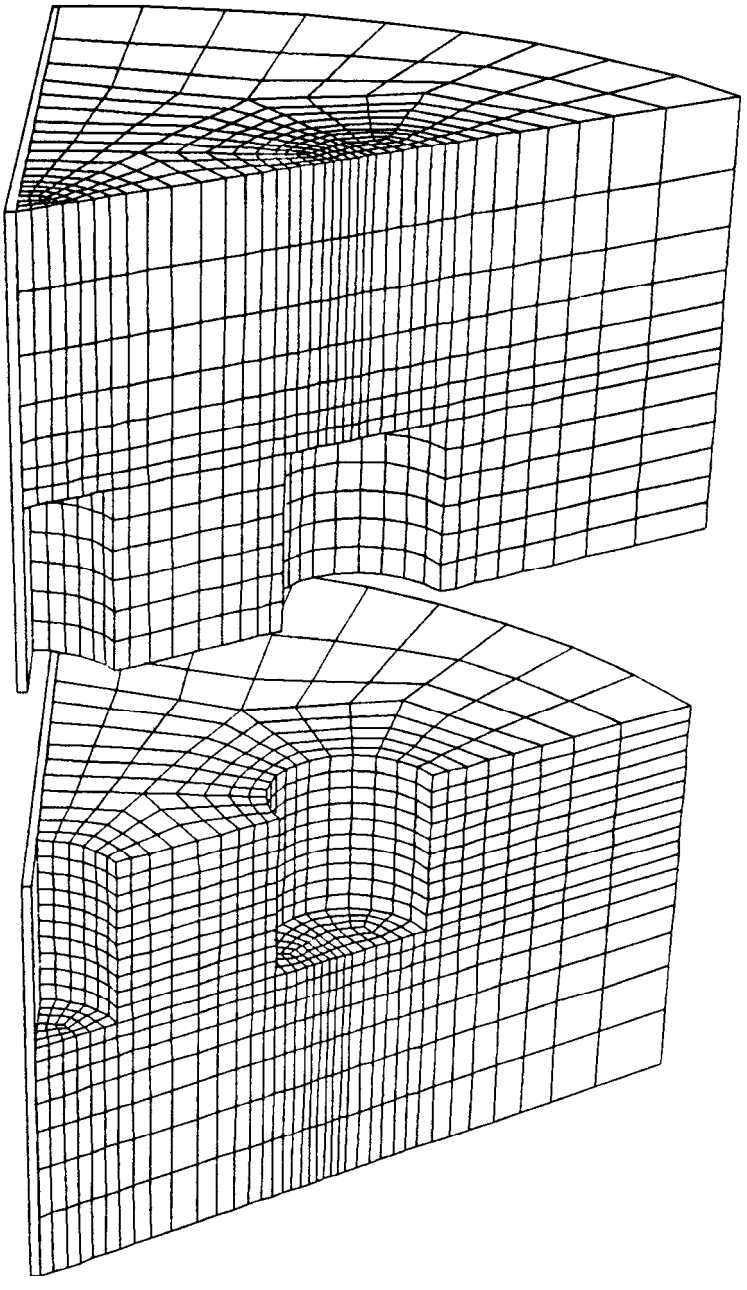

Figure 34: Sectioned 3-D Finite Element Model of Multiple Cavity Centrifuge Experiment With P/D = 1.0.

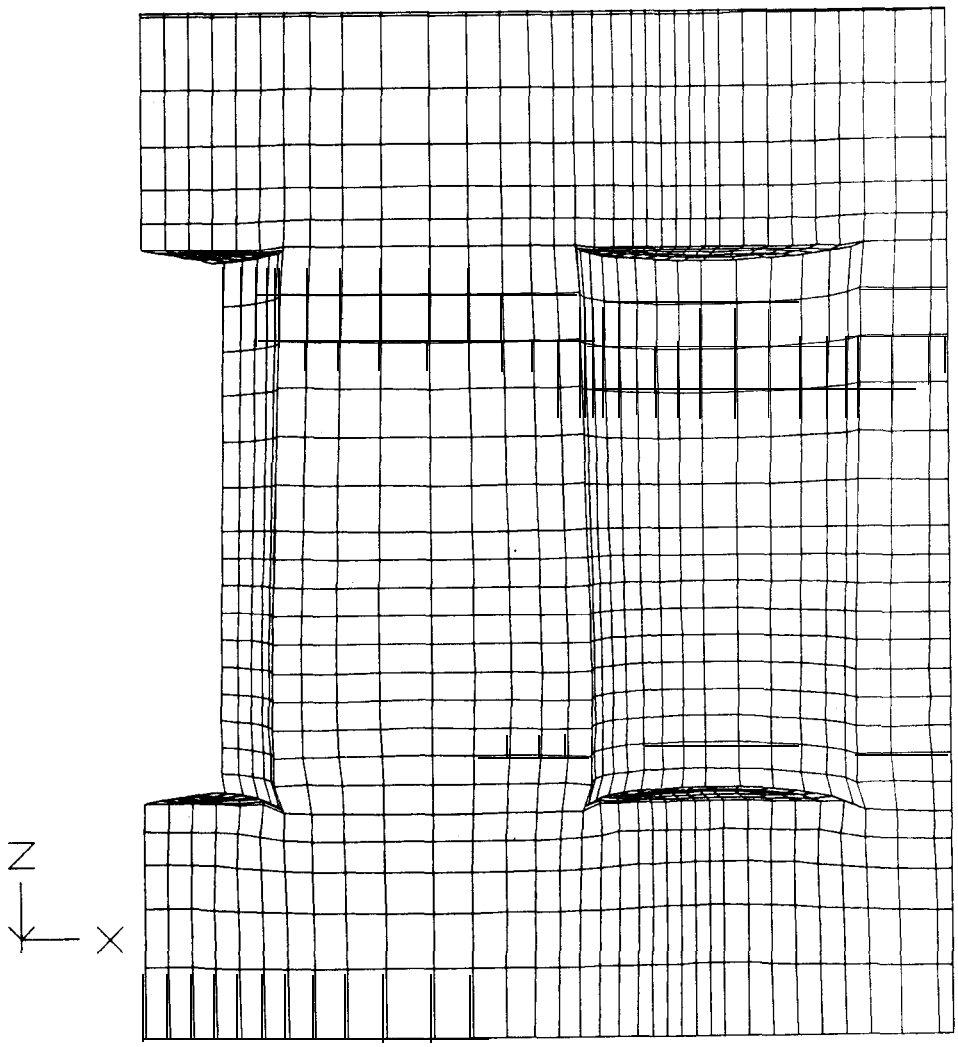

Figure 35: Deformed 3-D Finite Element Model of Multiple Cavity Centrifuge Experiment Immediately Before 100 g Gravity Load is Removed. P/D =1.0.

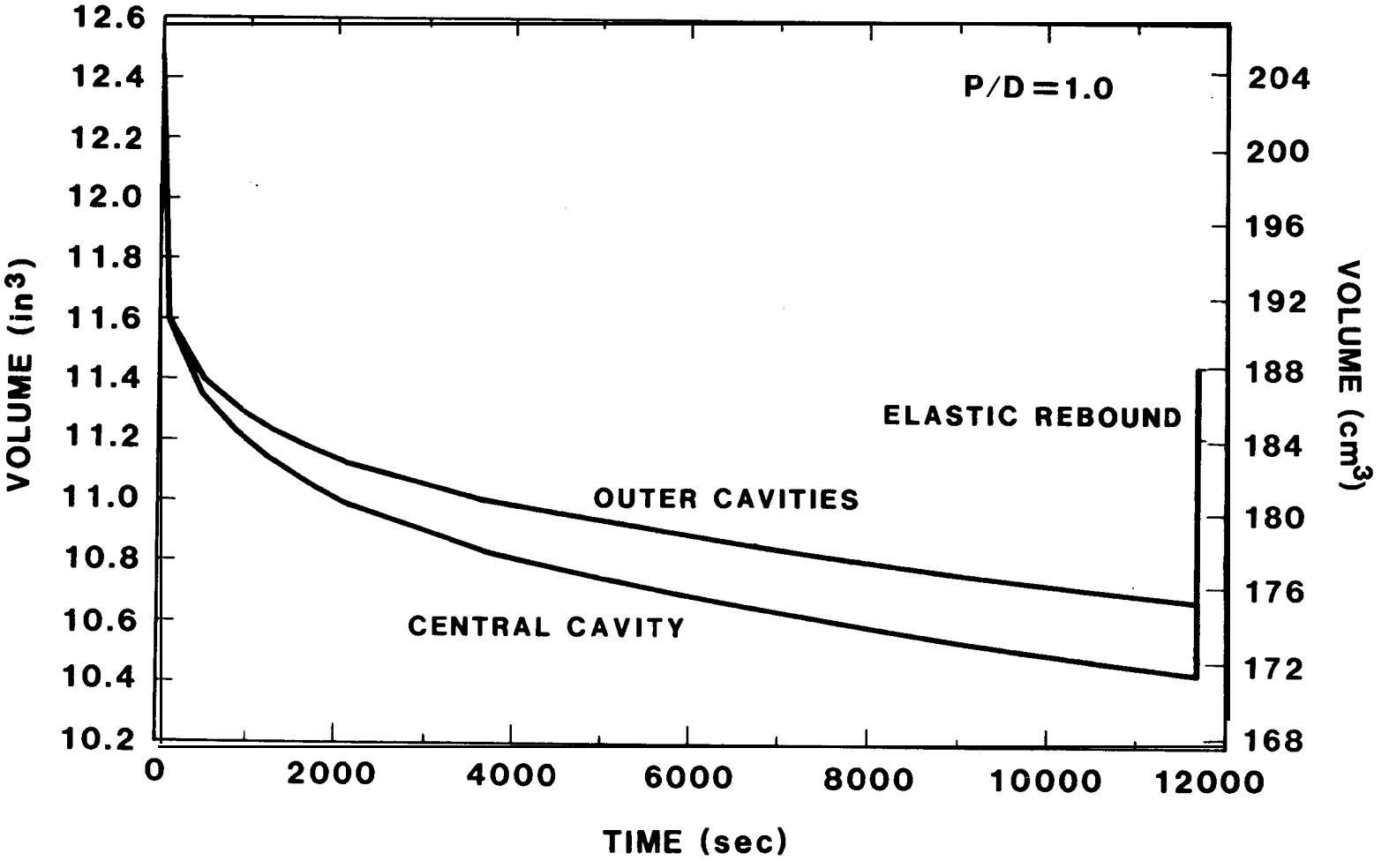

Figure 36: Calculated Volume Versus Time for Inner and Outer Cavities. P/D = 1.0.

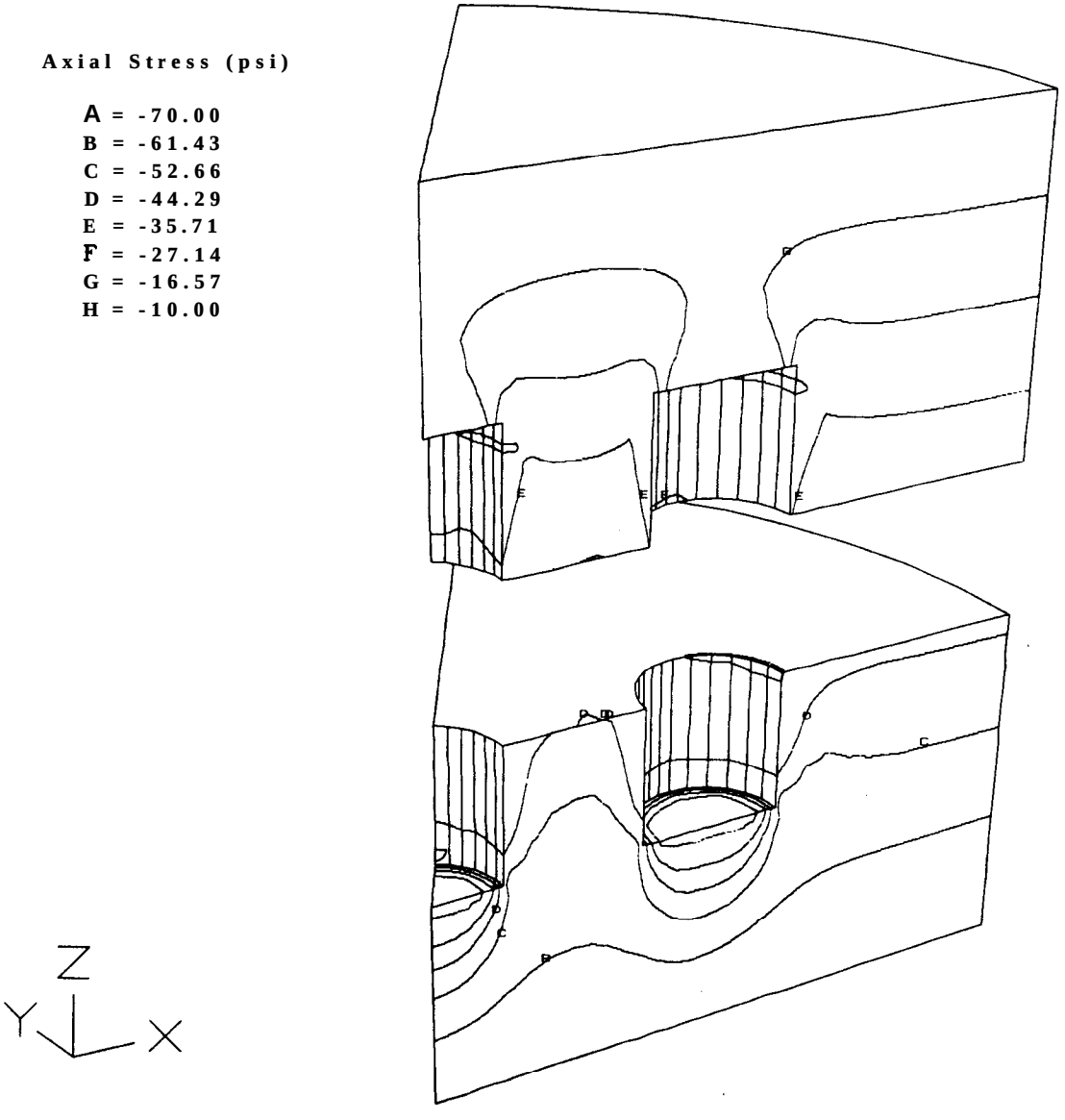

Figure 37: Calculated Axial Stress Immediately After 100 g Gravity Load is Reached. P/D = 1.0, Sectioned Model.

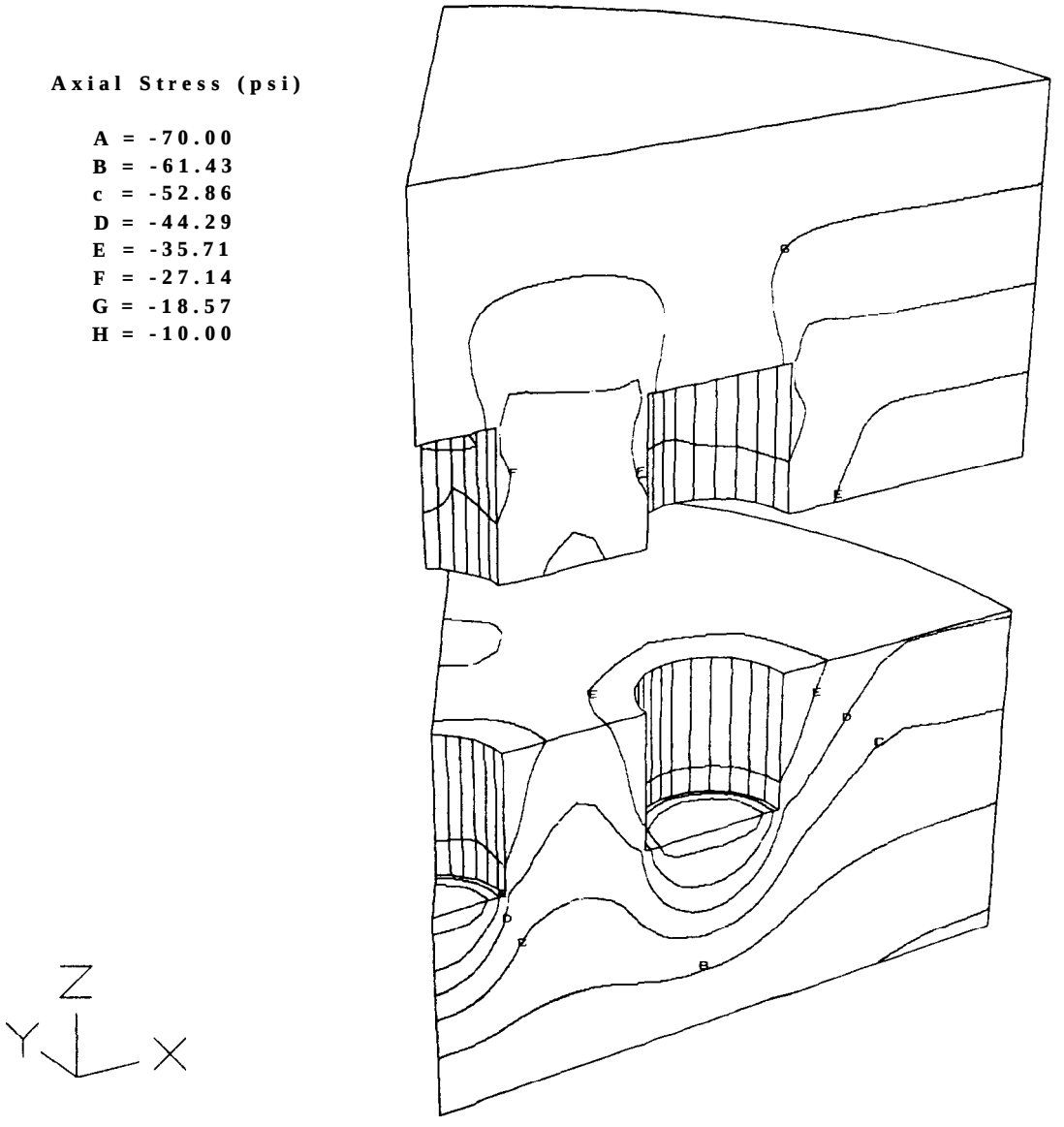

Figure 38: Calculated Axial Stress Immediately Before 100 g Gravity Load is Removed. P/D = 1.0, Sectioned Model.

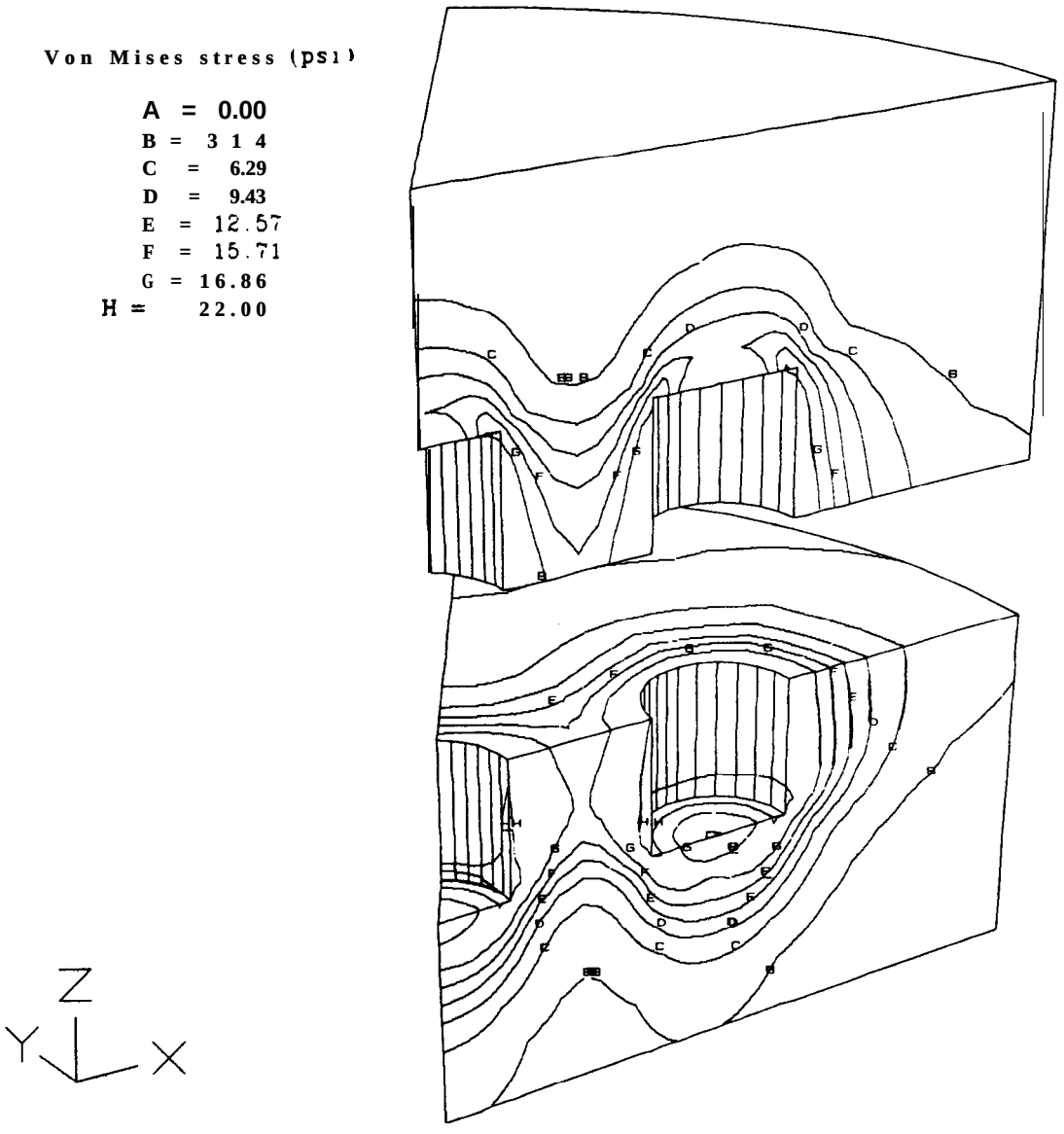

Figure 39: Calculated Von Mises Stress Immediately **After** 100 g **Gravity Load is Reached. P/D** = 1.0, **Sectioned Model.**

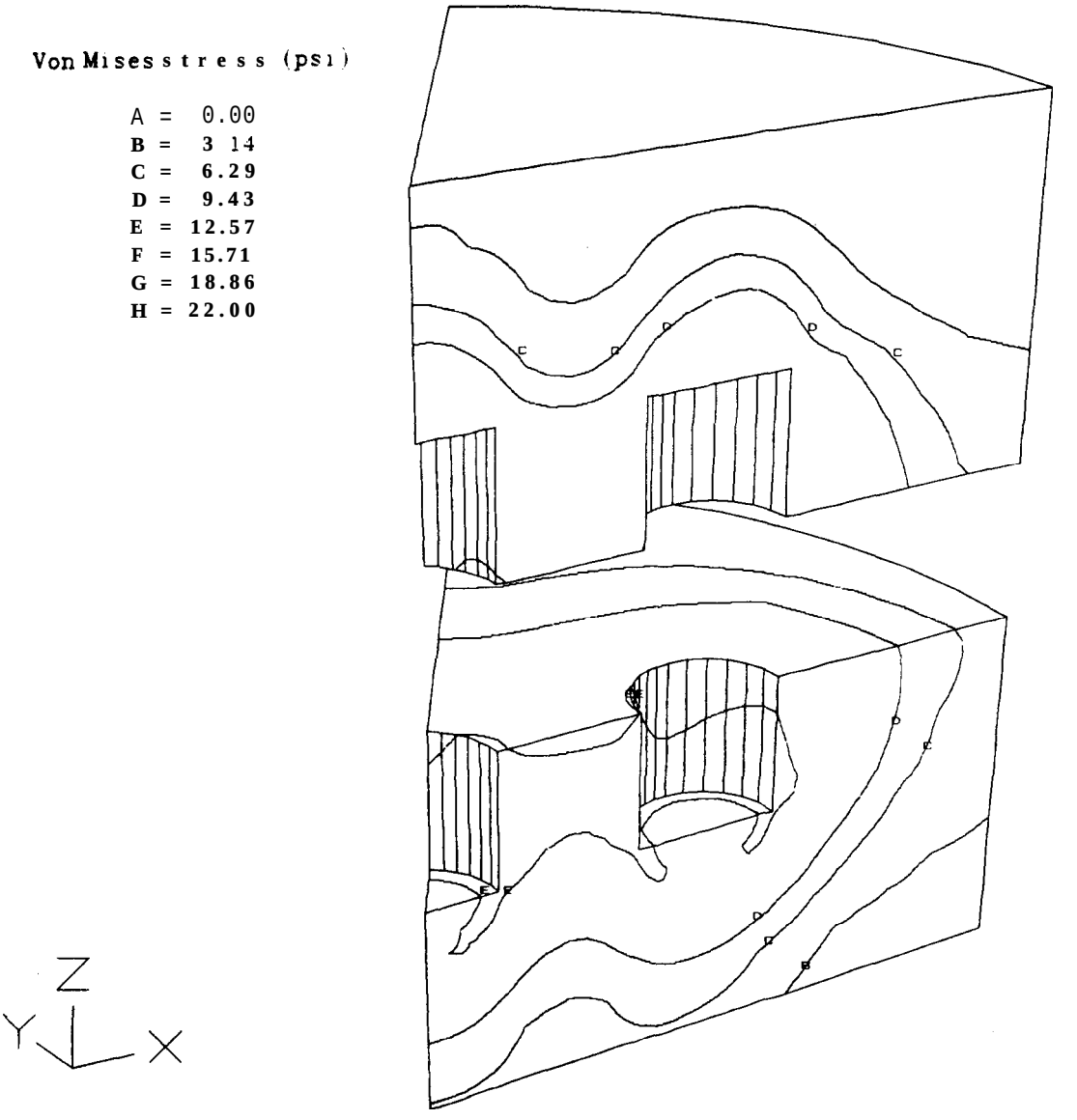

Figure 40:: Calculated Von Mises Stress Immediately Before 100 g Gravity Load is Removed. P/D = 1.0, Sectioned Model.

material at the highest Von Mises stress in the 1.0 P/D model than in the 0.5 P/D model which explains why there is less asymmetric deformation on the 1.0 P/D model than on the 0.5 P/D model. The Von Mises stress at the end of the experiment and after creep relief shows a stress envelope represented by the "C" and "D" contours completely surrounding the cavities. A result of this envelope is that' the cavities each influence the creep response of the other. Evidence of this is also shown in Figure 36 where the volume versus time curves for the two cavities are still separated. The two curves would be the same if the two cavities were acting independently of each other.

Finite Element Analysis of Centrifuge Experiment With P/D = 1.5

The finite element model of the 1.5 P/D centrifuge experiment is shown in Figure 41. This model is identical to the 0.5 P/D and 1.0 P/D models in loading and boundary conditions except that there is a 3 inch (76.2 mm) spacing between the cavities. Figure 42 shows this model mathematically clipped at midheight to display the mesh immediately adjacent to the cavities. The greater cavity spacing required more three-dimensional elements between the cavities than the other models. This model had 7468 nodal points and 6067 three-dimensional elements.

The calculated pillar deformation at the end of the experiment but before the gravity load is removed is shown in Figure 43. An analysis of the displacements shows slightly more deformation on the pillar side of the cavity but the difference in deformation between the two sides of the cavity is less than for the 0.5 or 1.0 P/D models. This is reasonable and indicates that the two cavities act more as individual cavities as their spacing is increased. Figure 44 shows calculated volume histories for the two cavities. As with the 0.5 and 1.0 P/D models the central cavity experiences more closure than the satellite cavities. However the curves in Figure 44 have a slightly different shape than the curves in Figures 28 and 36. They are more linear after 2000 sec and have a slope change after 6000 sec. A close study of Von Mises contour plots over the range of experimental time (two of which are shown in Figures 47 and 48) shows this shape change to be due to two factors. First, the cavities are acting more

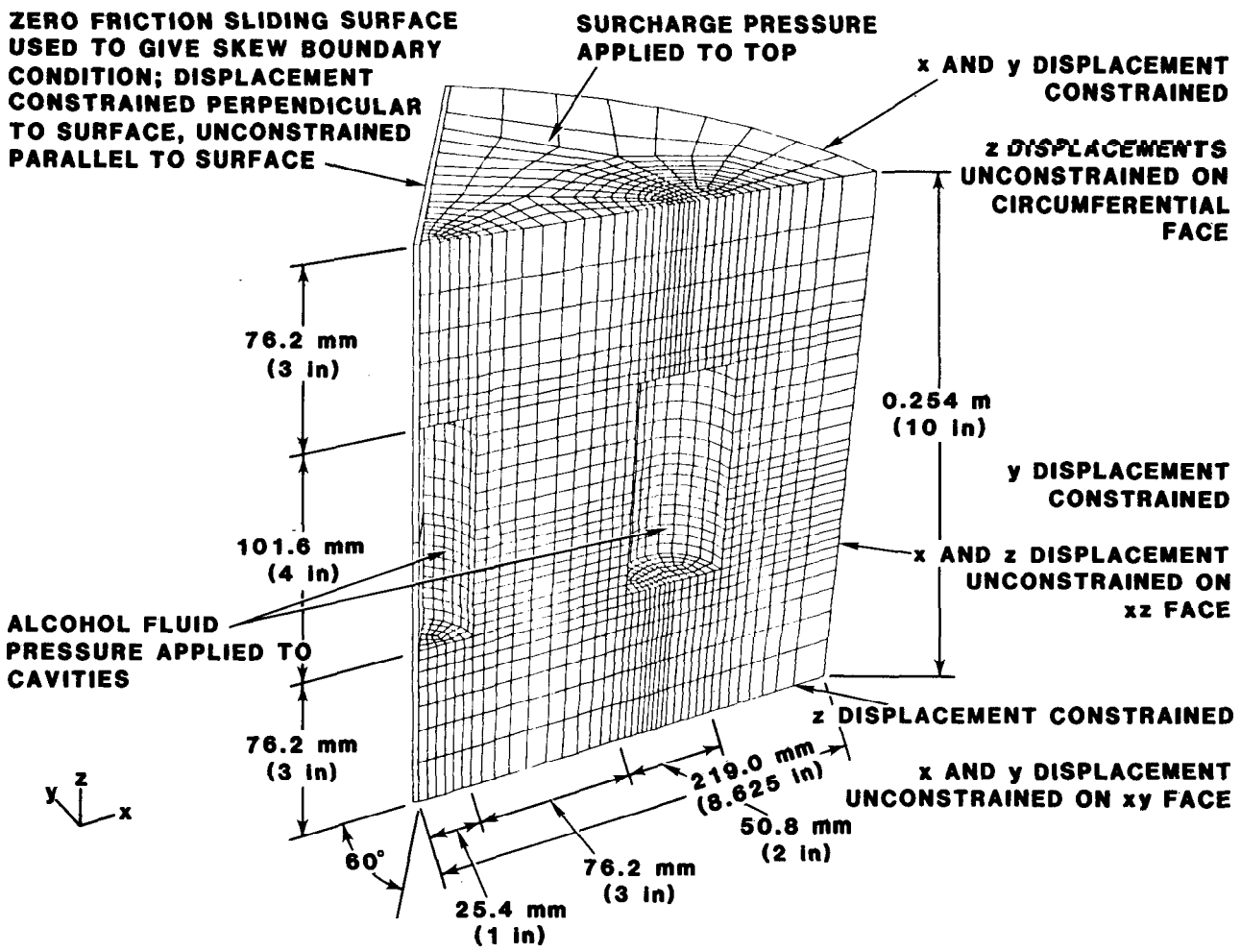

Figure 41: 3-D Finite Element Model of Multiple Cavity Centrifuge Experiment With P/D = 1.5.

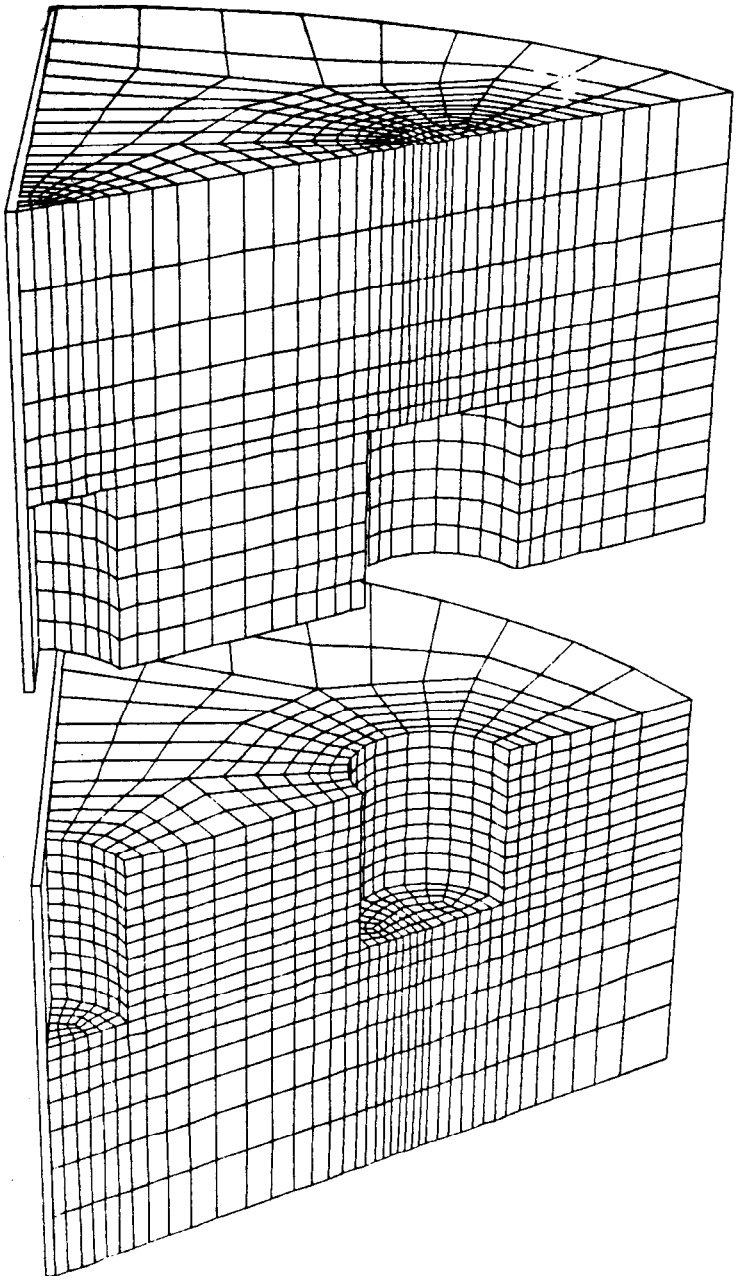

Figure 42: Sectioned 3-D Finite Element Model of Multiple Cavity Centrifuge Experiment With P/D = 1.5.

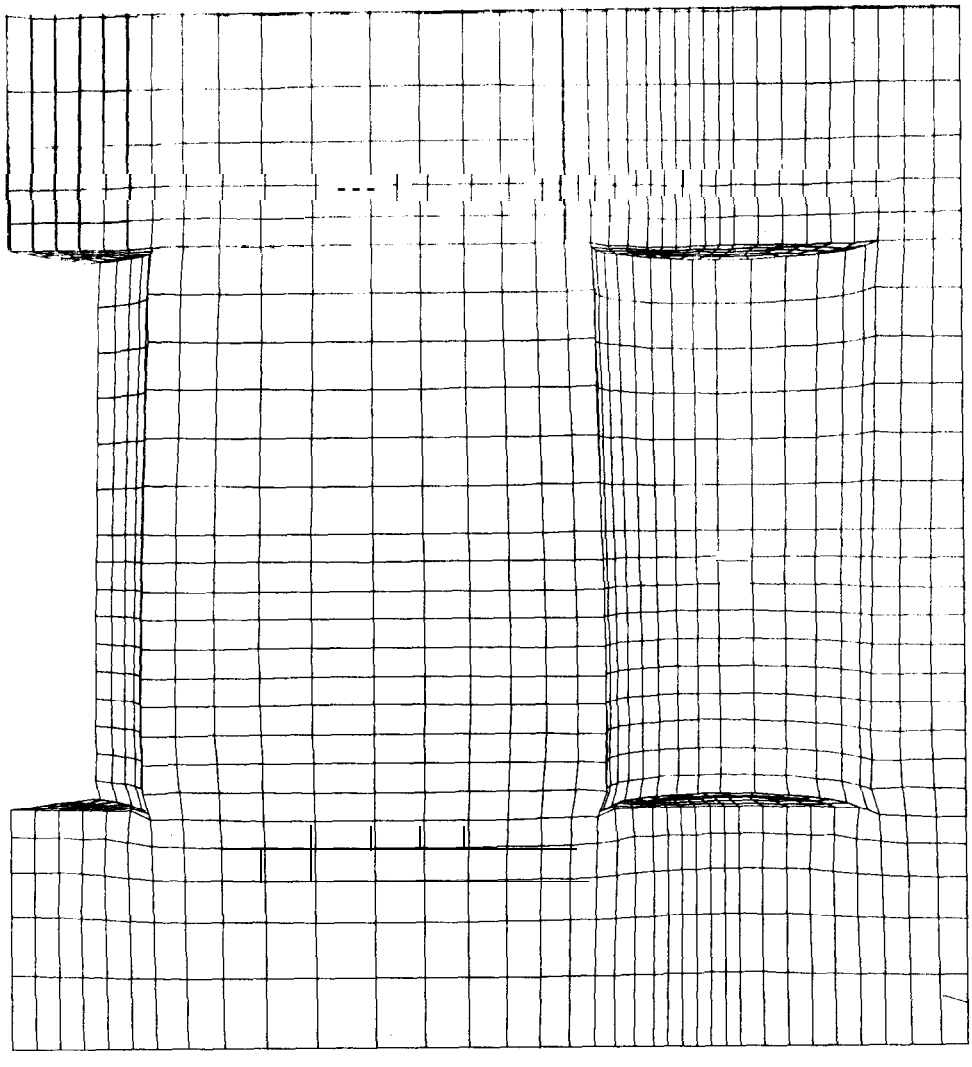

Figure 43: Deformed 3-D Finite Element Model of Multiple Cavity Centrifuge Experiment Immediately Before 100 g Gravity Load is Removed. P/D = 1.5.

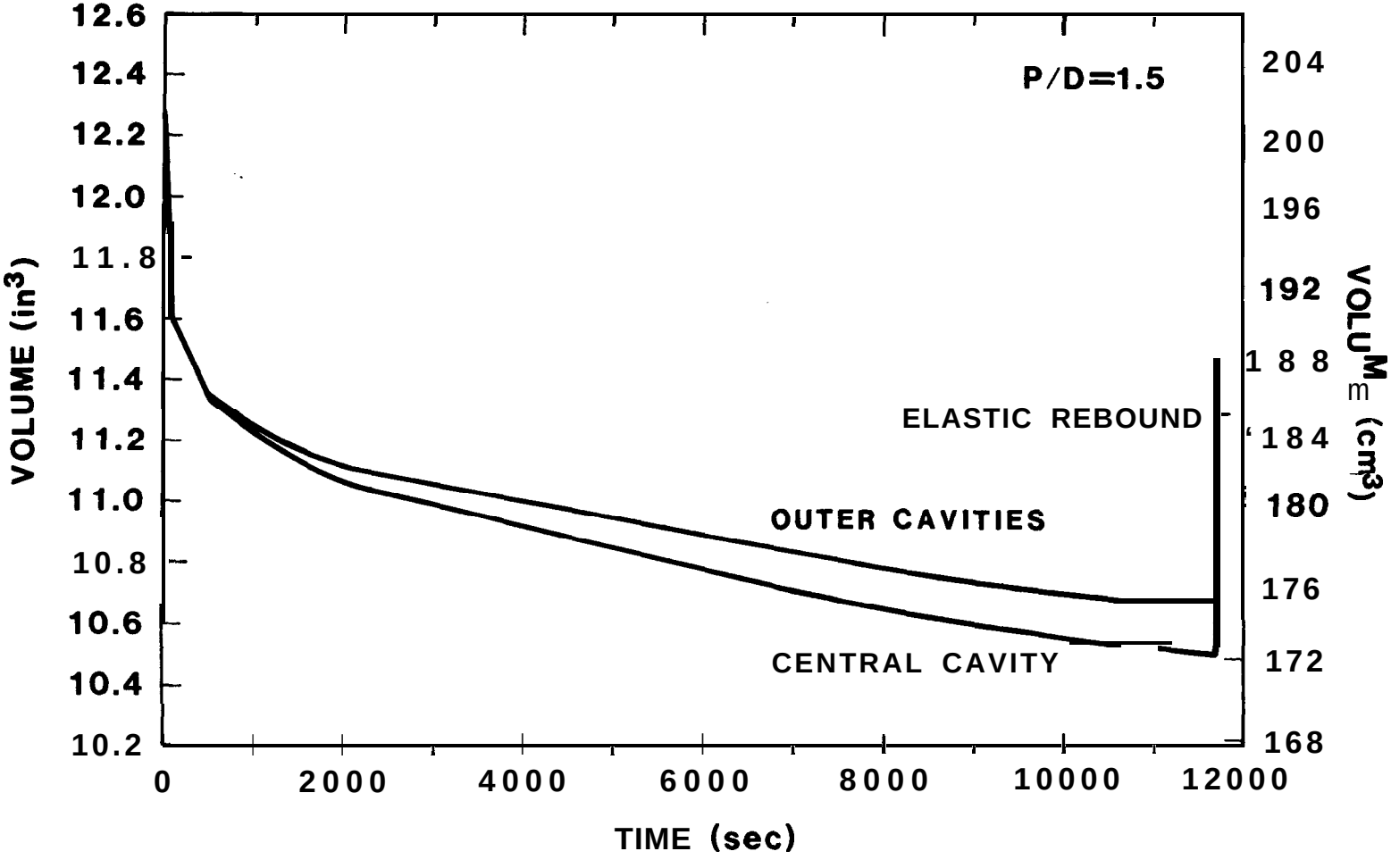

Figure 44: Calculated Volume Versus Time for Inner and Outer Cavities. P/D = 1.5.

independently of each other and follow the pattern of the single cavity which also becomes linear after 2000 sec (see Figure 23) whereas the 0.5 and 1.0 P/D models tend to become linear after 4000 sec (see Figures 28 and 36). Second, the Von Mises stress envelope enclosed by the "C" contour begins to touch the outer surface of the model at approximately 6000 sec. Interference of the outer surface-with the stress envelope of the cavity is shown by the "C" contour in Figure 48 and slightly increases the closure of the outer cavity. This phenomenon is also discussed later in the section titled, "Comparison of Results From the 0.5, 1.0 and 1.5 P/D Models."

Contours of axial stress immediately after loading and immediately before unloading are shown in Figures 45 and 46 respectively. Stress relief around the cavities is evident, however it should be noted that the maximum axial stress in the center of the pillar is just slightly lower than lithostatic. This is shown by the position of the "E", "D" and "C" contours on the pillar compared with their position on the right side of the model. Contours of Von Mises stress are shown at the beginning and end of the experiment in Figures 47 and 48. The Von Mises stress envelope around each cavity is more symmetric than it was for the other two models which explains the more uniform deformation of each cavity seen in Figure 43. It is also evident from Figure 48 that an envelope represented by the "D" contour encompasses both cavities implying that they should still influence each other. The influence of each cavity on the other is also evident in the volume versus time curves in Figure 44.

Comparison of Results from the 0.5, 1.0 and 1.5 P/D Models

The calculated percent volume loss for the three multi-cavity models at the end of the experiment and after the 100 g gravity load has been removed is given in Table VI. It can be seen that the central cavity always experiences more closure than the outer cavities. It should also be noted that the closure of both cavities is higher for the smaller spacings and decreases as the spacing is increased. The one exception to this is the outer cavity for the 1.5 P/D case. As has been discussed previously the closure of this cavity is increased slightly due to the interference of the

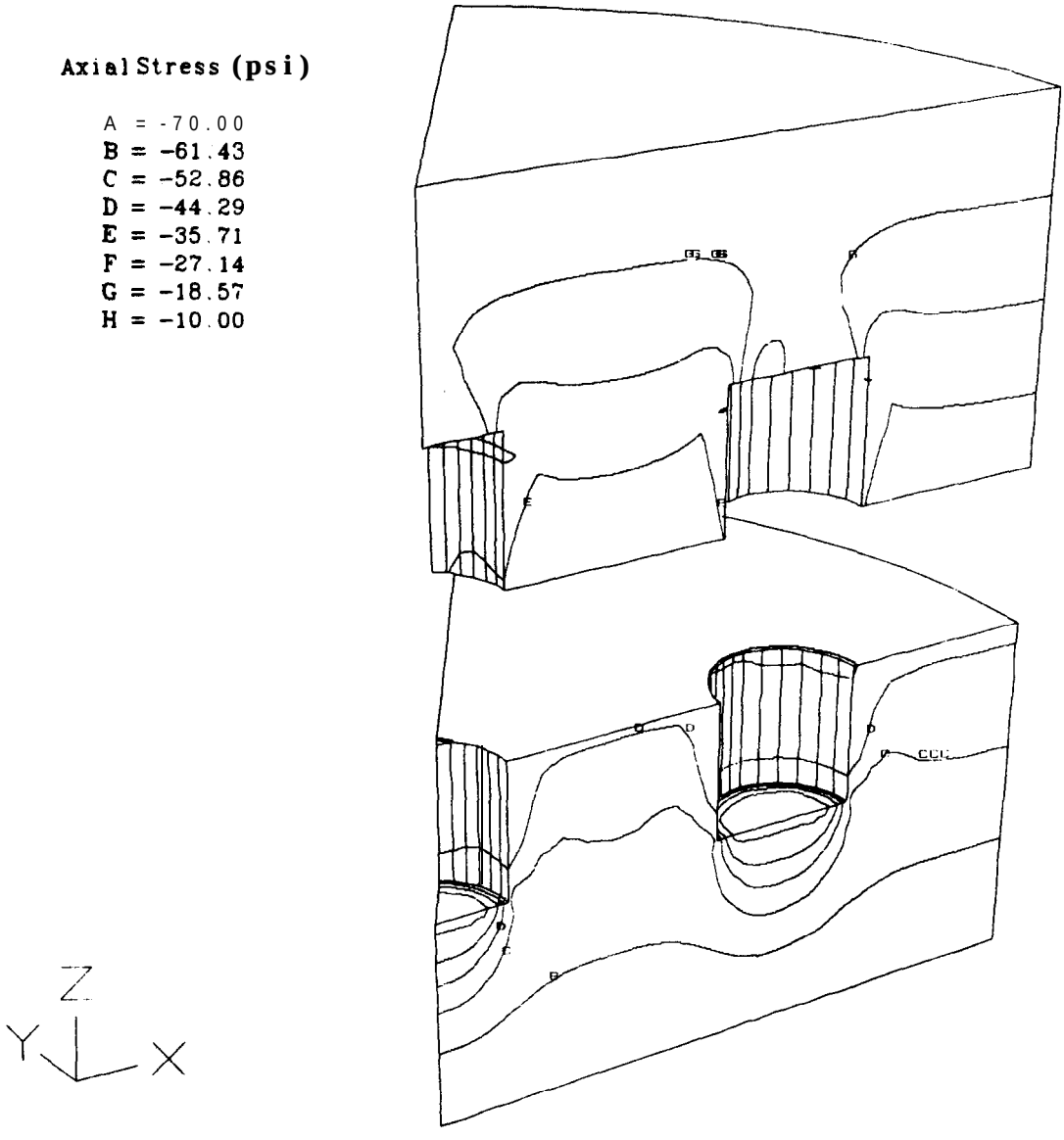

Figure 45: Calculated Axial Stress Immediately After 100 g Gravity Load is Reached. P/D = 1.5, Sectioned Model.

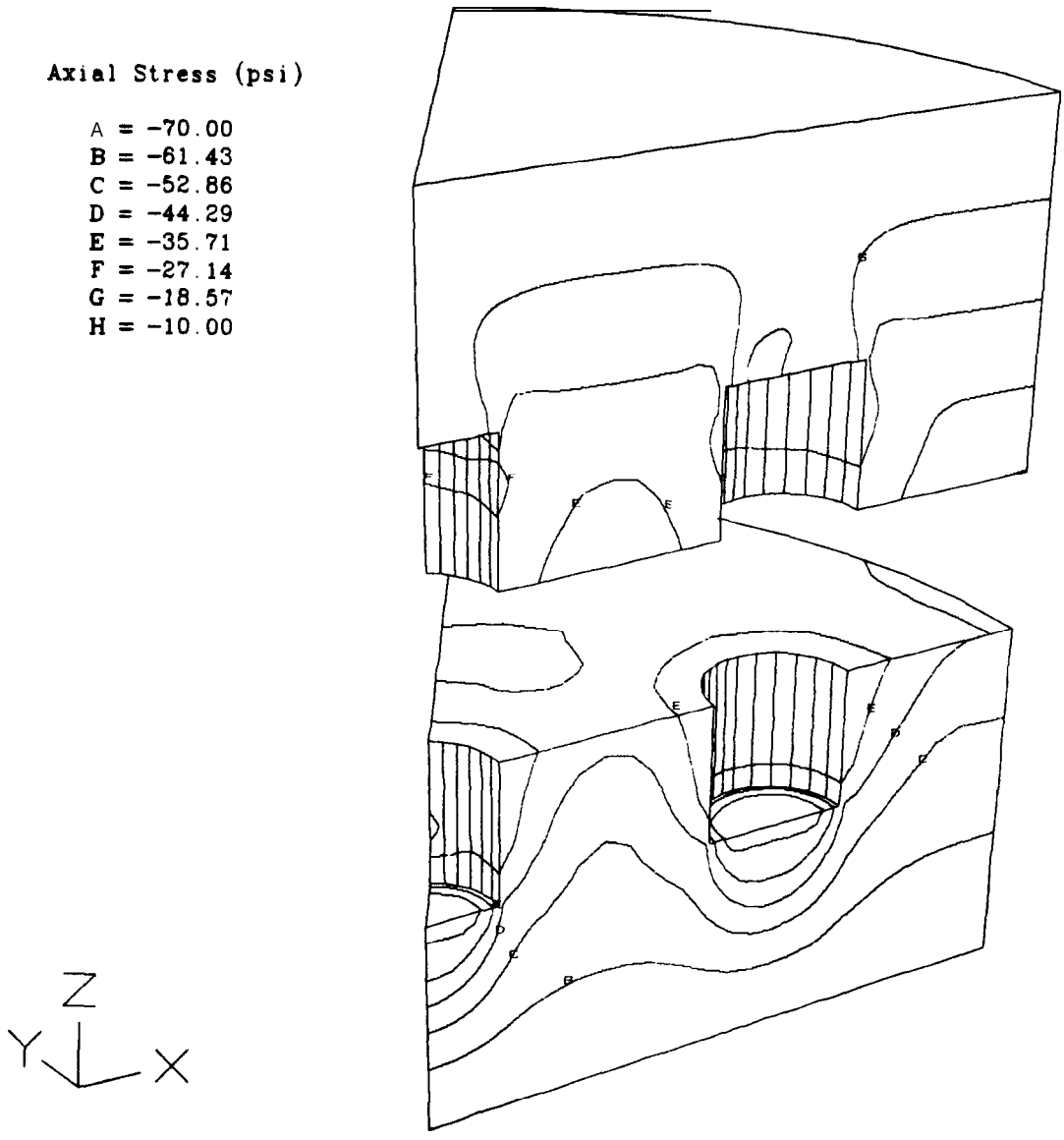

Figure 46: Calculated Axial Stress Immediately Before 100 g Gravity Load is Removed. P/D = 1.5, Sectioned Model.

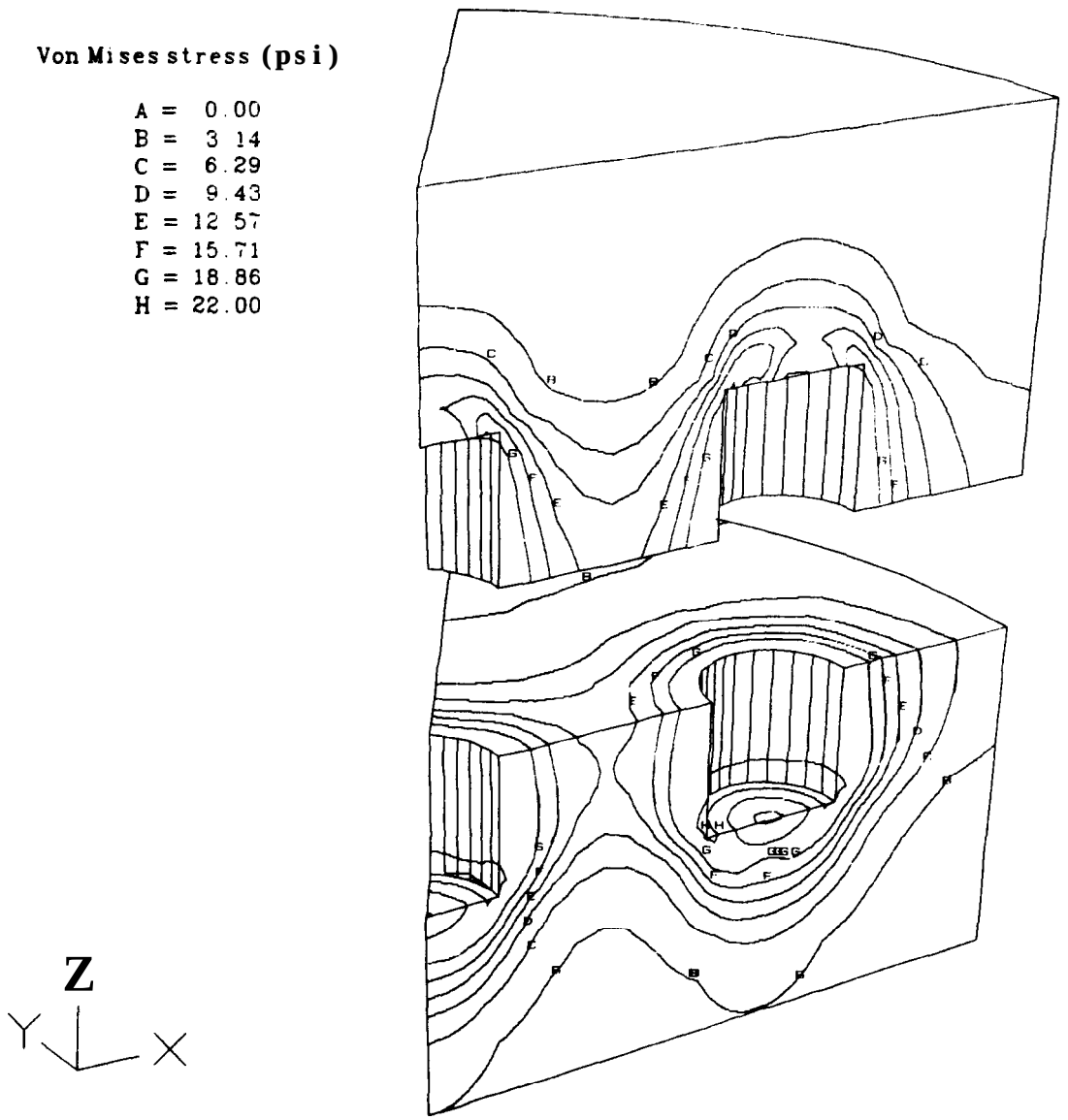

Figure 47: Calculated Von Mises Stress Immediately After 100 g Gravity Load is Reached. P/D = 1.5, Sectioned Model.

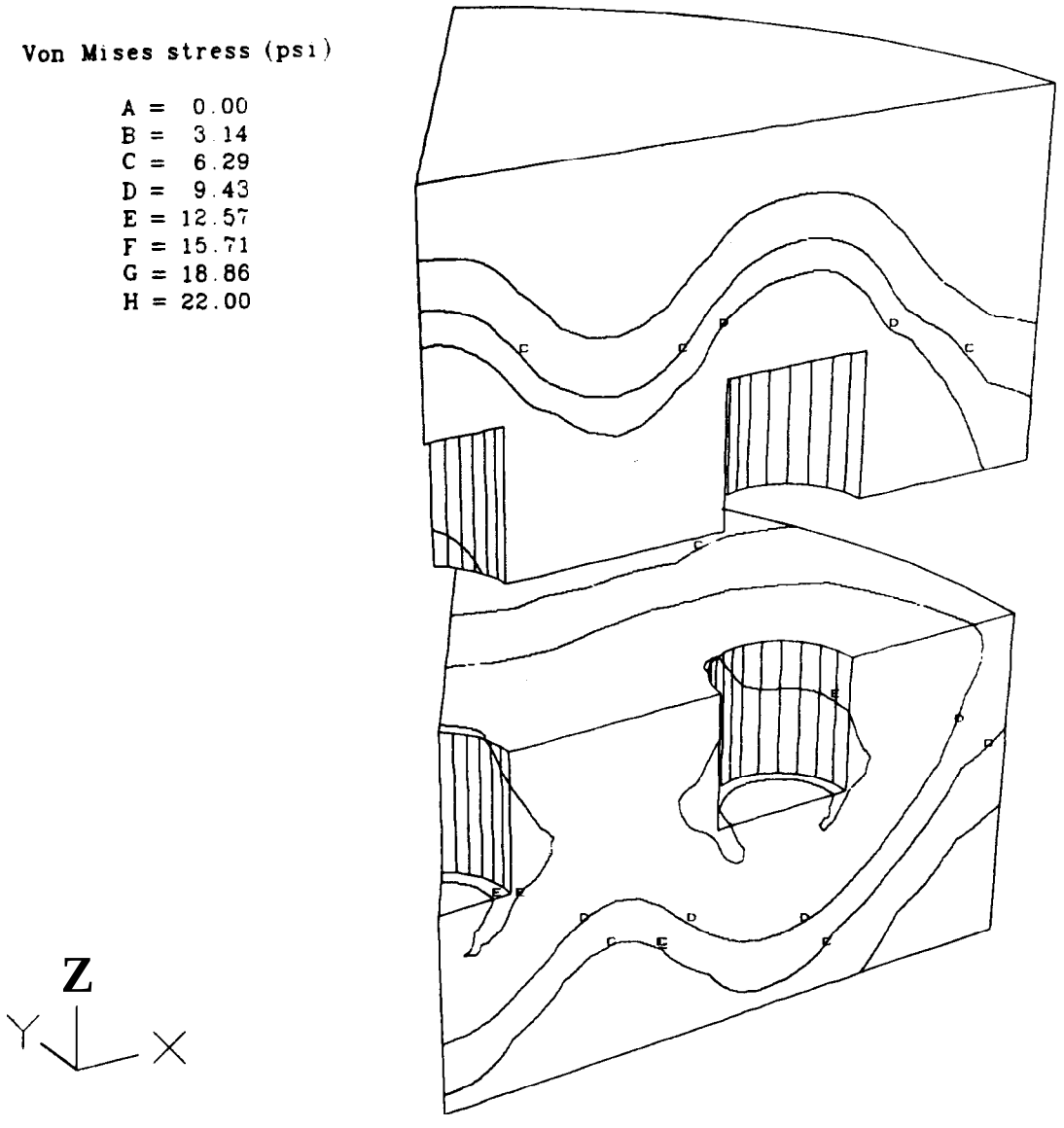

Figure 48: Calculated Von Mises Stress Immediately Before 100 g Gravity Load is Removed. P/D = 1.5, Sectioned Model.

cavity stress envelope with the outer boundary. A linear extrapolation of the outer cavity closures for the 0.5 and 1.0 P/D models to 1.5 P/D would result in a closure of 8.63 percent. This is not significantly different from 8.67 percent obtained from a single cavity model with the same dimensions and loading as the multi-cavity models. An important lesson from this study is that the outer boundary was not far enough away from the outer cavities and that stress envelopes generated by creep stress relief are usually significantly larger than elastic stress envelopes. Had the outer boundary been further away from the outer cavities, the closure of those cavities would probably have been very close to that of the single cavity. It is interesting to note that the creep closure of the outer cavities is closer to that of the single cavity and becomes even closer as the spacing is increased. The closure of the central cavity is also decreasing with increasing P/D but it appears that a relatively large spacing would be necessary before the closure approached that of the single cavity. This is due to the fact that the central cavity is surrounded by other cavities each of which has an influence on central cavity response. Figures 32, 40 and 48 show contours of Von Mises stress for the three models immediately before unloading and all three figures show that the two cavities are enveloped by the "C" and "D" contours. This indicates that the cavities still influence each other and it is logical that the volume versus time curves for the two cavities are separated for all three models.

The relationship between closure and P/D for the central cavity is nonlinear. An exponential curve fit of P/D and percent volume loss results in a fitting coefficient of 0.94 and predicts that the central cavity will have the same closure as a single cavity at a P/D of 4.1. A linear curve fit of P/D and percent volume loss also results in a fitting coefficient of 0.94 and predicts that the central cavity will experience the single cavity closure at a P/D of 3.8. It should be kept in mind that these are extrapolations and may not accurately predict the closures at larger P/D's.

Comparison of Multi-Cavity Numerical and Experimental Results

The multi-cavity experiments were performed using two different types of plasticine each with a slightly different creep model. This was done to provide a check on the dimensional analysis which was used to extrapolate the performance of plasticine models to that of caverns in rock salt. (The three-dimensional finite element calculations were all performed using green plasticine material properties). The dimensional analysis is discussed in detail by Sutherland and Preece [6]. In order to compare results from the green and gray plasticine models a finite element analysis of the single cavity model was performed with creep models for both green and gray plasticine. The green plasticine model had a percent volume loss that was 2.13 times that of the gray plasticine. Table VII gives a summary of the percent volume losses of the cavities obtained on the centrifuge and with the finite element models. The centrifuge and numerical results were extracted from Tables III and VI respectively.

Table VII

Comparison of Experimental and Numerical Results for the Multi-Cavity Experiments

P/D	Cavity	%loss	Adjusted %loss	Finite Element %loss
0.5	central	11.3		10.89
"	outer	11.4		8.91
"	"	9.5		8.91
"	"	9.6		8.91
1.0	central	5.1	10.9	10.69
"	outer	6.8	14.5	8.77
"	"	6.5	13.8	8.77
"	"	5.1	10.8	8.77
1.5	central	20.1		10.21
"	outer	35.8		8.96
"	"	14.1		8.96
"	"	14.1		8.96

Note: The Adjusted percent loss converts the gray plasticine of the 1.0 P/D experiment to the green plasticine of the other two experiments. The conversion factor of 2.13 was determined by performing finite element calculations on identical models using both gray and green plasticine.

As discussed in Sutherland and Preece [6] the first multi-cavity centrifuge experiment performed was the 1.5 P/D experiment which was made from green plasticine. This model developed leaks from two of the cavities (the central and one outer cavity) that reduced the fluid head and caused excessive closure of the two leaky cavities and above normal closure of the others. The above normal closure of the two non-leaky cavities is plausible

because the finite element analyses showed that the cavity stress envelopes overlap causing the cavities to influence each other. It is reasonable then that reduced fluid head in one cavity would also have an effect on satellite cavities which is what was seen in this experiment. This experiment also illustrates the significant impact internal fluid pressure has on the creep closure of the cavities. From dimensional analysis [6] it appears that the fluid level for cavity B in the 1.5 P/D experiment was at the cavity roof instead of 4.75 in (120.65 mm) above the cavity roof. A finite element analysis of this model with reduced fluid.head was considered but not done because of the expense of these three-dimensional calculations and because a similar exercise had been done on the two-dimensional single cavity model (see Figure 24). As can be seen in Table VII there is not a very good comparison between the centrifuge and numerical results for the 1.5 P/D but the reduced fluid head during the experiment is a plausible explanation.

The 1.0 P/D experiment was performed second. The sample was made from gray plasticine which is slightly stiffer in creep than the green plasticine. The model did not appear to lose fluid from any of the cavities but undetected small amounts may have been lost that could affect the creep closure of the cavities. The comparison between the centrifuge and numerical results is good for the central cavity but two of the outer cavities experienced more closure experimentally than the central cavity. It is possible that undetected leaks developed in these cavities or that the relatively small closures caused more error in the experimental volume calculations. Both experimental and numerical volume losses fall in the range between 8.77 and 14.5 percent. This implies the lack of gross errors and hints that the experiments had difficulty detecting some of the subtleties such as more closure of the central cavity.

The 0.5 P/D experiment was performed last and consequently was considered the best in terms of controlling leaky cavities. There was no evidence of any alcohol leakage from any of the cavities during the experiment. The comparison of experimental and numerical volume losses for this experiment is relatively good. The central cavity experimental loss of 11.4 percent compares well with the finite element loss of 10.89 percent. Outer cavity experimental losses of 9.5 and 9.6 percent compare well with

the finite element loss of 8.91 percent. One of the outer cavities experienced almost the same closure as the central cavity. The most plausible explanation for this is a small leak. All of the experimental and numerical volume losses fall between 8.91 and 11.5 percent and indicates good correlation in terms of gross cavity behavior.

An important point to make is that the final cavity volumes from the experiments were calculated from the average of the volumes of four axisymmetric nodal loops derived from post-test photographs [6]. This volume calculation process by its very nature tends to smear out nonsymmetric closure of the cavities. To quantify this error, the nodal loop method of calculating cavity volumes was exercised on the deformed satellite cavity in the 0.5 P/D finite element model shown in Figure 27. The two nodal loops each began at the node in the center of the roof. One loop circumscribed the right side of the cavity and the other the left side. The left nodal loop produced a final cavity volume of 11.1590 in^3 (183.0 cm^3) compared to 11.5921 in^3 (190.0 cm^3) for the right nodal loop. The average of the two is 11.3756 in^3 (186.4 cm^3) which results in a volume loss of 9.48% compared to 8.91% (Table VII) calculated for the same cavity using the same set of displacements with the hexahedral method. This indicates that the experimental cavity closures which were calculated by averaging volumes produced by four nodal loops are probably high by approximately 0.5%. This implies that the experimental cavity closures are probably 0.5% less than what is given in Tables III and VII. This would improve the correlation between experimental results and numerical calculations.

CONCLUSIONS

It has been demonstrated that centrifuge creep testing of fluid-filled cavities in the modeling material plasticine is feasible. In these experiments the uncertainty in boundary conditions, loading and geometry then is much less than for measurements taken in actual petroleum-filled caverns in rock salt. Because of this, these experiments have been used as a finite element program qualification exercise. It has been demonstrated that finite element computer programs employing a material creep model for plasticine can be used to calculate the creep closure of the cavities in plasticine with reasonable agreement. This implies the validity of finite element calculations with a creeping material such as plasticine. Extension of this capability to rock salt must be done with care since salt is a crystalline material that creeps by very different mechanisms than plasticine.

The single cavity 100 g experiment was simulated numerically with both two-dimensional and three-dimensional versions of the same finite element creep program. The same results in terms of displacements, cavity closure and stress distributions were obtained with both programs, making this a successful benchmark exercise.

The three-dimensional finite element analyses of the multi-cavity experiments provided further qualification of the three-dimensional program since the finite element and experimental results compared reasonably well for two of the three experiments. The experiment that did not compare well experienced difficulties with leaky cavities and fluid head loss.

The multi-cavity geometry, consisting of a central cavity and three satellite cavities, was designed to model an array of cavities. The experiments revealed the gross behavior of the array but did not produce some of the subtleties that became obvious from the three-dimensional finite element analyses. For example, it was demonstrated numerically that the central cavity always experiences slightly more creep closure than the outer cavities in the array. One of the experiments (P/D = 0.5) indicated this but another (P/D = 1.0) indicated slightly less closure from the central

cavity. It would have been impossible to predict that the central cavity closes slightly more than the others based on experimental evidence alone. The finite element calculations indicated several other characteristics of array behavior. First, it was shown that the closure of both cavities is greatest for the closest spacing and decreases slightly as the spacing is increased. Second, it was demonstrated that the zone of influence generated by each cavity through creep stress relief is relatively large. These zones significantly overlap for cavities with a P/D of 1.5 and the cavities considerably influence each other's creep closure. Extrapolation of P/D versus closure data to the closure of a single cavity indicates that the cavities will begin to act independently at a P/D of approximately 4. Third, the zone of influence of the outer cavities began to touch the outer cylindrical surface of the plasticine sometime during the 1.5 P/D experiment. This implies that the cylindrical blocks of plasticine were not quite large enough in diameter.

ACKNOWLEDGEMENTS

The authors are indebted to Paul Hatch, who conducted the constant strain rate experiments on plasticine, and to Carl Goodrich, Tim George, Jim Ross and Eugene Chavez for their assistance in performing the experiments. Also, John Gieske and Phil Walkington who performed the ultra-sound experiments on plasticine and Johnny Biffle who wrote both finite element programs (JAC and JAC3D) used to do the creep calculations.

REFERENCES

1. R. J. Hart and T. S. Ortiz, "Strategic Petroleum Reserve (SPR) Geological Site Characterization Report Big Hill Salt Dome," SAND81-1045, Sandia National Laboratories, Albuquerque, NM.

2. D. S. Preece and W. R. Wawersik, "Leached Salt Cavern Design Using a Fracture Criterion for Rock Salt," Proceedings of the 25th U. S. Symposium on Rock Mechanics, Northwestern University, June 1984.

3. H. Ramberg, Gravity, Deformation and the Earth's Crust, Academic Press, London, 1981.

4. K. R. McClay, "The Rheology of Plasticine", Tectonophysics, Vol. 33, 1976, pp. T7-T15.

5. S. H. Crandall, L. G. Kurzweil, and A. K. Nigam, "On the Measurement of Poisson's Ratio for Modeling Clay," Experimental Mechanics, September 1971, pp. 402-407.

6. H. J. Sutherland and D. S. Preece, "Physical Simulations of Cavity Closure in a Creeping Material," SAND85-0505, Sandia National Laboratories, Albuquerque, NM.

7. J. S. Rinehart, Stress Transients in Solids, Hyperdynamics, Santa Fe, New Mexico, 1975.

8. J. H. Biffle, "JAC - A Two-Dimensional Finite Element Computer Program for the Non-Linear Quasistatic Response of Solids with the Conjugate Gradient Method," SAND81-0998, Sandia National Laboratories, Albuquerque, NM.

9. H. S. Morgan, R. D. Krieg, and R. V. Matalucci, "Comparative Analysis of Nine Structural Codes Used in the Second WIPP Benchmark Problem," SAND81-1389, Sandia National Laboratories, Albuquerque, NM.

10. F. P. Beer and E. R. Johnson, Jr., Vector Mechanics for Engineers: Statics, McGraw Hill, New York, 1972.

11. D. S. Preece and C. M. Stone, "Verification of Finite Element Methods Used to Predict Creep Closure of Leached Salt Caverns," Proceedings of the 23rd U. S. Symposium on Rock Mechanics, Berkeley, California, August 1982.

12. D. S. Preece and J. T. Foley, "Finite Element Analysis of Salt Caverns Employed in the Strategic Petroleum Reserve," Proceedings of the 6th International Symposium on Salt, Toronto, Ontario, Canada, May 1983.

13. D. S. Preece and J. T. Foley, "Long Term Performance Predictions for Strategic Petroleum Reserve (SPR) Salt Caverns," SAND83-2343, Sandia National Laboratories, Albuquerque, NM.

14. K. H. Huebner, The Finite Element Method for Engineers, John Wiley & Sons, New York, 1975, pp. 150.

15. L. E. Malvern, Introduction to the Mechanics of a Continuous Medium, Prentice-Hall, Inc.,, Englewood Cliffs, New Jersey, 1969, pp. 280-281.

16. H. S. Morgan, C. M. Stone, and R. D. Krieg, "Effects of Elastic Properties on the Time-Dependent Response of WIPP Rooms," Internal memorandum to D. E. Munson, 6332, Sandia National Laboratories, December 15, 1983.

17. PDA Software Products Division, PATRAN User's Guide, PDA Engineering, Santa Ana, California.

18. D. P. Flanagan, "DETOUR - Preliminary User's Guide," Internal memorandum, Sandia National Laboratories.

19. H. N. Christiansen, and M. B. Stephenson, "MOVIE.BYU - Computer Graphics Software System," Journal of the Technical Councils of ASCE, Vol. 5, No. TCI, April 1979, pp. 3-12.

20. C. S. Desai and H. J. Siriwardane, Constitutive Laws for Engineering Materials With Emphasis on Geologic Materials, Prentice-Hall, Inc., pp. 213-214.

21. J. Prij and J. Mengelers, "On The Derivation of a Creep Law From Isothermal Bore Hole Convergence," ECN-80-169, Stiching Energieonderzoek Centrum Nederland, October 1980.

22. M. B. Stephenson, and H. N. Christiansen, "A Polyhedron Clipping and Capping Algorithm and a Display System for Three-Dimensional Finite Element Models," Computer Graphics, Vol. 9, No. 3, Fall 1975, pp. 1-16.

Appendix A

Computer Program for Calculating Finite Element Model Cavity Volumes Using Nodal Loops

```
      PROGRAM  VOLCAV
      COMMON  /DEFINE/  NCAV,N,NNODES
      REAL  MOIL,MBR
      DIMENSION  DETHTIM(10)
      DIMENSIONTITLE(10),R(4,10000),Z(4,10000),D(10000,6),IX(8,10000)
      DIMENSION A(4), NNODES(4), OVOL(4), VOL(4), XBAR(4), YBAR(4)
      DIMENSION S(4,10000), T(4,10000), U(4,10000), V(4,10000)
      DIMENSION X(4,10000), Y(4,10000)
      DIMENSION XC(10000,3), CVOL(4,10000), TME(10000), PRES(10000)
      DIMENSION N(4,100), FLR(4), XVOL(10000)
      CHARACTER*8   TITLE,CNAME,CDATE,CTIME,MNAME,MDATE,MTYME
      CHARACTER*8  LNAME(6)
      DATA LNAME/'VOLUME 1','VOLUME 2','VOLUME 3','FLRATE 1','FLRATE 2',
     1'FLRATE 3'/
      NSTE=0.0
      JJ=1
      PRINT 10
   10 FORMAT (' CAVITY VOLUME CALCULATION PROGRAM - USING NODAL LOOPS')
   20 CONTINUE
C
C     READ CAVITY NODES, FLUID PROPERTIES AND DEATH TIMES
C
      CALL  READ
C
C     READ DATA FROM STANDARD POST-FEM DATABASE
C
      IERROR=0
   30 CALL OPEN ('PLOT',11,0,IERROR)
      IF (IERROR) 30, 220, 40
   40 READ (11) TITLE
      READ (11) NDIM,NUMNP,NUMEL,NUMIX,NUMAT,NVARNP,NVAREL,NGLBV,
     1          IBLKNP,IBLKEL,IPACK
      PRINT 50, TITLE
   50 FORMAT (' ',///,2X,'TITLE:',2X,8A8)
      PRINT  60,  NDIM,NUMNP,NUMEL,NUMIX,NUMAT,NVARNP,NVAREL,NGLBV,
     1         IBLKNP,IBLKEL,IPACK
   60 FORMAT (/3X,
     1         'NUMBER OF COORDINATES PER NODE (NDIM)---------- 'I10/3X,
     2         'NUMBER OF NODAL POINTS (NUMNP)----------------- 'I10/3X
     3         'NUMBER OF ELEMENTS (NUMEL)--------------------- 'I10/3X
     4         'NUMBER OF NODES PER ELEMENT (NUMIX)------------ 'I10/3X
     5         'NUMBER OF MATERIALS (NUMAT)-------------------- 'I10/3X
     6         'NUMBER OF VARIABLES AT EACH NODE (NVARNP)------ 'I10/3X
     7         'NUMBER OF VARIABLES FOR EACH ELEMENT (NVAREL)-- 'I10/3X
     8         'NUMBER OF GLOBAL VARIABLES (NGLBV)------------- 'I10/3X
     9         'NODAL POINT BLOCKING FLAG (IBLKNP)------------- 'I10/3X
     $         'ELEMENT BLOCKING FLAG (IBLKEL)----------------- 'I10/3X
     $         'PACKED  DATA  FLAG  (IPACK)---------------------  'I10/3X
```

```
     $        )
C
C      DUMMY READS OF DATA THAT IS NOT NEEDED
C
       IF (NDIM.GT.0)   READ (11)
       IF (NVARNP.GT.0) READ (11)
       IF (NVAREL.GT.0) READ (11)
       IF (NGLBV.GT.0)  READ (11)
C
C      READ COORDINATES FROM UNIT 11
C
       READ (11) ((XC(I,J),I=1,NUMNP),J=1,NDIM)
C
C      TRANSFER X(I,J) TO R(K,I) AND Z(K,I)
C
       DO 70 K=1,NCAV
          DO 70 I=1,NUMNP
          R(K,I)=XC(I,1)-XC(N(K,1),1)
          Z(K,I)=XC(I,3)
   70     CONTINUE
C
C      DUMMY READ OF CONNECTIVITY
C
       DO 80 J=1,NUMEL
   80     READ (11)
C
C      DUMMY READ OF MATERIAL ARRAY
C
       IF (NUMAT.GT.1) READ (11)
C
C      CALCULATE UNDEFORMED CAVITY VOLUMES
C
       CALL CALCVOL (R,Z,NCAV,N,NNODES,OVOL)
C
C      ADD UNDEFORMED CAVITY VOLUMES
C
       TOVOL = 0.0
       DO 90 K=1,NCAV
   90     PRINT 100, K,OVOL(K)
  100  FORMAT (/' ',' CAVITY ',I2,2X,'UNDEFORMED VOLUME ='G12.6//)
       PRINT 110
  110  FORMAT (/'0',' DEFORMED CAVITY VOLUMES')
C
C      READ TIME DISPLACEMENT DATA FROM TAPE
C
  120  READ (11, END=210) TYME
C
C      NODAL TIME DATA
C
       NWRDS=((NUMNP-1)/IPACK)+1
       DO 130 J=1,NVARNP
  130     READ (11, END=210) (D(I,J),I=1,NWRDS)
C
C      ELEMENT TIME DATA
C
```

```
      NWRDS=((NUMEL-1)/IPACK)+1
      DO 140 J=1,NVAREL
  140    READ (11, END=210)
C
C     GLOBAL TIME DATA
C
      IF (NGLBV.GT.0) READ (11, END=210)
C
C     SKIP IF DATA TAPE TIME IS LESS THAN MOST RECENT TIME
C
      IF (NSTE.EQ.0) GO TO 150
      TEST = TME(NSTE)
      IF (TYME.LE.TEST) GO TO 200
  150 NSTE=NSTE+1
      TME(NSTE)=TYME
C
C     ADD COORDINATES AND DISPLACEMENTS
C
      DO 160 K=1,NCAV
         DO 160 I=1,NUMNP
         S(K,I)= R(K,I)+D(I,1)
         T(K,I)= Z(K,I)+D(I,3)
  160    CONTINUE
C
C     CALCULATE DEFORMED CAVITY VOLUMES
C
      CALL CALCVOL (S,T,NCAV,N,NNODES,VOL)
C
C     PRINT VOLUMES OF CAVITIES
C
      PRINT 170, NSTE,TYME
  170 FORMAT ('O',' STEP'I2,1X,' TIME = '612.6)
      DO 190 K=1,NCAV
         CVOL(K,NSTE)=VOL(K)
         PRINT 180, K,CVOL(K,NSTE)
  180    FORMAT (' ',' CAVITY ',I2,' VOLUME = ',G12.6)
  190    CONTINUE
  200 CONTINUE
      GO TO 120
  210 CONTINUE
      GO TO 20
  220 CONTINUE
C
C     SET UP UNIT 12 TO WRITE PLOT DATA
C
      CALL OPEN ('PLOT',12,-1,IERROR)
C
C     DEFINE CREATION NAME DATE AND TIME
C
      CNAME='SANCHO  '
      CTIME='        '
      CDATE='        '
C
C     DEFINE MODIFICATION NAME DATE AND TIME
C
```

```
      MNAME='VOLCAV  '
      CALL DATE (MDATE)
      CALL TIME (MTYME)
C
C     ALLOW USER TO CHANGE TITLE
C
      PRINT 230
  230 FORMAT (' ','<CHANGE PLOT TITLE?> ',$)
      READ (5, 240) ANS
  240 FORMAT (A1)
      IF (ANS.EQ.'N') GO TO 270
      IF (ANS.EQ.' ') GO TO 270
      PRINT 250
  250 FORMAT (' ', '<ENTER NEW TITLE> ',$)
      READ (5, 260) TITLE
  260 FORMAT (10A8)
  270 CONTINUE
C
C     WRITE PRELIMINARY PLOT DATA
C
      WRITE (12) TITLE,CNAME,CDATE,CTIME,MNAME,MDATE,MTYME
      WRITE (12) 0,0,0,0,0,0,0,6,0,0,0
      WRITE (12) LNAME(1),LNAME(2),LNAME(3),LNAME(4),LNAME(5),LNAME(6)
C
C     DO LOOP THROUGH ALL TIME INCREMENTS TO CALCULATE
C     AND WRITE PLOT VARIABLES TO UNIT 12
C
      DO 350 I=1,NSTE-2
C
C     SET FLOW RATE FOR TIME = 0
C
         IF (I.GT.1) GO TO 280
         FLR(1)=0.0
         FLR(2)=0.0
         FLR(3)=0.0
         GO TO 310
C
C     CALCULATE FLOWRATE FOR FIRST TIME STEP AFTER ELASTIC RESPONSE
C
  280    CONTINUE
         IF (I.GT.2) GO TO 290
         FLR(1)=(CVOL(1,I+1)-CVOL(1,I))/(TME(I+1)-TME(I))
         FLR(2)=(CVOL(2,I+1)-CVOL(2,I))/(TME(I+1)-TME(I))
         FLR(3)=(CVOL(3,I+1)-CVOL(3,I))/(TME(I+1)-TME(I))
         GO TO 310
C
C     CALCULATE FLOWRATE FOR OTHER TIMES BY LINEAR REGRESSION
C
  290    CONTINUE
         DO 300 K=1,NCAV
            CALL REGRESS (I,K,TME,CVOL,XNUM,DEN)
            FLR(K)=XNUM/DEN
  300       CONTINUE
  310    CONTINUE
         PRINT 320, I,TME(I)
```

```
  320     FORMAT (1X,//'TIME INC. = 'I5,5X,'TIME = '612.6)
          DO 330 K=1,NCAV
  330        PRINT 340, K,CVOL(K,I),FLR(K)
  340     FORMAT (1X,'CAVITY',I2,1X,'VOLUME = '612.6,
     1     'FLOW RATE ='G12.6)
C
C     WRITE TIME AND GOLBAL VARIABLES TO UNIT 12
C
          WRITE (12) TME(I)
          WRITE (12) CVOL(1,I),CVOL(2,I),CVOL(3,I),FLR(1),FLR(2),FLR(3)
  350     CONTINUE
      STOP
      END
C
      SUBROUTINE CALCVOL (X,Y,NCAV,N,NNODES,VOL)
      DIMENSION X(4,1), Y(4,1), N(4,1), NNODES(1), VOL(1)
      DIMENSION A(4), XBAR(4), YBAR(4)
      DATA PI/3.141592654/
C
C     CALCULATE CAVITY AREAS
C
      DO 20 K=1,NCAV
         SUM=X(K,N(K,1))*Y(K,N(K,1))
         MAXN = NNODES(K)-1
         DO 10 J=1,MAXN
            I=J+1
   10       SUM = SUM+(Y(K,N(K,I))-Y(K,N(K,J)))*(X(K,N(K,I))+
     1      X(K,N(K,J)))
         SUM=SUM-Y(K,N(K,NNODES(K)))*X(K,N(K,NNODES(K)))
         A(K)=-SUM/2.0
C
C     CALCULATE  XBAR
C
         INDEX = 1
         CALL   CNTRD   (X,Y,INDEX,N,NNODES,K,A,XBAR)
C
C     CALCULATE  YBAR
C
         INDEX = 2
         CALL   CNTRD   (Y,X,INDEX,N,NNODES,K,A,YBAR)
C
C     CALCULATE  CAVITY  VOLUMES
C
         VOL(K)=2*PI*XBAR(K)*A(K)
   20    CONTINUE
      RETURN
      END
```

```
      SUBROUTINE  CNTRD  (U,V,INDEX,N,NNODES,K,A,CENTER)
      DIMENSION U(4,1), V(4,1), N(4,1), NNODES(1), A(1), CENTER(1)
      SUM = V(K,N(K,1))/8*(U(K,N(K,1))**2+.33333333*U(K,N(K,1))**2)
      MAXN=NNODES(K) - 1
      DO 10 J=1,MAXN
         I=J+1
         SUM=SUM+(V(K,N(K,I))-V(K,N(K,J)))/8.0*((U(K,N(K,I))+
     1   U(K,N(K,J)))**2+0.333333*(U(K,N(K,I))-U(K,N(K,J)))**2)
   10    CONTINUE
      NSH=NNODES(K)
      SUM=SUM-V(K,N(K,NSH))/8.0*(U(K,N(K,NSH))**2+
     10.333333*U(K,N(K,NSH))**2)
      CENTER(K)=1.0/A(K)*SUM
      IF (INDEX.EQ.1) CENTER(K)=-CENTER(K)
      RETURN
      END
C
      SUBROUTINE  OPEN  (FILEID,IUNIT,IOP,IERROR)
      BYTE  BLANK,NULL,XNAME
      DIMENSION  XNAME(16)
      DATA BLANK/' '/,NULL/0/
      IERROR=0
      IF (IOP.LT.0) PRINT 30, FILEID
      IF (IOP.GE.0) PRINT 40, FILEID
      READ (5, 20) (XNAME(I),I=1,15)
      IF (XNAME(1).EQ.BLANK) RETURN
      IERROR=1
      XNAME(16)=NULL
      IF (IOP.LT.0) OPEN (UNIT=IUNIT, FILE=XNAME, TYPE='NEW', FORM='UNFO
     1RMATTED', ERR=10)
      IF (IOP.EQ.0) OPEN (UNIT=IUNIT, FILE=XNAME, TYPE='OLD', READONLY,
     1FORM='UNFORMATTED', ERR=10)
      IF (IOP.GT.0) OPEN (UNIT=IUNIT, FILE=XNAME, TYPE='OLD', ERR=10)
      RETURN
   10 IERROR=-1
      R E T U R N
   20 FORMAT (15A1)
   30 FORMAT (/'+<WRITE',1X,A4,' FILE> '$)
   40 FORMAT (//'+<READ',1X,A4,' FILE> '$)
      END
C
      SUBROUTINE  REGRESS  (I,K,X,Y,XNUM,DEN)
```

```
      DIMENSION X(1), Y(4,1)
C
      XBAR=(X(I-1)+X(I)+X(I+1))/3.0
      YBAR=(Y(K,I-1)+Y(K,I)+Y(K,I+1))/3.0
C
      XNUM=0.0
      DEN=0.0
C
      DO 10 KK=1,3
         L=KK-2
         XNUM=XNUM+((X(I+L)-XBAR)*(Y(K,I+L)-YBAR))
         DEN=DEN+(X(I+L)-XBAR)**2
   10    CONTINUE
C
      RETURN
      END
C
```

```
      SUBROUTINE READ
      COMMON /DEFINE/ NCAV,N,NNODES
      DIMENSION N(4,100), NNODES(4), DETHTIM(10)
C
C     OPEN FILE CONTAINING INPUT INFORMATION
C
      IERROR=0
   10 CALL OPEN ('DATA',15,1,IERROR)
      IF (IERROR) 10, 100, 20
C
C     READ AND PRINT CAVITY NODE DESCRIPTION
C
   20 READ (15, 30) NCAV
   30 FORMAT (215)
      PRINT 40, NCAV
   40 FORMAT ('0',' NUMBER OF CAVITIES = '15)
C
      DO 90 I=1,NCAV
         READ (15, 30) ICAVNO,NNODES(I)
         PRINT 50, ICAVNO,NNODES(I)
   50    FORMAT (///' CAVITY NO. ='I5'       NUMBER OF NODES ='I5)
         NUM = NNODES(I)
         READ (15, 60) (N(ICAVNO,J),J=1,NUM)
   60    FORMAT (1615)
         PRINT 70, ICAVNO
   70    FORMAT (' NODES DESCRIBING CAVITY NO. '15)
         PRINT 80, (N(ICAVNO,J),J=1,NUM)
   80    FORMAT (' ',15I5)
   90    CONTINUE
  100 CONTINUE
      RETURN
      END
```

Appendix B

Computer Program for Calculating Finite Element Model Cavity Volumes Using Displacement Hexahedrons

```
      PROGRAM VOL3D
      DIMENSION XTITLE(72),TITLE(lO)
      DIMENSION X(10000,3), ICON(10000,8), IPC(2000), IFLAG(2000)
      DIMENSION IFACE(2000,4), XC(10000,3), D(10000,6)
      DIMENSION CVOL(4,10000), CHVOL(4), TME(lOOOO)
      DIMENSION FLR(4), FAC(4)
      COMMON /NODEC/ HX(8),HY(8),HZ(8)
      CHARACTER*8  TITLE,CNAME,CDATE,CTIME,MNAME,MDATE,MTYME
      CHARACTER*8 LNAME(6)
      DATA LNAME/'VOLUME 1','VOLUME 2','VOLUME 3','FLRATE 1','FLRATE 2',
     1'FLRATE 3'/
C
C     DEFINE MODEL SPECIFIC DATA
C
      FAC(1)=6.0
      FAC(2)=2.0
      NCAV=2
C
      NSTE=0
C
      PRINT 10
   10 FORMAT (' ','3-D HEXAHEDRAL CAVITY VOLUME CHANGE PROGRAM'/)
C
C      OPEN JAC3D.BDF INPUT FILE
C
   20 CALL OPEN ('BDF ',11,1,IERROR)
      IF (IERROR) 20, 330, 30
C
C      READ TITLE
C
   30 CONTINUE
      READ (11, 40) (XTITLE(I),I=1,72)
      PRINT 40, (XTITLE(I),I=1,72)
   40 FORMAT (72A1)
C
C      READ FIRST, CARD
C
      READ (11, 50) NUMAT,NUMNP,NUMEL,NUMPC
      PRINT 50, NUMAT,NUMNP,NUMEL,NUMPC
   50 FORMAT (415)
C
C      READ COORDINATE ARRAY
C
      DO 70 I=1,NUMNP
         READ (11, 60) NUM1,NUM2, (X(I,J),J=1,3)
   60    FORMAT (2I5,3F10.5)
   70    CONTINUE
C
```

```
C       READ CONNECTIVITY
C
      DO,90 ,I=1,NUMEL
         READ (11, 80) NUM1,NUM2, (ICON(I,J),J=1,8)
   80    FORMAT (1015)
   90    CONTINUE
C
C       READ PRESSURE BOUNDARY VALUES
C
      DO 110 I=1,NUMPC
         READ (11, 100) IPC(I),IFLAG(I),(IFACE(I,J),J=1,4)
  100    FORMAT (615)
  110    CONTINUE
C
C     BEGINNING OF TAPE11.BIN READ LOOP (IN CASE OF RESTARTS)
C
  120 CONTINUE
C
C     READ DATA FROM STANDARD POST-FEM DATABASE
C
      IERROR=0
  130 CALL OPEN ('PLOT',11,0,IERROR)
      IF (IERROR) 130, 330, 140
  140 READ (11) TITLE
      READ (11) NDIM,NUMNP,NUMEL,NUMIX,NUMAT,NVARNP,NVAREL,NGLBV,
     1          IBLKNP,IBLKEL,IPACK
      PRINT 150, TITLE
  150 FORMAT (1X,///,2X,'TITLE:',2X,10A8)
      PRINT 160, NDIM,NUMNP,NUMEL,NUMIX,NUMAT,NVARNP,NVAREL,NGLBV,
     1           IBLKNP,IBLKEL,IPACK
  160 FORMAT (/3X,
     1        'NUMBER OF COORDINATES PER NODE (NDIM)----------'I10/3X,
     2        'NUMBER OF NODAL POINTS(NUMNP)-----------------'I10/3X
     3        'NUMBER OF ELEMENTS (NUMEL)--------------------'I10/3X
     4        'NUMBER OF NODES PER ELEMENT (NUMIX)-----------'I10/3X
     5        'NUMBER OF MATERIALS (NUMAT)-------------------'I10/3X
     6        'NUMBER OF VARIABLES AT EACH NODE (NVARNP)------'I10/3X
     7        'NUMBER OF VARIABLES FOR EACH ELEMENT (NVAREL)-- 'I10/3X
     8        'NUMBER OF GLOBAL VARIABLES (NGLBV)------------'I10/3X
     9        'NODAL POINT BLOCKING FLAG (IBLKNP)------------'I10/3X
     $        'ELEMENT BLOCKING FLAG (IBLKEL)----------------'I10/3X
     $        'PACKED DATA FLAG (IPACK)----------------------'I10/3X
     $      )
C
C     DUMMY READS OF DATA THAT IS NOT NEEDED
C
      IF (NDIM.GT.0)   READ (11)
      IF (NVARNP.GT.0) READ (11)
      IF (NVAREL.GT.0) READ (11)
      IF (NGLBV.GT.0) READ (11)
C
C     READ COORDINATES FROM UNIT 11
C
      READ (11) ((XC(I,J),I=1,NUMNP),J=1,NDIM)
C
```

```
C     DUMMY READ OF CONNECTIVITY
C
      DO 170 J=1,NUMEL
  170    READ (11)
C
C     DUMMY READ OF MATERIAL ARRAY
C
      IF (NUMAT.GT.1) READ (11)
C
      PRINT 180
  180 FORMAT (/'0',' DEFORMED CAVITY VOLUMES')
C
C     READ TIME DISPLACEMENT DATA FROM TAPE
C
  190 READ (11, END=320) TYME
C
C     NODAL TIME DATA
C
      NWRDS=((NUMNP-1)/IPACK)+1
      DO 200 J=1,NVARNP
  200    READ (11, END=320) (D(I,J),I=1,NWRDS)
C
C     ELEMENT TIME DATA
C
      NWRDS=((NUMEL-1)/IPACK)+1
      DO 210 J=1,NVAREL
  210    READ (11, END=320)
C
C     GLOBAL TIME DATA
C
      IF (NGLBV.GT.0) READ (11, END=320)
C
C     SKIP IF DATA TAPE TIME IS LESS THAN MOST RECENT TIME
C
      IF (NSTE.EQ.0) GO TO 220
      IF (TYME.LE.TME(NSTE)) GO TO 310
  220 NSTE=NSTE+1
      TME(NSTE)=TYME
C
C     DEFINE ORIGINAL VOLUME CAVITIES
C
      DO 230 K=1,4
  230    CHVOL(K)=0.0
      NFACE1 = 0
      NFACE2 = 0
C
C     PROCESS ALL PRESSURIZED FACES FOR VOLUME CHANGE
C
      DO 260 I=1,NUMPC
C
C     SKIP FACES WITH FLAGS OF 1 (CAVITIES HAVE FLAGS OF 2 AND 3)
C
         IF (IFLAG(I).EQ.1) GO TO 260
C
C     COUNT NUMBER OF PRESSURE FACES IN EACH CAVITY
```

```
C
          IF (IFLAG(I).EQ.2) NFACE1=NFACE1+1
          IF (IFLAG(I).EQ.3) NFACE2=NFACE2+1
C
C     CREATE HEXAHEDRON FROM CAVITY FACE ELEMENT AND ITS DISPLACEMENTS
C
          DO 240 JJ=1,4
             HX(JJ)=X(IFACE(I,JJ),1)
             HY(JJ)=X(IFACE(I,JJ),2)
             HZ(JJ)=X(IFACE(I,JJ),3)
  240        CONTINUE
          DO 250 JJ=5,8
             KK=JJ-4
             HX(JJ)=X(IFACE(I,KK),1)+D(IFACE(I,KK),1)
             HY(JJ)=X(IFACE(I,KK),2)+D(IFACE(I,KK),2)
             HZ(JJ)=X(IFACE(I,KK),3)+D(IFACE(I,KK),3)
  250        CONTINUE
C
C     CALCULATE DEFORMED CAVITY VOLUMES
C
          CALL HEXVOL (HVOL)
C
C     SUM HVOL TO OBTAIN TOTAL VOLUME CHANGE
C
          KK=IFLAG(I)-1
          CHVOL(KK)=CHVOL(KK)+FAC(KK)*HVOL
  260     CONTINUE
C
C     SUBTRACT TOTAL VOLUME CHANGE FROM ORIGINAL VOLUME
C
      DO 270 K=1,NCAV
  270    CVOL(K,NSTE)=12.56637062-CHVOL(K)
C
C     PRINT VOLUMES OF CAVITIES
C
      PRINT 280, NSTE,TYME
  280 FORMAT ('0',/' STEP '12,1X,'TIME = '612.6)
      DO 290 K=1,NCAV
  290    PRINT 300, K,CVOL(K,NSTE)
  300 FORMAT (' ',' CAVITY ',I2,' VOLUME = ',G12.6)
  310 CONTINUE
      GO TO 190
  320  CONTINUE
      GO TO 120
  330 CONTINUE
C
C     SET UP UNIT 12 TO WRITE PLOT DATA
C
      CALL OPEN ('PLOT',12,-1,IERROR)
C
C     DEFINE CREATION NAME DATE AND TIME
C
      CNAME='SANCHO  '
      CTIME='        '
      CDATE='
```

```
C
C     DEFINE MODIFICATION NAME DATE AND TIME
C
      MNAME='VOL3D   '
      CALL DATE (MDATE)
      CALL TIME (MTYME)
C
C     ALLOW USER TO CHANGE TITLE
C
      PRINT 340
  340 FORMAT ('','<CHANGE PLOT TITLE?> ',$)
      READ (5, 350) ANS
  350 FORMAT (A1)
      IF (ANS.EQ.'N') GO TO 380
      IF (ANS.EQ.' ') GO TO 380
      PRINT 360
  360 FORMAT (' ', '<ENTER NEW TITLE> ',$)
      READ (5, 370) TITLE
  370 FORMAT (10A8)
  380 CONTINUE
C
C     WRITE PRELIMINARY PLOT DATA
C
      WRITE (12) TITLE,CNAME,CDATE,CTIME,MNAME,MDATE,MTYME
      WRITE (12) 0,0,0,0,0,0,0,6,0,0,0
      WRITE (12) LNAME(1),LNAME(2),LNAME(3),LNAME(4),LNAME(5),LNAME(6)
C
C     DO LOOP THROUGH ALL TIME INCREMENTS TO CALCULATE
C     AND WRITE PLOT VARIABLES TO UNIT 12
C
      DO 460 I=1,NSTE-1
C
C     SET FLOW RATE FOR TIME = 0
C
         IF (I.GT.1) GO TO 390
         FLR(1)=0.0
         FLR(2)=0.0
         FLR(3)=0.0
         GO TO 420
C
C     CALCULATE FLOWRATE FOR FIRST TIME STEP AFTER ELASTIC RESPONSE
C
  390    CONTINUE
         IF (I.GT.2) GO TO 400
         FLR(1)=(CVOL(1,I+1)-CVOL(1,I))/(TME(I+1)-TME(I))
         FLR(2)=(CVOL(2,I+1)-CVOL(2,I))/(TME(I+1)-TME(I))
         FLR(3)=(CVOL(3,I+1)-CVOL(3,I))/(TME(I+1)-TME(I))
         GO TO 420
C
C     CALCULATE FLOWRATE FOR OTHER TIMES BY LINEAR REGRESSION
C
  400    CONTINUE
         DO 410 K=1,NCAV
            CALL REGRESS (I,K,TME,CVOL,XNUM,DEN)
            FLR(K)=XNUM/DEN
```

```
  410        CONTINUE
  420     CONTINUE
          PRINT 430, I,TME(I)
  430     FORMAT (1X,//' TIME INC. = 'I5,5X,'TIME = '612.6)
          DO 440 K=1,NCAV
  440        PRINT 450, K,CVOL(K,I),FLR(K)
  450     FORMAT (1X,'CAVITY',I2,1X,'VOLUME = '612.6,
     1      'FLOW RATE ='G12.6)
C
C     WRITE TIME AND GLOBAL VARIABLES TO UNIT 12
C
          WRITE (12) TME(I)
          WRITE (12) CVOL(1,I),CVOL(2,I),CVOL(3,I),FLR(1),FLR(2),FLR(3)
  460     CONTINUE
      STOP
      END
C
```

```
      SUBROUTINE HEXVOL (HVOL)
C ***************************************************************************
      COMMON /NODEC/ HX(8),HY(8),HZ(8)
C
      DATA O64TH/0.0156250/
C
C     JACOBIAN MATRIX
C
      X17=HX(7)-HX(1)
      X28=HX(8)-HX(2)
      X35=HX(5)-HX(3)
      X46=HX(6)-HX(4)
      Y17=HY(7)-HY(1)
      Y28=HY(8)-HY(2)
      Y35=HY(5)-HY(3)
      Y46=HY(6)-HY(4)
      Z17=HZ(7)-HZ(1)
      Z28=HZ(8)-HZ(2)
      Z35=HZ(5)-HZ(3)
      Z46=HZ(6)-HZ(4)
C
      AJ1=X17+X28-X35-X46
      AJ2=Y17+Y28-Y35-Y46
      AJ3=Z17+Z28-Z35-Z46
      A17=X17+X46
      A28=X28+X35
      B17=Y17+Y46
      B28=Y28+Y35
      C17=Z17+Z46
      C28=Z28+Z35
C
      AJ4=A17+A28
```

```
      AJ5=B17+B28
      AJ6=C17+C28
      AJ7=A17-A28
      AJ8=B17-B28
      AJ9=C17-C28
C
C     JACOBIAN
C
      AJ5968=AJ5*AJ9-AJ6*AJ8
      AJ6749=AJ6*AJ7-AJ4*AJ9
      AJ4857=AJ4*AJ8-AJ5*AJ7
C
      HVOL=064TH*(AJ1*AJ5968+AJ2*AJ6749+AJ3*AJ4857)
C
      RETURN
C
      END
C
```

```
      SUBROUTINE OPEN (FILEID,IUNIT,IOP,IERROR)
C*********************************************************************
      BYTE BLANK,NULL,XNAME
      DIMENSION XNAME(16)
      DATA BLANK/' '/,NULL/0/
      IERROR=0
      IF (IOP.LT.0) PRINT 30, FILEID
      IF (IOP.GE.0) PRINT 40, FILEID
      READ (5, 20) (XNAME(I),I=1,15)
      IF (XNAME(1).EQ.BLANK) RETURN
      IERROR=1
      XNAME(16)=NULL
      IF (IOP.LT.0) OPEN (UNIT=IUNIT, FILE=XNAME, TYPE='NEW', FORM='UNFO
     1RMATTED', ERR=10)
      IF(IOP.EQ.0) OPEN (UNIT=IUNIT, FILE=XNAME, TYPE='OLD', READONLY,
     1FORM='UNFORMATTED', ERR=10)
      IF (IOP.GT.0) OPEN (UNIT=IUNIT, FILE=XNAME, TYPE='OLD', ERR=10)
      RETURN
   10 IERROR=-1
      RETURN
   20 FORMAT (15A1)
   30 FORMAT (/'+<WRITE',1X,A4,' FILE> '$)
   40 FORMAT (//'+<READ',1X,A4,' FILE> '$)
      END
C
```

```
      SUBROUTINE REGRESS (I,K,X,Y,XNUM,DEN)
C*************************************************************************
      DIMENSION X(1), Y(4,1)
C
      XBAR=(X(I-1)+X(I)+X(I+1))/3.0
      YBAR=(Y(K,I-1)+Y(K,I)+Y(K,I+1))/3.0
C
      XNUM=0.0
      DEN=0.0
C
      DO 10 KK=1,3
         L=KK-2
         XNUM=XNUM+((X(I+L)-XBAR)*(Y(K,I+L)-YBAR))
         DEN=DEN+(X(I+L)-XBAR)**2
   10    CONTINUE
C
      RETURN
      END
```

DISTRIBUTION:'

US DOE SPR PMO (8)
900 Commerce Road East
New Orleans, LA 70123
Attn: E. E. Chapple, PR-632 (6)
TDCS (2)

US Department of Energy (2)
Strategic Petroleum Reserve
1000 Independence Avenue, SW
Washington, DC 20585
Attn: D. Johnson
D. Smith

US DOE (1)
Oak Ridge Operations Office
P.O. Box E
Oak Ridge, TN 37831
Attn: J. Milloway

Walk-Haydel & Associates, Inc.
600 Carondelet St.
New Orleans, LA 70130
Attn: J. Mayes

Boeing (2)
880 Commerce Rd., W.
New Orleans, LA 70123
Attn: Ken Mills

PB/KBB (4)
880 Commerce Rd. W.
New Orleans, LA 70123
Attn: H. Lombard

Gerald J. Parker
DOE/AP1
FE-33, D-128
Washington, DC 20585

A. M. Hartstein
Department of Energy
FE-34, D-124
Washington, DC 20585

Paul McWilliams (4)
U.S. Bureau of Mines
Spokane Mining Research Center
E. 315 Montgomery Avenue
Spokane, WA 92007

Phil Halleck
405 Deike Building
State College, PA 16851

Prof. S. H. Advani
Department of Engineering Mechanics
Ohio State University
Columbus, OH 43201

Prof. S. Benzley
Department of Civil Engineering
Brigham Young University
Provo, UT 84601

Department of Materials Science (2)
and Materials Engineering
University of California
Berkeley, CA 94720
Attn: Prof. N.G.W. Cook
M. Hood

Prof. Hon-Kim Ko
Department of Coal & Environmental Engineering
University of Colorado
Boulder, CO 80202

Dr. D. J. Goodings
Department of Civil Engineering
University of Maryland
College Park, MD 20742

Prof. S. K. Saxena
Department of Civil Engineering
Armour College of Engineering
Illinois Institute of Technology
Chicago, IL 60616

Prof. A. N. Schofield
University of Cambridge
Department of Engineering
Trumpington Street
Cambridge CB2 IPZ, ENGLAND

P. R. Dawson
Cornell University
Sibley School of Mechanical
& Aerospace Engineering
254 Upson Hall
Ithaca, NY 14853

Erick J. Reinhard
AFWL/NTED, USAF
Kirtland AFB, NM 87117

Ted S. Vinson
Department of Civil Engineering
Oregon State University
Corvallis, OR 97331

James Cheney
Department of Civil Engineering
University of California, Davis
Davis. CA 95616

Dr. W. H. Craig
Simon Engineering Laboratories
University of Manchester
Manchester M13 9PL
UNITED KINGDOM

John M. Dixon
Department of Geological Sciences
Queen's University
Kingston, Ontario
CANADA

Exxon Production Research Co. (3)
P.O. Box 2189
Houston, TX 77001
Attn: R. T. Weiss
Raymond Finucane

Enrique Garjardo Wolff
Supervisor, Unidad de Geotecnia
Dept. de Ingenieria General
Edificio Los Tres Puentes
Piso 2 - Los Teques
Apartado 76343
Caracas 1070A, VENEZUELA

Solution Mining Research Institute, Inc. (3)
812 Muriel Street
Woodstock, IL 60098

SANDIA INTERNAL

1510 J. W. Nunziato
1512 J. C. Cummings
1512 A. J. Russo
1520 D. J. McCloskey
1521 R. D. Krieg
1521 D. S. Preece (30)
1522 R. C. Reuter, Jr.
1523 J. H. Biffle
1524 A. K. Miller
1530 L. W. Davison
1540 W. C. Luth
1542 W. R. Wawersik
1821 N. E. Brown
3141 S. A. Landenberger (5)
3144 W. R. Roose (5)
3151 W. L. Garner (3)
3154-3 C. H. Dalin (28) for DOE/OSTI

Sandia Internal Continued:

6200 V. L. Dugan
6250 B. W. Marshall
6256 D. Engi
6256 H. J. Sutherland (10)
6257 J. K. Linn (10)
6257 R. R. Beasley
6257 J. L. Todd
6330 W. D. Weart
8024 P. W. Dean (1)